The evolution of dust-disk sizes from a homogeneous analysis of 1-10 Myr-old stars

Nathanial Hendler,[1] Ilaria Pascucci,[1] Paola Pinilla,[2] Marco Tazzari,[3] John Carpenter,[4] Renu Malhotra,[1] and Leonardo Testi[5]

[1]*Lunar and Planetary Laboratory, The University of Arizona, Tucson, AZ 85721, USA*
[2]*Max-Planck-Institut für Astronomie, Königstuhl 17, 69117, Heidelberg, Germany*
[3]*Institute of Astronomy, University of Cambridge, Madingley Road, CB3 0HA Cambridge, UK*
[4]*Joint ALMA Observatory, Avenida Alonso de Córdova 3107, Vitacura, Santiago, Chile*
[5]*European Southern Observatory, Karl-Schwarzschild-Strasse 2, 85748 Garching bei Mnchen, Germany*

ABSTRACT

We utilize ALMA archival data to estimate the dust disk size of 152 protoplanetary disks in Lupus (1-3 Myr), Chamaeleon I (2-3 Myr), and Upper-Sco (5-11 Myr). We combine our sample with 47 disks from Tau/Aur and Oph whose dust disk radii were estimated, as here, through fitting radial profile models to visibility data. We use these 199 homogeneously derived disk sizes to identify empirical disk-disk and disk-host property relations as well as to search for evolutionary trends. In agreement with previous studies, we find that dust disk sizes and millimeter luminosities are correlated, but show for the first time that the relationship is not universal between regions. We find that disks in the 2-3 Myr-old Cha I are not smaller than disks in other regions of similar age, and confirm the Barenfeld et al. (2017) finding that the 5-10 Myr USco disks are smaller than disks belonging to younger regions. Finally, we find that the outer edge of the Solar System, as defined by the Kuiper Belt, is consistent with a population of dust disk sizes which have not experienced significant truncation.

Keywords: protoplanetary disks, stars: pre-main sequence, submillimeter: planetary systems

1. INTRODUCTION

Protoplanetary disks, consisting of gas and dust around young ($\sim$1–10 Myr) stars, are the sites of planet formation. Because the expected population of planetesimals (km-sized bodies) or larger planetary embryos within these disks is not directly observable, we rely on millimeter observations sensitive to the largest detectable dust grains to constrain the timing, location, and mechanics of planet formation. The radial distribution of these mm/cm sized grains within the disk is a key parameter governing the planet making potential of a disk. For instance, in the pebble accretion scenario, the total amount of millimeter-sized grains and their inward flux are critical to form planets (e.g Ormel et al. 2017).

Millimeter surveys of protoplanetary disks reveal typical disk properties, as well as their spread, and can be used to identify empirical relationships between disk properties and disk/host-star properties. Such relations are essential to test and inform planet formation (e.g. Mulders et al. 2015; Pascucci et al. 2018), as well as in understanding the diversity of observed exo-planetary systems.

ALMA surveys of the nearby low-mass star-forming regions of Lupus, Cha I and USco (Ansdell et al. 2016; Pascucci et al. 2016; Barenfeld et al. 2016, respectively) each found a positive correlation between the mass in millimeter grains (hereafter, $M_{\rm dust}$) and stellar mass (hereafter, $M_\star$) for their respective region. It was also shown that the relationship steepens with the age of the region (Pascucci et al. 2016), suggesting that the amount of pebbles available to form planets decreases faster for disks around low-mass stars.

Pre-ALMA observations of the brightest disks in different star-forming regions reported dust disk outer radii ranging from 22 to 440 au (Isella et al. 2009; Andrews et al. 2010; Guilloteau et al. 2011). In addition, a correlation between disk size and disk luminosity ($L_{\rm mm}$) was identified early on (Andrews et al. 2010). However, only the $\sim$ 3 times larger SMA sample analyzed by Tripathi et al. (2017) could quantify the relation and found that $L_{\rm mm}$ scales as the square of the dust disk radius.

Corresponding author: Nathanial Hendler
nathanhendler@gmail.com

Dust disk size estimates from ALMA surveys have been carried out for Lupus (Tazzari et al. 2017; Andrews et al. 2018a), USco (Barenfeld et al. 2017) and the Orion Nebula Cluster (Eisner et al. 2018), yet each has been performed with different modeling techniques and assumptions. Tazzari et al. (2017) estimated Lupus disk sizes by fitting a two layer model (Chiang & Goldreich 1997) to visibilities, and found that Lupus disks tend to be larger than previously reported disk sizes in Tau/Aur and Oph observed at similar angular resolutions. Andrews et al. (2018a) estimated the disk sizes of Lupus by fitting Nuker brightness profiles, and compared them to the disk sizes of Tau/Aur and Oph as estimated by Tripathi et al. (2017) and did not come to the same conclusion that the Lupus disks are generally larger. While both works analyzed sub-samples of the same ALMA campaign, the Andrews et al. (2018a) sample was ~ 2 times larger than the Tazzari et al. (2017) sample which had a 4 mJy cutoff, excluded unresolved disks as well as disks with resolved gaps or cavities. However, both works determined that disks within Lupus have a positive correlation between disk size and L_{mm}. Barenfeld et al. (2017) estimated the sizes of disks within the older USco region by fitting radiative transfer models to visibilities using a truncated power law for surface density. They found USco disks to be typically three times smaller than the disks in Oph, Tau/Aur and Lupus, and suggested that USco followed the same positive correlation between disk size and L_{mm} as Tripathi et al. (2017). Finally, Eisner et al. (2018) measured disks within the Orion Nebula Cluster by fitting a 2D elliptical Gaussian to ALMA continuum maps. Their work found a correlation between disk size and L_{mm} as well, and additionally suggested that Cha I disks, using HWHM measurements from Pascucci et al. (2016) for Cha I disk sizes, are significantly smaller than Oph, Tau/Aur, and Lupus.

While trends seen within each region are robust, inferences among regions might be compromised by the use of varying modeling techniques (i.e. image plane measurements, radiative transfer modeling, visibility fitting with profiles generated by different functions) and assumptions (i.e. opacity, paramaterized disk height, fixed surface density slope, disk temperature, inner radius location). Andrews et al. (2018a) addressed this problem by comparing the regions of Oph, Tau/Aur and Lupus in a homogeneous way, finding that mm-luminosity scales as the square of the dust-disk radius was common to all three regions. This suggests that the scaling law between disk radius and stellar luminosity may be universal.

In this work we expand on the results of Tripathi et al. (2017) and Andrews et al. (2018a), using the same modeling techniques in order to present a homogeneously derived census of disk sizes within five regions of varying ages. In Section 2 we discuss our sample selection, consisting of a combination of disk size estimates from literature for Oph and Tau/Aur (Section 2.1) with our own estimates for disks within Lupus, Cha I and USco (Section 2.2). Our reduction of the ALMA observations is discussed in Section 3. To estimate disk sizes, we model observed sky brightnesses using axisymmetric radial-profile models which are fit to ALMA visibilities (see Section 4). Because not every source is detected, or results in a model that provides a disk size estimate, Section 4.1 provides details on the selection criteria we use for the final sample of disks used in our analysis. In Section 5 we summarize our results and compare disk sizes between regions. We use a variety of statistical tests to assess if relationships exist between disk properties and stellar-host properties in Section 5.1. Finally, we discuss and summarize our results in Sections 6 and 7.

2. INITIAL SAMPLE SELECTION

We aim to obtain a representative sample of stars with protoplanetary disks from different regions spanning a range of ages. In order to make a proper comparison, we have also chosen regions observed at similar wavelengths and spatial scales (see Table 1). Each of the disks included in this work belongs to the following 5 regions: Ophiuchus which is $\sim$ 1-2 Myr (Wilking et al. 2005; Luhman & Rieke 1999), hereafter Oph; the Taurus & Auriga Complex which is $\sim$ 1-3 Myr (Luhman 2004), hereafter Tau/Aur; Lupus which is $\sim$ 1-3 Myr (Comerón 2008; Alcalá et al. 2014); Chamaeleon I which is $\sim$ 2-3 Myr (Luhman et al. 2008), hereafter Cha I; and the Upper Scorpius OB association which is $\sim$ 5-11 Myr (Preibisch et al. 2002; Pecaut et al. 2012; Slesnick et al. 2008), hereafter USco.

We use previously published disk sizes for Oph and Tau/Aur with observations obtained by the Submillimeter Array (SMA; see Section 2.1 for more details), while we estimate sizes for disks in Lupus, Cha I, and USco from archival ALMA data (Section 2.2). Stellar masses are also derived homogeneously for the latter three regions after re-scaling literature stellar luminosities to the Gaia DR2 distances (Section 2.2.1).

2.1. Oph and Tau/Aur

We include in our analysis previously derived disk sizes for sources in the Oph and Tau/Aur star-forming regions (Tripathi et al. 2017), relying on the Gaia-updated values reported in Andrews et al. (2018a). From the entire sample of 50 disks we exclude TW Hya, HD 163296,

Table 1. Regions included in our analysis

Region	Telescope	λ	Typical Beam
		(μm)	(arcsec)
Oph	SMA	880	$0.41 - 0.78$
Tau/Aur	SMA	880	$0.41 - 0.78$
Lupus	ALMA	935-954	$0.28 - 0.35$
Cha I	ALMA	884-887	$0.5 - 0.7$
USco	ALMA	876-975	$0.35 - 0.75$

and LkHα 330 because they do not belong to Oph nor Tau/Aur.

Andrews et al. (2018a) derived disk sizes also for 56 sources belonging to the Lupus star-forming region, from ALMA observations originally presented in Ansdell et al. (2016). We use these literature values only to verify that our modeling approach delivers the same results (Section 2.2 and Appendix A.1) and justify the extended comparison of disk sizes carried out here. We note, however, that the Oph and Tau/Aur samples come from flux-limited SMA observations, and consequently are biased towards brighter objects than the Lupus, Cha I, and USco samples. We take this bias into account when interpreting the results.

2.2. *Lupus, Cha I, and USco*

To test if our approach for estimating disk sizes delivers the same results as Tripathi et al. (2017) and Andrews et al. (2018a), we re-reduce and re-analyze the ALMA data from the Lupus star-forming region. We include in our sample all the 62 detections from the ALMA project 2013.1.00220.S (PI: Johnathan Williams) as presented in Ansdell et al. (2016). As discussed in Appendix A.1 and shown in Figures 10 and 11, our method retrieves the same disk sizes as those in Andrews et al. (2018a) for most sources, as well as the same disk size-millimeter luminosity relation within the quoted uncertainties. Because the uncertainties reported in Andrews et al. (2018a) are systematically lower than ours (see Appendix A.1), we prefer to use the inferred disk sizes from our modeling in the analysis and discussion sections of this paper in order to have consistent uncertainties across all of our samples.

For the Cha I region, we include as part of our sample the 66 detections reported in Pascucci et al. (2016) from ALMA project 2013.1.00437.S (PI: Pascucci, I.). Five detections and nine non-detections from that project were re-observed at 5 times higher sensitivity in project 2015.1.00333.S (PI: Pascucci, I.). We use the 11 de-

tections reported in Long et al. (2018), giving us a total of 72 Cha I disks.

Finally, USco was observed in projects 2011.0.00526.S and 2013.1.00395.S (PI: Carpenter, J.) and results were originally presented in Carpenter et al. (2014) and Barenfeld et al. (2016) respectively. To estimate disk sizes we have selected those 50 USco targets that were detected.

2.2.1. *Stellar masses*

For Lupus, Cha I, and USco we also re-derive stellar masses in order to (a) have self-consistent values for the ALMA datasets, and (b) take advantage of the newer Gaia DR2 distances. Stellar masses are determined following the Bayesian inference approach described in Pascucci et al. (2016). First, we collect stellar effective temperatures and bolometric luminosities from the literature: For Lupus we rely on Alcalá et al. (2014); Biazzo et al. (2017); Frasca et al. (2017); Andrews et al. (2018a); For Cha I on Manara et al. (2016, 2017); while for USco we rely on Barenfeld et al. (2016). Then, we scale these luminosities to the new Gaia DR2 distances. For sources in Cha I and USco we query distances from the Bailer-Jones et al. (2018) Gaia catalogue. When there is no DR2 distance available, we use the median sample distance of 190 pc for Cha I and 144 pc for USco, both of which agree with the values obtained from all members of each region (see Roccatagliata et al. 2018 and de Zeeuw et al. 1999). For our Lupus sample, we take the GAIA DR2 distances as presented in Andrews et al. (2018a). J11072825-7652118 (Cha I) and J16141107-2305362 (USco) have anomalously large DR2 distances (744 pc, and 6011 pc respectively). For these three sources we also use the median distance of each region as given above. Following Pascucci et al. (2016), we assume an uncertainty of 0.02 dex in the stellar temperature for spectral types earlier than M3 and 0.01 dex for later spectral types and a 0.1 dex uncertainty on all stellar luminosities. Table 7 within Appendix B summarizes the adopted and inferred stellar parameters for Lupus, Cha I, and USco.

3. ALMA OBSERVATIONS AND DATA REDUCTION: LUPUS, CHA I AND USCO

We re-reduce band 7 ($\sim 880 - 975\mu$m) observations of similar sensitivity for the sample of disks presented in Section 2.2. The data reduction steps that lead to the calibrated visibilities are described below.

In general, the raw data is taken from the ALMA archive and measurement sets are built using the calibration scripts created by the North American ALMA Science Center (NAASC). For this step we use the same

version of the Common Astronomy Software Applications (CASA, McMullin et al. 2007) as used by the NAASC noted within the downloaded scripts. These scripts perform phase, bandpass and flux calibrations and create the standard CASA measurement sets containing the visibilities.

Because the 8 outermost edge channels in each spectral window are typically noisy, we remove them from our measurement sets. Next, we average the measurement sets in time and by channel. The parameters used to do time averaging and spectral window averaging are unique to each source with the goal of ending up with similarly sized (in number of data points) data sets. Typically, we average spectral windows by widths of 19 channels. We average our data in time by a variable number of seconds based on the total amount of data available to us (this varies by exposure time and number of baselines). However, we constrain all time averaging to be between 2 and 30 seconds. For these steps, we use `CASA` version `4.7.2-el6`.

Measurement sets from the project `2011.0.00526.S` (USco) were directly provided by the PI and co-author J. Carpenter. For these sources we used a width of 22 channels for the spectral window averaging.

Calibration of the sources in projects `2015.1.00333.S` (Cha I) and `2013.1.00395.S` (USco) were performed using `CASA` version `4.7.2-el6`. Calibration of the sources in science goal `A001_X11d_X13` (Cha I) and project `2013.1.00220.S` (Lupus) was performed using `CASA` version `5.1.1-5.el7`. These exceptions were required due to incompatibilities between the NAASC provided calibration scripts and system libraries.

In addition, for the 10 brightest Cha I disks[1], we use self-calibrated visibilities from Pascucci et al. (2016). The disk sizes resulting from self-calibrated visibilities are the same as those derived from non-self-calibrated visibilities, hence we do not apply self calibration to the other regions.

4. MODELING METHOD

In this section we describe our approach to model the calibrated continuum visibilities and our procedure for determining the dust disk outer radius ($R_{\rm eff}$). To expand upon the results presented in Tripathi et al. (2017) and Andrews et al. (2018a), we use a similar method to derive disk sizes for Lupus, ChaI and USco.

---

[1] These disks are: J10581677–7717170, J10590699–7701404, J11022491–7733357, J11040909–7627193, J11074366–7739411, J11080297–7738425, J11081509–7733531, J11092379–7623207, J11094742–7726290, and J11100010–7634578.

As high-contrast asymmetries seem to be uncommon even in high-resolution ALMA images (Long et al. 2018; Andrews et al. 2018b), we assume axisymmetric disks and use a parametric radial intensity profile to fit the disk intensity in the visibility domain.

For all modeling, we fit disk inclination (i), position angle (PA), and disk center offsets (dRA, dDec) in addition to the free parameters connected to the chosen radial profile function described below. All modeling also includes a *nuisance* parameter (lnwcorr) defined as the natural logarithm of the factor by which the weights of the observed visibilities are overestimated.

For all disks, we test two different functions for generating the radial profile shape: a Nuker profile (Lauer et al. 1995) and a Dirac delta function (point source). By comparing the best-fit models of each function (using the reduced χ^2) for a given source, we are able to determine if the disk is resolved (Nuker fits better) or not (point source fits better).

The Nuker profile was shown by Tripathi et al. (2017) to be a useful radial profile function thanks to its ability to reproduce the sky brightness of both full and transition disks. The radial intensity of a Nuker profile is expressed as:

$$I(r) = F_0 \left(\frac{r}{R_{\rm t}} \right)^{-\gamma} \left[1 + \left(\frac{r}{R_{\rm t}} \right)^{\alpha} \right]^{(\gamma - \beta)/\alpha} \quad (1)$$

where r is the radial distance, F_0 is the amplitude coefficient, $R_{\rm t}$ is the transition radius, α is the transition index, while γ and β are indexes that define the inner and outer cutoff, respectively. Figure 2 in Tripathi et al. (2017) nicely illustrates how each parameter affects the shape of the Nuker profile.

For a given profile (Nuker or point source), we produce a synthetic disk image which is Fourier transformed and sampled at the same spatial frequencies as our observational data using `GALARIO` (Tazzari et al. 2018). Our modeled visibilities are fit to the real and imaginary parts of the observed visibilities using the `emcee` implementation (Foreman-Mackey et al. 2013) of the Markov Chain Monte Carlo method (MCMC). Uniform priors are used over a parameter space defined as: $R_{\rm t} \in [0.005, 3]\,{\rm au}$, $\gamma \in [-11, 4]$, $\log \alpha [0.3, 1.3]$, $\beta \in [1, 17]$, $\log F_0 \in [3, 12]\,{\rm Jy/Sr}$, $i \in [0, 90]\,{\rm deg}$, PA $\in [0, 179]\,{\rm deg}$, dRA $\in [-3, 3]\,{\rm arcsec}$, dDec $\in [-3, 3]\,{\rm arcsec}$, lnwcorr $\in [-10, 10]$. We cover this parameter space with 70 chains (ensemble sample walkers) which individually take 100,000 steps in order to sample the posterior probability distribution function (PDF). The location of each walker is initialized using random draws from a truncated normal distribution about the median value for each parameters following an initial MCMC burn in cy-

cle using 100 walkers and 1000 steps. An example best fit model for the source J16085468-3937431, is given in Figures 1 and 2, all other fits are provided in the electronic version of this paper.

MCMC fitting produces a chain of models. We use the autocorrelation length as a guide to understand at what point in the chain convergence occurs. This typically happens well before 10^4 steps per walker, leaving us with approximately 6.99×10^6 samples per disk. We then conservatively ignore half of the converged chain length and only consider the 3.5×10^6 samples from the end of the MCMC chain to estimate the posterior probability density function (PDF), and parameter uncertainties.

The bounds of the parameter space explored by the MCMC walkers for the variables i, PA, dRA, dDec and lnwcorr is the same for all regions. The remaining free parameters explored is determined by the radial profile being modeld (Nuker or point-source). For these parameters, the bounds are adjusted for each star-forming region based on prior exploration of the parameter space to ensure no truncation of the posterior distributions. The boundaries we chose are similar to those in Tripathi et al. (2017) and Andrews et al. (2018b), and are chosen to cover well the posterior distribution.

At this point it is important to point out that the physical parameter we are interested in, disk size, is not one of the free parameters being fit, and additionally, the Nuker profile has no distinct outer edge. To deal with these two issues and following Tripathi et al. (2017), we estimate the *effective radius* ($R_{\rm eff}$), the radius at which a given fraction (x) of the cumulative flux is contained. Here, we compute two $R_{\rm eff}$: R_{68}, the radius containing 68% of the flux, to connect our results to the low- and medium-resolution disk surveys (Tripathi et al. 2017; Andrews et al. 2018a); and R_{90}, the radius containing 90% of the flux. The latter is done primarily to test how well low- and medium-resolution surveys recover disk radii obtained via high-resolution ALMA surveys (Long et al. 2018; Huang et al. 2018), although we also find it useful when comparing our disk sizes with dynamical features in the Solar System (see Section 6.2).

We randomly sample 5000 models from the second half of our MCMC chain, and for each model we calculate $R_{\rm eff}$. This gives us a posterior distribution of disk sizes. We take the median value to be our $R_{\rm eff}$ estimate, and quantiles of 16 and 84% as our upper and lower confidence intervals.

In order to determine wheter the observations resolve the source or not, we independently fit and test models created by both a Nuker profile (resolved) and a point source (unresolved) for each observation. The reduced chi-square statistic of the best Nuker profile and best point source model are compared. In cases where the point-source results in a better fit, we determine that the source is unresolved. To compute the upper-limit on the size of unresolved sources, we take the results of the Nuker model, and use the 84th percentile $R_{\rm eff}$ (what would be the upper confidence interval on a resolved source) as the $R_{\rm eff}$ upper limit. We expect that these disks are most likely limited by the resolution of the telescope, but take this conservative approach in order to not misinterpret disks that are large and faint (sensitivity limited).

Occasionally we notice walkers stuck within local minima of our posteriors. This appears to happen in less than 15% of our sources. Because not all of these stuck walkers are identifiable by eye, we make no attempt to remove them in order to safeguard against introducing systematic errors. However, we measured the impact of stuck walkers on several sources and found that the decision to leave the chains unaltered ultimately results in small changes, and slightly larger errors, in our $R_{\rm eff}$ estimates. For example, an estimation of R_{68} for J16000236-4222145 with, and without stuck walkers results in values of $81.67^{+1.97}_{-2.95}$ and $85.28^{+2.62}_{-2.30}$ arcsec respectively.

4.1. *Subsample of systems with estimated disk sizes*

While we have modeled all of the detected sources within the Lupus, Cha I, and USco regions, we do not use every source in the remainder of our analysis.

Unless otherwise noted, we have removed from our sample, disks around multiple star systems with separations ≤ 2.0" in order to make our sample consistent with those in Tripathi et al. (2017) and Andrews et al. (2018a). These papers imposed the separation threshold to exclude disks that might have their sizes truncated by dynamical interactions with their companions (see, e.g. Manara et al. 2019). However, we do not impose a flux cutoff of 2 mJy as in Andrews et al. (2018a).

Additionally, we find 15 disks with best-fit models that we do not trust, hence we remove them from our analysis. The details and further discussion of the excluded models is given in Appendix C. This leaves us with 152 disks: 50 from Lupus, 58 from Cha I and 44 from USco which we include in our analysis.

To better determine if our final disk samples are representative, or biased (being a subset of each region's complete disk population), we attempt to reproduce previously reported disk-host ($\log M_{\rm dust} - \log M_\star$) relationships with our subset of disks (using the equivalent $\log L_{\rm mm} - \log M_\star$ relationship). With the exception of Oph, this relationship has been quantified in Ansdell et al. (2016) and Pascucci et al. (2016), and we use the fitting slopes reported in Pascucci et al. (2016) for our
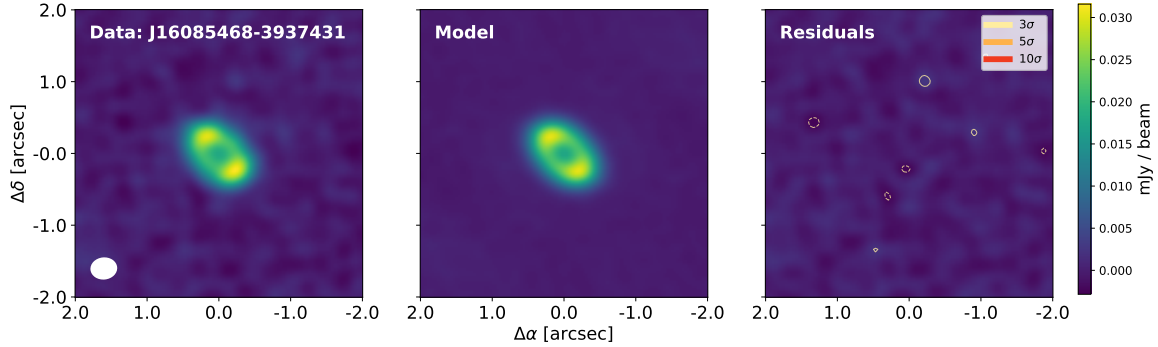
Figure 1. Comparison of the ALMA 887 μm observation of J16085468-3937431 with our best-fit model. The first panel shows the ALMA observation as a continuum map generated using the CASA `clean` command with Briggs weighting with a robustness parameter of 0.5. The middle panel shows a continuum map generated from our model using the same UV spacings as the ALMA observation. The last panel shows the residuals between the first two panels (residuals of 3, 5, and 10 sigma are denoted as outlines).
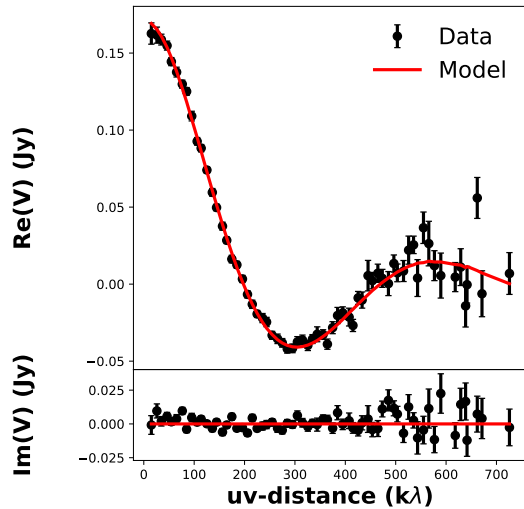

Figure 2. A comparison of our model with the observed visibilities for the source J16085468-3937431. The real and imaginary components of the observed visibilities (filled circles) are azimuthally averaged and deprojected. For the clarity of the figure, the visibility data is further binned in increments of 10kλ. Our best-fit (Nuker profile) model is plotted in red. Plot made with the UVPLOT package (Tazzari 2017).

(see Section 4 in Pascucci et al. 2016). The results of our modeling for individual sources is given in Table 10.

Appendix E shows that R_{90} and R_{68} are strongly correlated and we derive an equation to convert R_{68} into R_{90} based on our modeling of the Lupus, Cha I and USco disks. Additionally, we compare in Appendix A.2 disk radii obtained here from those obtained at high-resolution for 26 sources and demonstrate that these lower resolution surveys are sufficient to determine dust disk sizes.

comparison given that stellar masses in this paper are estimated in the same way. In those works, a larger sample size for each region (than we use here) is included in the analysis because they are able to include flux density non-detections. We find that for our subset of disks in each region, $\log L_{\mathrm{mm}} - \log M_\star$ is correlated for Lupus, Cha I and USco, and is not correlated for the regions Oph and Tau/Aur (see Appendix D; Figure D and Table 8). For the regions with correlations (Lupus, Cha I and USco) we find consistently shallower slopes as it is expected from samples lacking the faintest disks
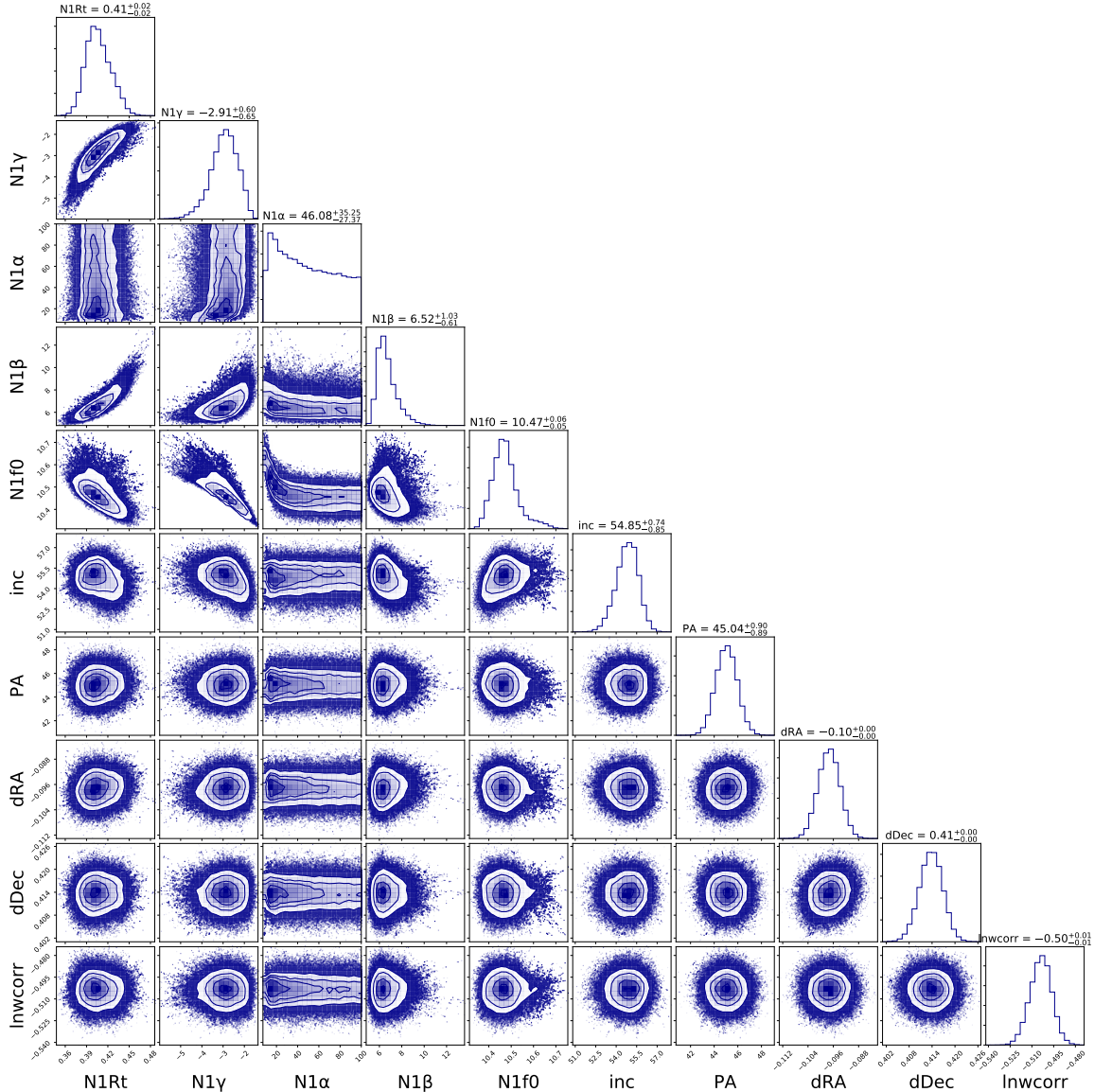
Figure 3. Corner plot of the free parameters generated from the MCMC fitting of J16085468-3937431. Marginalized distributions are shown as histograms at the top of each column. Parameters with names preceded by "N1" refer to the corresponding Nuker parameters (see Equation 1). Parameters used to deproject and center the disk are inclination (inc), position angle (PA), right ascension offset (dRA), and declination offset (dDec). The last column is the fitted weight correction factor (lnwcorr; see Section 4).

5. RESULTS

We present a census of 199 homogeneously derived dust-disk sizes from five star-forming regions and associations. In this paper, we estimate the sizes of 152 disks: 50 from Lupus, 58 from Cha I and 44 from USco. Of the 152 disks we model, we find 85 to be resolved, and 67 to be unresolved. Of the unresolved disks, 20 are in Lupus, 25 in Cha I and 22 in USco[2]. To this we add

the literature values for 20 Oph disks and 27 Tau/Aur disks; these disk size estimations were originally modeled in Tripathi et al. (2017) but we use the updated values reported in Andrews et al. (2018a).

Table 2 summarizes the median and maximum R_{68} and R_{90} sizes of resolved disks within each region. Both interpretations of $R_{\rm eff}$ are useful to consider. R_{68} is necessary in order to compare all 5 regions, since only R_{68} sizes are available for Oph and Tau/Aur. Consequently, the majority of our analysis uses R_{68} as a proxy for $R_{\rm eff}$. However, R_{90} better approximates the full extent of the

---

[2] The modeling results of individual sources are given in Appendix F

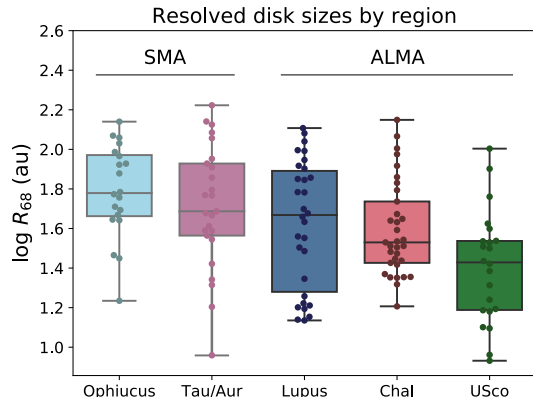disk, and we find it useful to consider in the discussion (Section 6).

Figure 4. Swarmplots for resolved disks in different regions, ordered by age. The boxplots include a shaded region surrounding the R_{68} 25-75% quartiles, the horizontal line denotes the median disk size, while whiskers define the 0-25% and 75-100% quartiles. The regions observed with the SMA are greyed out because they are biased to the brightest millimeter disks, hence their size distributions should not be directly compared to the regions observed by ALMA.

A comparison of the size distribution for each region is shown in Figure 4. Individual resolved disks within each region are shown as swarmplots with a shaded box surrounding the distribution's 25-75% quartiles and a horizontal line denoting the median disk size. Whiskers extend from the shaded boxes defining the 0-25% and 75-100% quartiles. While it may be tempting to infer a trend of decreasing disk size with age, it is important to recall that the Oph and Tau/Aur samples are biased towards higher luminosity disks, and therefore, a direct comparison of size distributions, in particular of the minimum and median size, between the SMA and ALMA samples is unjustified. The largest disks, being also among the brightest (see Section 5.1), are the least affected by the bias mentioned above, as well as by differences in survey sensitivity and spatial resolution. Table 2 and Figure 4 show that all regions, except USco, have multiple disks with R_{68} greater than 115 au (while USco has only one disk with R_{68} larger than 80 au), hinting that USco disks are smaller than those in other regions. This is in agreement with Barenfeld et al. (2017) who used a different approach to determine USco disk sizes[3] and concluded that that they are ~ 3 times smaller than those in Oph, Tau/Aur and

the subset of the Lupus disks modelled by Tazzari et al. (2017).

Table 2. Summary statistics for resolved disks

region	count	R_{68} (au)		R_{90} (au)	
		median	max	median	max
Oph	20	60.1	138.0	...	...
Tau/Aur	25	48.6	167.0	...	...
Lupus	30	46.6	128.1	63.2	213.1
Cha I	33	33.9	140.9	43.1	231.3
USco	22	26.8	100.8	33.4	126.2

NOTE— Oph and Tau/Aur R_{68} values are from Andrews et al. (2018a).
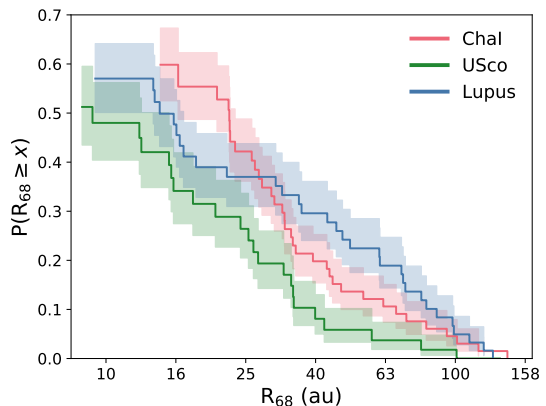
Figure 5. Cumulative disk sizes distributions for our modeled regions: Lupus, Cha I and USco. Shaded regions indicate 1σ confidence intervals.

To further examine if there is a difference in the observed distributions of the now homogeneously-derived disk sizes, we focus on the three ALMA regions observed with similar sensitivity and spatial resolution (Lupus, Cha I and USco) and show the R_{68} cumulative distribution functions (CDF) in Figure 5. Uncertainties on the CDF are determined using the Kaplan-Meier estimator[4] and include unresolved disks with upper limits. However, the CDF uncertainties do not consider our disk size uncertainties. There are two features in Figure 5 that are worth noting. First, there is a deficit of large disks in USco when compared to Lupus and Cha I. Second, all regions host small disks (as small as ~ 15 au), and

---

[3] Barenfeld et al. (2017) fit power-law models to the dust surface density and carry out continuum radiative transfer calculations to compute the surface brightness and visibilities.

[4] We use the Python lifelines (Davidson-Pilon et al. 2019) Kaplan-Meier implementation.

USco in particular appears to have a population of even smaller disks. However, the smaller end of the disk-size distributions are impacted by the source distance combined with the chosen beam size and sensitivity. For this reason we make no inferences regarding the smallest disks.

In order to test if two regions are drawn from the same empirical distribution function, we compare each region with every other using the Anderson-Darling test (Anderson & Darling 1952). We report the Anderson-Darling statistic and significance level (sig.) in Table 3. The significance level is the level at which we cannot reject the null hypothesis that the samples are drawn from the same distribution. The small values of 0.013 and 0.014 suggest that the USco sample is unlikely to be drawn from the same parent disk-size distribution of Lupus and Cha I, respectively. With a significance level of 0.1 we are not able to determine if Lupus and Cha I are drawn from differing distributions or not with any high degree of confidence. Oph and Tau/Aur, with their similarly biased samples have a significance level $> 25\%$, suggesting that there is no difference in the distribution from which the two regions' brightest disks are drawn.

To test if these results depend on the selection of R_{68} or R_{90}, we produced a R_{90} version of Figure 5, and performed the Anderson-Darling tests on Lupus, Cha I and USco using our R_{90} disk sizes and found no significant change in the observed trends.

Table 3. Comparison of R_{68} size distributions

R_{68} Distributions		Anderson-Darling	
Region 1	Region 2	stat	sig.[a]
USco	Cha I	3.4	0.014
USco	Lupus	3.4	0.013
Cha I	Lupus	1.2	0.105
Lupus	Oph	1.2	0.104
Tau/Aur	Oph	-0.2	> 0.25

[a]sig., also known as the error rate, indicates the significance level at which the null hypothesis that samples are drawn from the same distribution cannot be rejected.

5.1. *Relations between stellar and disk properties*

The following two subsections examine the disk size-disk luminosity ($\log R_{\mathrm{eff}} - \log L_{\mathrm{mm}}$) and the disk size-stellar properties ($\log R_{\mathrm{eff}} - \log M_\star$ and $\log R_{\mathrm{eff}} - \log L_\star$) relations. In order to determine if empirical relation-ships can be established, we apply several statistical tests to the data.

We begin with the Shapiro−Wilk normality test (Shapiro & Wilk 1965) to determine if the distribution of our bivariate data is normal or not. This is important as many correlation tests, e.g. the Pearson's r test, are based on the assumption that the data follow a normal distribution. The Shapiro−Wilk p-value is the null hypothesis probability that the sample is normally distributed. In cases where the p-value is < 0.05 we reject the null hypothesis and conclude that the distribution is not normal. Otherwise, we conclude that the distribution is likely normal. The result of this determines which correlation test we use afterward and is described in further detail below.

For all regions we calculate both the Pearson correlation coefficient (hereafter Pearson r test) and Spearman's rank correlation coefficient (hereafter Spearman ρ test) and the corresponding p-values. For both tests, the p-value gives the probability of rejecting the null hypothesis that there is no statistically significant relationship between the variables, more specifically a linear relation for the Pearson's r test and a monotonic one for the Spearman ρ test. In cases where the p-value for the chosen statistic is < 0.05 we consider the data to be correlated. As mentioned above, the Pearson's r test requires the data to be bivariate normal. For this reason, we use the Pearson's r test to establish if there is a linear correlation only when our data are normally distributed, as found by the Shapiro−Wilk test. In all other cases, we rely on the Spearman ρ to test for the existence of a monotonic relationship between variables. Note that while the Spearman ρ does not need the variables to be normally distributed, it does require that they are converted into a rank-order (ordinal) data set.

A limitation of all these statistical tests is that they do not include upper-limits and uncertainties in the assessment. As such, and for comparison with results already reported in the literature, we might fit linear relationships even if our correlation tests result in a probability larger than 0.05 that the variables are not correlated.

5.1.1. *Disk radii and millimeter luminosities*

Recently, Andrews et al. (2018a) demonstrated that the dust disk effective radius (R_{eff}) and the millimeter luminosity (L_{mm}) scale in the same way for their Oph, Tau/Aur, and Lupus samples as $R_{\mathrm{eff}} \propto L_{\mathrm{mm}}^{0.5}$. Thus, one might infer that such a relationship is universal and apply to all star-forming regions. Here, we demonstrate that this is not the case and that the $\log R_{\mathrm{eff}} - \log L_{\mathrm{mm}}$ slope flattens moving from the younger to the older star-forming regions.
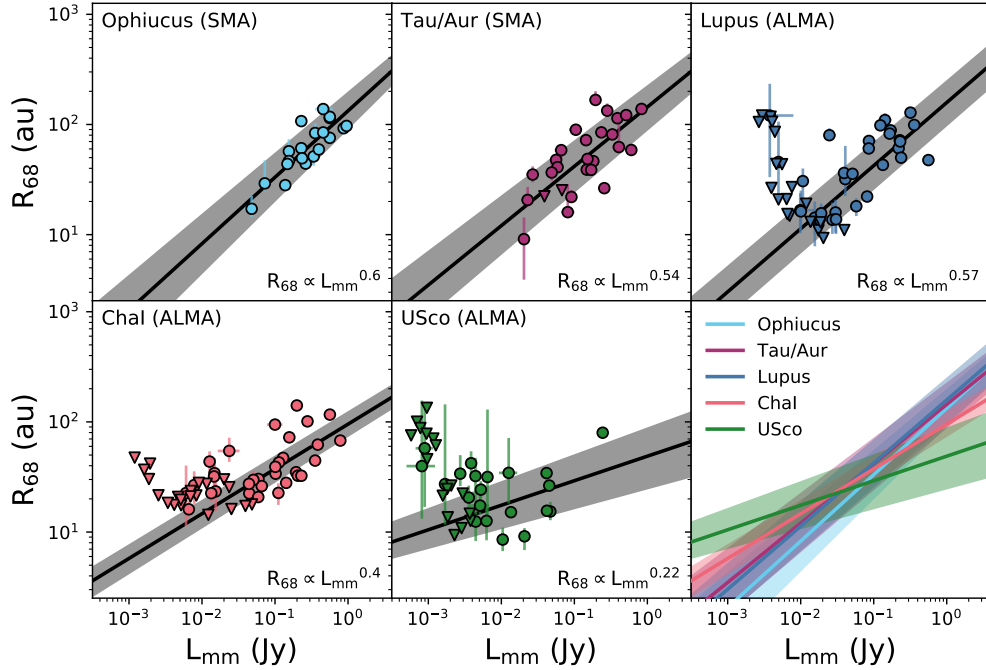
Figure 6. Fitting of $\log R_{\mathrm{eff}} - \log L_{\mathrm{mm}}$. The first 5 panels (left to right; top to bottom; ordered by region age) show the model results of each region as circles (resolved) and triangles (upper-limits). The best fit from MCMC linear regression is plotted as a black line, and surrounded by our 68% confidence intervals in grey. The last panel replots the bests fits of each region (and the corresponding 68% confidence intervals) so that they can be directly compared. Fit parameters for each region are given in Table 4.

Table 4. $\log R_{68} - \log L_{\mathrm{mm}}$ Statistical tests

Region	Shapiro L_{mm} stat	p-value	Shapiro R_{eff} stat	p-value	Pearson r stat	p-value	Spearman ρ stat	p-value	Regression Parameters α	β	σ	$\hat{\rho}$
Oph	0.91	5.7e-02	0.96	5.9e-01	0.67	1.3e-03	0.75	1.4e-04	$2.11^{+0.06}_{-0.06}$	$0.60^{+0.11}_{-0.11}$	$0.14^{+0.03}_{-0.02}$	$0.92^{+0.04}_{-0.06}$
Tau/Aur	0.84	9.9e-04	0.91	3.4e-02	0.59	2.0e-03	0.70	1.0e-04	$2.16^{+0.11}_{-0.11}$	$0.53^{+0.12}_{-0.12}$	$0.24^{+0.05}_{-0.04}$	$0.86^{+0.05}_{-0.08}$
Lupus	0.81	8.8e-05	0.91	1.9e-02	0.44	1.4e-02	0.55	1.8e-03	$2.20^{+0.14}_{-0.13}$	$0.57^{+0.10}_{-0.10}$	$0.30^{+0.06}_{-0.05}$	$0.88^{+0.04}_{-0.05}$
Cha I	0.75	4.5e-06	0.77	1.3e-05	0.53	1.7e-03	0.64	7.7e-05	$1.97^{+0.08}_{-0.08}$	$0.40^{+0.06}_{-0.06}$	$0.21^{+0.03}_{-0.03}$	$0.90^{+0.03}_{-0.04}$
USco	0.45	7.7e-08	0.87	1.0e-02	0.60	4.1e-03	-0.27	2.4e-01	$1.68^{+0.23}_{-0.22}$	$0.22^{+0.11}_{-0.10}$	$0.28^{+0.07}_{-0.05}$	$0.67^{+0.12}_{-0.18}$

NOTE—Values we consider unreliable are greyed out (see Section 5.1).

Figure 6 shows the inferred disk sizes (circles) or upper limits (downward triangles) as a function of L_{mm}. Values for Oph and Tau/Aur are from Andrews et al. (2018a) while for the other three regions are from this work (see Sections 2.1 and 2.2). For all regions, we see the general trend of larger disk sizes for brighter disks, although USco covers a smaller range in L_{mm} than other regions and the scatter is large. Indeed, when we apply the non-parametric Spearman's rank correlation test to

the disks with a measured dust radius (circles), we find positive values (R_{eff} increases with L_{mm}) and probabilities (p-value) lower than 5% that the two quantities are uncorrelated in all regions except USco (see Table 4).

Next, following Andrews et al. (2018a), we fit the $\log R_{\mathrm{eff}} - \log L_{\mathrm{mm}}$ relation in each individual region taking into account measured R_{eff}, the associated uncertainties, as well as upper limits in R_{eff}. For this task we use the Bayesian method of linear regression described

in Kelly (2007) (as implemented in the `linmix` code by Joshua E. Meyers) and specifically fit the following linear relation:

$$\log R_{\mathrm{eff}} = \alpha + \beta \log L_{\mathrm{mm}} \qquad (2)$$

where α and β are the intercept and the slope, respectively. The best fit parameters for each region, together with the scatter of the relation (σ) and the correlation coefficient ($\hat{\rho}$), are reported in Table 4.

We find that $\hat{\rho}$, which is estimated accounting for uncertainties and upper limits (but assumes bivariate-normal data), is positive and larger than the Spearman ρ correlation coefficient in all regions. This may be particularly important for USco, where the Spearman ρ coefficient of -0.27 and large p-value suggest no $\log R_{\mathrm{eff}} - \log L_{\mathrm{mm}}$ correlation for sources with measured disk sizes, while the `linmix` $\hat{\rho}$ value of 0.67 points to a positive correlation, albeit less strong than in the other younger star-forming regions. The first five panels of Figure 6 visualize the best fit for each region with the grey shadowing highlighting the 68% confidence intervals. The sixth panel of Figure 6 summarizes the results and emphasizes the main finding of our analysis that the $\log R_{\mathrm{eff}} - \log L_{\mathrm{mm}}$ relation is not universal.

We do not perform a fitting for the combined sample of all regions due to differences in the estimated disk size uncertainties between the SMA and the ALMA samples and our finding that not all regions share the same $\log R_{\mathrm{eff}} - \log L_{\mathrm{mm}}$ relation.

5.1.2. *Disk radii and stellar properties*

Several works have pointed out that L_{mm}, which (if optically thin) probes the dust disk mass, is positively correlated with stellar properties like stellar bolometric luminosity ($L_\star$) and stellar mass ($M_\star$) in most star-forming regions, (e.g., Andrews et al. 2013; Ansdell et al. 2016; Pascucci et al. 2016). However, the relationship between R_{eff} and these same stellar properties has been less explored. Andrews et al. (2018a) find $\log R_{\mathrm{eff}} - \log M_\star$ and $\log R_{\mathrm{eff}} - \log L_\star$ to be correlated ($R_{\mathrm{eff}} \propto M_\star{}^{0.6} \propto L_\star{}^{0.3}$) for the combined Tau/Aur and Lupus samples but to a lesser degree than $\log R_{\mathrm{eff}} - \log L_{\mathrm{mm}}$. In this section we investigate whether such relations are present in individual regions.

Figures 7 and 8 show the inferred disk sizes (circles) or upper limits (downward triangles) as a function of $M_\star$ and $L_\star$, respectively. Tables 5 and 6 report the statistical tests described in Section 5.1 as well as the `linmix` best fit parameters and correlation coefficient $\hat{\rho}$. For the two regions that are most biased to bright millimeter disks (Oph and Tau/Aur), we can confidently

conclude that there is no correlation in $\log R_{\mathrm{eff}} - \log M_\star$ nor in $\log R_{\mathrm{eff}} - \log L_\star$.

The three remaining regions (Lupus, Cha I, and USco) have Spearman ρ correlation coefficients (0.29-0.34) and p-values (0.07-0.20) where we can not completely rule out a weak or marginal correlation between R_{eff} and $M_\star$, but correlations are not strongly supported.

Interestingly, for Cha I, which covers the largest range in $L_\star$, we can rule out a $\log R_{\mathrm{eff}} - \log L_\star$ correlation with a high level of confidence (correlation coefficient=0.17 and p-value=0.35).

The situation is different for USco where we can not rule out a weak $\log R_{\mathrm{eff}} - \log L_\star$ relation, the Spearman ρ correlation coefficient is 0.29 with a p-value of 0.19 and $\hat{\rho}$ is 0.72.

Finally, the Lupus region appears to have some degree of correlation in $\log R_{\mathrm{eff}} - \log L_\star$, but likely not in $\log R_{\mathrm{eff}} - \log M_\star$. When we combine the Oph, Tau/Aur, and Lupus samples and refit the $\log R_{\mathrm{eff}} - \log M_\star$ relation with `linmix` we find $\hat{\rho} = 0.63^{+0.07}_{-0.09}$, the same as for Lupus. Thus, we conclude that the weak $\log R_{\mathrm{eff}} - \log M_\star$ correlation reported by Andrews et al. (2018a) for the SMA+ALMA samples (mostly Oph, Tau/Aur, and Lupus) with a coefficient of $\hat{\rho} = 0.54$ is mostly driven by the Lupus sample. Similarly, when we combine Oph, Tau/Aur, and Lupus samples and refit the $\log R_{\mathrm{eff}} - \log L_\star$ relation, we find a coefficient of $\hat{\rho} = 0.64^{+0.07}_{-0.09}$, consistent with the findings in Andrews et al. (2018a) for the same joint sample.
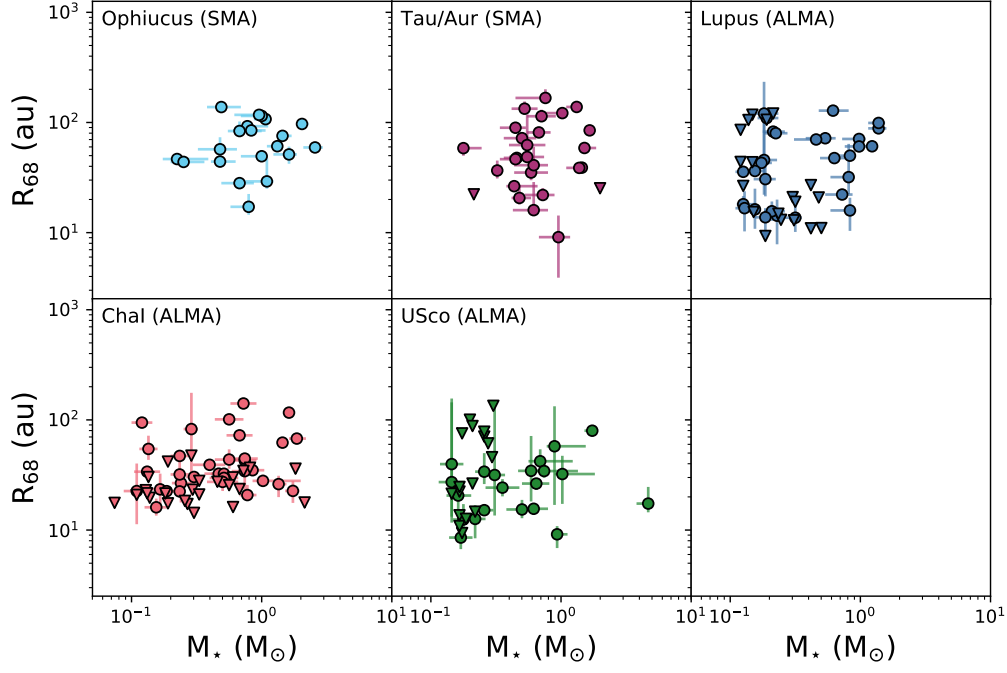
Figure 7. Fitting of $\log R_{\mathrm{eff}} - \log M_\star$. The first 5 panels (left to right; top to bottom; ordered by region age) show the model results of each region as circles (resolved) and triangles (upper-limits).

Table 5. $\log R_{68} - \log M_\star$ statistical tests

	Shapiro $M_\star$		Shapiro R_{eff}		Pearson r		Spearman ρ		Regression Parameters			
Region	stat	p-value	stat	p-value	stat	p-value	stat	p-value	α	β	σ	$\hat{\rho}$
Oph	0.91	6.7e-02	0.96	5.9e-01	0.08	7.2e-01	0.24	3.2e-01	$1.81^{+0.06}_{-0.06}$	$0.20^{+0.25}_{-0.24}$	$0.24^{+0.05}_{-0.04}$	$0.47^{+0.22}_{-0.11}$
Tau/Aur	0.87	3.7e-03	0.91	3.4e-02	0.16	4.3e-01	0.18	3.8e-01	$1.71^{+0.08}_{-0.09}$	$0.18^{+0.30}_{-0.29}$	$0.34^{+0.07}_{-0.05}$	$0.38^{+0.23}_{-0.10}$
Lupus	0.82	2.3e-04	0.91	1.6e-02	0.31	1.0e-01	0.34	7.2e-02	$1.66^{+0.13}_{-0.13}$	$0.57^{+0.23}_{-0.22}$	$0.43^{+0.08}_{-0.06}$	$0.62^{+0.10}_{-0.14}$
Cha I	0.85	4.0e-04	0.80	2.7e-05	0.23	2.0e-01	0.23	2.0e-01	$1.50^{+0.07}_{-0.08}$	$0.31^{+0.14}_{-0.14}$	$0.33^{+0.06}_{-0.04}$	$0.58^{+0.11}_{-0.15}$
USco	0.56	7.4e-07	0.87	1.0e-02	0.13	5.8e-01	0.29	1.9e-01	$1.41^{+0.08}_{-0.08}$	$0.47^{+0.16}_{-0.15}$	$0.26^{+0.06}_{-0.05}$	$0.72^{+0.09}_{-0.13}$

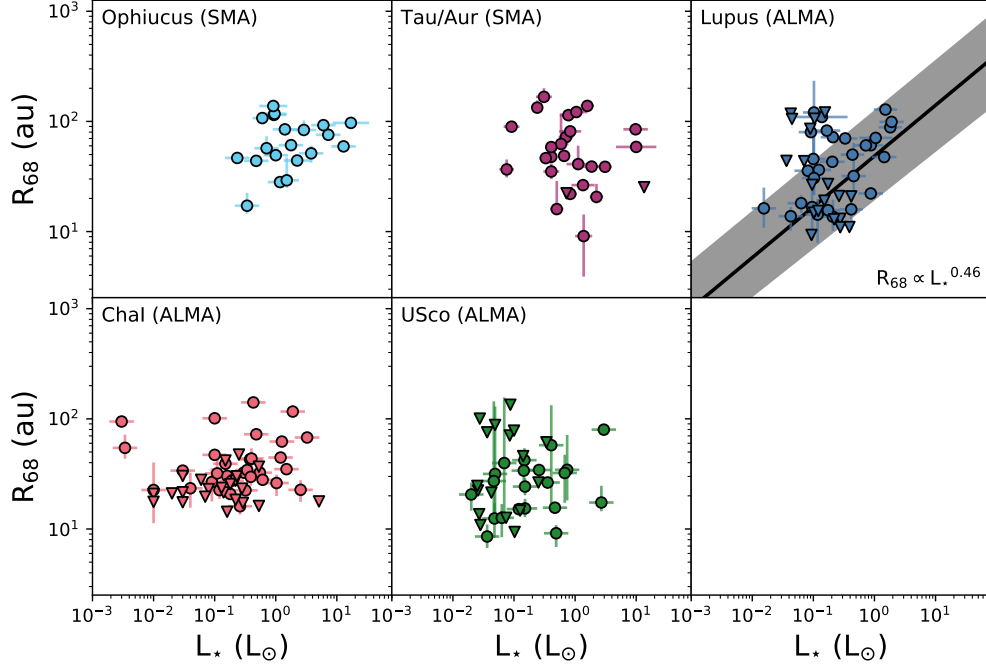NOTE—Values we consider unreliable are greyed out (see Section 5.1).

Figure 8. Fitting of $\log R_{\rm eff} - \log L_\star$. The first 5 panels (left to right; top to bottom; ordered by region age) show the model results of each region as circles (resolved) and triangles (upper-limits).

Table 6. $\log R_{68} - \log L_\star$ statistical tests

| Region | Shapiro $L_\star$ | | Shapiro $R_{\rm eff}$ | | Pearson r | | Spearman ρ | | Regression Parameters | | | |
	stat	p-value	stat	p-value	stat	p-value	stat	p-value	α	β	σ	$\hat{\rho}$
Oph	0.66	1.3e-05	0.96	5.9e-01	0.15	5.4e-01	0.17	4.6e-01	$1.77^{+0.06}_{-0.06}$	$0.14^{+0.13}_{-0.13}$	$0.24^{+0.05}_{-0.04}$	$0.54^{+0.19}_{-0.38}$
Tau/Aur	0.54	9.5e-08	0.91	3.4e-02	-0.02	9.3e-01	-0.18	3.9e-01	$1.67^{+0.07}_{-0.07}$	$-0.15^{+0.13}_{-0.14}$	$0.33^{+0.06}_{-0.05}$	nan^{+nan}_{-nan}
Lupus	0.75	1.4e-05	0.91	1.6e-02	0.45	1.4e-02	0.42	2.3e-02	$1.68^{+0.13}_{-0.13}$	$0.46^{+0.17}_{-0.16}$	$0.41^{+0.08}_{-0.06}$	$0.67^{+0.10}_{-0.13}$
Cha I	0.71	1.2e-06	0.77	1.3e-05	0.18	3.2e-01	0.17	3.5e-01	$1.45^{+0.08}_{-0.09}$	$0.10^{+0.09}_{-0.08}$	$0.36^{+0.06}_{-0.05}$	$0.45^{+0.15}_{-0.24}$
USco	0.57	8.9e-07	0.87	1.0e-02	0.45	3.9e-02	0.35	1.2e-01	$1.49^{+0.10}_{-0.10}$	$0.33^{+0.11}_{-0.10}$	$0.25^{+0.06}_{-0.05}$	$0.77^{+0.08}_{-0.12}$

NOTE—Values we consider unreliable are greyed out (see Section 5.1), including the result of *nan* which denotes a value below the floating point precision of our analysis.

6. DISCUSSION

In the following sections we compare the size distributions found in each region (Section 6.1), define and compare our inferred disk sizes with the outer edge of the Solar System (Section 6.2), and discuss disk-disk and disk-host scaling relations (Section 6.3).

6.1. *Comparison between regions*

In Section 5 we use several statistical approaches to assess how similar, or different, the distributions of disk sizes are in our sample regions.

When compared to other regions USco lacks large dust disks. The vast majority ($\geq 75\%$) of resolved disks within USco have sizes that fall below the Lupus and Cha I median disk sizes. Barenfeld et al. (2017) compared their USco disk sizes with the inhomogeneously derived sizes of Oph, Tau/Aur and Lupus [5] and concluded that USco disks are three times smaller. We also find that the typical disk in USco is smaller than the typical disk in Lupus or Cha I. However, the difference is not as great: the median disk size in USco is 1.7 times smaller than that in Lupus and 1.3 times smaller than that in Cha I. We believe that the difference between our results and Barenfeld et al. (2017) is due to the fact that the latter has used inhomogeneous disk size estimations as well as samples biased to the brightest disks in Oph, Tau/Aur, and Lupus. Because the disks from Oph and Tau/Aur are biased towards only the brightest disks, the only conclusion we can make is that USco lacks the large disks seen in both of those regions. The decrease in median disk size from the younger Lupus and Cha I to the older USco may be interpreted as an evolution of the disk outer edge caused by e.g. efficient inward drift of millimeter grains (Pinilla et al. 2013; Krijt et al. 2015; Pascucci et al. 2016); growth of millimeter grains into planetesimals (Barenfeld et al. 2017; Gerbig et al. 2019; Lenz et al. 2019); or external photoevaporation in the higher UV field of the USco OB association (Facchini et al. 2016; Barenfeld et al. 2017). Measuring gas disk sizes in these three regions should help to discriminate between internal vs external processes.

Eisner et al. (2018) reported that the population of disk sizes within Cha I was significantly smaller than that of disks in the younger regions of Oph, Tau/Aur, and Lupus. However, we do not arrive at the same conclusion. As previously mentioned, we find that Cha I

---

[5] The comparison by Barenfeld et al. (2017) made use of Lupus dust-disk sizes from Tazzari et al. (2018) which considered a sample that excluded edge-on disks, disks with sub-structures and disks with mm-flux < 4mJy, resulting in ~50% of the objects modelled in Andrews et al. (2018a) or this work.

disks are not significantly smaller than Lupus, and span a similar range in disk sizes. Cha I, when compared to Lupus in Figure 5, hints at a enhanced population of disks between 15 and 25 au, and a decreased population of disks between 30 and 65 au.

The differing result from Eisner et al. (2018) is likely due to several factors. First, their work compares inhomogeneously estimated disk sizes, e.g. FWHMs from Pascucci et al. (2016) for Cha I with exponential cutoff radii of a power-law disk from Tazzari et al. (2017) for Lupus. Second, the entire Cha I disk population is compared with luminosity biased samples in Oph, Tau/Aur, and even Lupus (only the sub-sample in Tazzari et al. (2017) was available at that time). Lastly, the cumulative disk-size distributions used for comparison in Eisner et al. (2018) are not consistently constructed, leading to a different definition for what a probability of unity means in each region. For instance, the Cha I sample appears to include all sources that were targeted in Pascucci et al. (2016), whether they were detected or not, the USco sample includes only resolved sources, while the Lupus sample appears to include detected sources, whether they were resolved or not.

6.2. *The outer edge of the Solar System*

Stellar encounters (e.g. Ida et al. 2000; Kenyon & Bromley 2004) and external photoevaporation by massive stars within a star cluster (e.g. Adams et al. 2004) have been suggested as mechanisms connected to the formation of the Solar System's outer edge. In this section we look into whether or not our results can test these models which utilize edge truncation to explain the size of the Solar System.

The region of the Solar System beyond Neptune (the trans-Neptune region or Edgeworth–Kuiper belt) is populated with icy bodies (TNOs) which fall into distinct classes based on their dynamical properties. There is a decrease in the population of TNOs beyond 48 au, and the population of objects with nearly circular orbits effectively ends at 45 au (e.g. Petit et al. 2011). This *outer edge* of the Kuiper belt appears well defined and is not an observational bias (Allen et al. 2001; Morbidelli et al. 2008). Because the region beyond this edge is dynamically stable on timescales longer than the Solar System's lifetime (Duncan et al. 1995), a primordial population of planetesimals beyond 45 au – had it existed – should have been retained.

Determining if the outer edge of the Solar System's primordial planetesimal disk was located at, beyond, or interior to the present Kuiper belt's edge would test hypotheses which evoke an outer-edge modifying event. This work does not directly probe the history of the
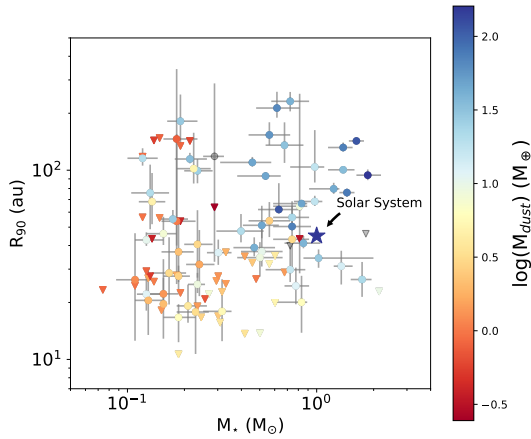
Figure 9. The R_{90} sizes and dust masses for disks in the 1-3 and 2-3 Myr old Lupus and Cha I star-forming regions are plotted along with the Solar System in order to determine if the Solar System (denoted in the figure with a star) should be considered *typical*, or a statistical outlier. Disks with constrained size estimates are shown as circles, and upper limits with triangles. The color of each symbol (including the Solar System) corresponds to the dust mass.

Solar System. However, if we take the location of dust observed in our disks to be an indicator of the location of planetesimals (or planetesimal formation), and if we interpret the outer edge at 45-48 au to be primordial, we can compare the Solar System's outer edge with our inferred disk sizes. It is important to be aware that this comparison is between the location of dust emission in 1-3 Myr old disks and the location of a dynamical and occurrence-rate feature found within a distribution of 4.5 Gyr old planetesimals. The validity of this comparison ultimately relies on whether or not the Solar System's outer-edge is a feature inherited from its proto-planetary disk.

While stellar encounters and external photoevaporation by massive stars may impact disk sizes in high-mass star-forming regions, these two mechanisms are most likely not affecting the disk sizes in Lupus and Cha I. Winter et al. (2018) compared the effect of external photoevaporation and close stellar encounters on disk sizes in typical cluster environments and concluded that tidal truncation due to stellar encounters are unlikely. They find that significant truncation due to stellar encounters requires a cluster stellar density of $5 \times 10^4 \text{pc}^{-3}$; far larger than the current stellar densities of Lupus (Nakajima et al. 2000; Merín et al. 2008; Winter et al. 2018) ($< 500\text{pc}^{-3}$) and Cha I (Sacco et al. 2017). By comparing Gaia observations of the structural properties of Cha I with N-body simulations, Sacco et al. (2017) concluded that Cha I likely did not form in a high-density

environment. The number of O- and B- stars in Lupus and Cha I is only 2 (Comerón 2008) and 3 (Luhman et al. 2008), respectively, ruling out external photoevaporation as the dominant mechanism setting disk sizes in these low-mass star-forming regions.

The Solar System, on the other hand, may have formed in a high-density cluster environment. The review by Adams (2010) argues for a large cluster ($N = 10^3 - 10^4$) as birth environment, and required a nearby supernova to produce the inventory of short-lived radio isotopes found in the meteoritic record at the time of writing. However, more recently Wasserburg et al. (2017) showed that the short-lived radionuclide abundances of ^{26}Al, ^{60}Fe, ^{182}Hf, and ^{107}Pd found in meteorites are not consistent with being injected via sources of mass $> 5\,\text{M}_\odot$ such as supernovae. A small fraction of presolar grains (X grains) may still link the early Solar System formation to a nearby supernova event (see Zinner 2014), but how nearby the supernova would need to be is not known. Low-mass star-forming regions such as Lupus and Oph are known to have been influenced by external Supernovae (e.g. Comerón 2008; Wilking et al. 2005). Therefore, it remains unclear if the presence of X grains limits the Solar System birth environment to that of a high-density cluster.

To compare our dust-disk sizes with the Solar System, we utilize the R_{90} estimates which better represent the full extent of the disk. In addition, we constrain ourselves to the younger and lower mass star-forming regions of Lupus and Cha I to exclude significant evolution and external processes affecting disk sizes. Figure 9 provides this comparison and shows that the Solar System's size falls within the range of R_{90} values found for both low-mass star-forming regions. We also test if the dust masses of the Lupus and Cha I disks is consistent, or discordant, with the Solar System. To get a rough estimate of the mass of the primordial Solar System's dust disk, we sum the masses of solids locked up within the major planets ($\sim 30\,M_\oplus$). Dust disk masses are estimated assuming optically thin emission and a fixed temperature of 20 K for the emitting grains as in the 20 K dust-mass calculation described in Pascucci et al. (2016). Figure 9 shows that the mass of solids in the Solar System is larger than the average dust disk mass but still falls within the range of masses observed in other disks.

When compared to the disks in Lupus and Cha I, the Solar System doesn't appear to be an outlier. It is neither small, nor does it appear to be missing dust mass. If the initial sizes of protoplanetary disks within high-density and low-density regions are similar, our results show that the Solar system's primordial disk requires

no external modification (e.g. stellar encounter or photoevaporation) to explain its size and mass since it is consistent with a population of disks lacking truncation. Radial drift of dust grains, which is common to all environments, may be setting disk sizes. However, if the Solar System formed in a high-density cluster, *and* the initial sizes of these disks is not similar to the initial sizes found in low-density regions, we can come to no conclusion about the history of the Solar System's outer edge.

6.3. *Disk size scaling relations*

In Section 5.1 we test for the existence of and, if found, quantify empirical relations between disk sizes ($R_{\rm eff}$), millimeter luminosities ($L_{\rm mm}$), stellar masses ($M_\star$), and stellar luminosities ($L_\star$). In this sub-section we discuss our findings in that order, starting with $\log R_{\rm eff} - \log L_{\rm mm}$.

We find that, in log scale, disk radii are linearly correlated with millimeter luminosities and that the slope of the $\log R_{\rm eff} - \log L_{\rm mm}$ relation is not the same for all regions investigated here (see Figure 6 and Table 4). The latter result is different from earlier works. Previous analysis by Tripathi et al. (2017) and Andrews et al. (2018a) found a slope of ~ 0.5 to be common to the Oph, Tau/Aur, and Lupus star-forming regions. Using a different technique, Barenfeld et al. (2017) showed that disk sizes in USco, while being a factor of ~ 3 times smaller than those in Oph and Tau/Aur, plot on the same $\log R_{\rm eff} - \log L_{\rm mm}$ relation with slope 0.5. This result has led to speculation that the $\log R_{\rm eff} - \log L_{\rm mm}$ relationship could be universal (e.g., Rosotti et al. 2019). As the relation implies that the millimeter luminosity scales with the square of the dust radius, the most commonly adopted interpretation is that the millimeter emission is mostly optically thick.

Assuming a simple parameterization for the dust temperature profile, Andrews et al. (2018a) considered whether their $\log R_{\rm eff} - \log L_{\rm mm}$ and $\log L_{\rm mm} - \log L_\star$ relationships for Oph, Tau/Aur and Lupus were consistent with disks being optically thin or thick. Ultimately, they concluded that neither of the two scenarios could be ruled out. Here, we focus on the optically thick scenario and repeat Andrews et al. (2018a) approach for Cha I and USco. Using the following temperature profile:

$$T_d(r) \propto \left(\frac{L_\star}{L_\odot}\right)^{0.25} \left(\frac{r}{r_0}\right)^{-q} \tag{3}$$

where $r_0 = 10\,{\rm au}$ for a solar luminosity star, Andrews et al. (2018a) derived a relationship connecting the dust effective radius to the stellar luminosity and millimeter

luminosity via the power law index (q) of the dust temperature profile:

$$R_{\rm eff} \propto L_\star^{-1/3(2-q)} L_{\rm mm}^{1/(2-q)} \tag{4}$$

We can then estimate q for each region using Equation 4 and our empirically measured $\log L_{\rm mm} - \log L_\star$ and $\log R_{\rm eff} - \log L_{\rm mm}$ relationships (see Table 11 in Appendix G and Table 4 in Section 5.1.1 respectively). With an estimate of q in hand, we can test if the resulting temperature profile is consistent with that expected for optically thin or thick disks. Doing so results in values of q of $0.32^{+0.33}_{-0.4}$ for Cha I and $-0.85^{+1.42}_{-3.1}$ for USco. At long millimeter wavelengths and in the case of optically thin emission, the radial temperature profile can be expressed as $T(r) \propto r^{-2/(4+\beta)}$ where β is the index of the dust absorption coefficient, e.g. Evans (1994). Thus, for the average β of 0.6 (Ricci et al. 2010), we find $T(r) \propto r^{-0.4}$ in the optically thin regime. Partially optically thick emission is characterized by a steeper dependence with radial distance (e.g., Fig. 5 in Pascucci et al. 2004) close to $r^{-0.5}$ for the midplane of an accretion disk irradiated by the central star (D'Alessio et al. 1998). The upper bounds of the confidence intervals encompass the optically thin and thick temperature profiles both for Cha I and USco. However, the mostly negative values of q for USco imply a temperature profile increasing with disk radius, which is highly unlikely, suggesting that the disk emission is not optically thick.

Andrews et al. (2018a) report finding weak scaling relationships for their joint sample of Oph, Tau/Aur and Lupus for both $\log R_{\rm eff} - \log M_\star$ and $\log R_{\rm eff} - \log L_\star$. We determine that $\log R_{\rm eff} - \log M_\star$ is not correlated for any of our regions, and for the $\log R_{\rm eff} - \log L_\star$ correlation we find a trend only for Lupus. Extending disk radii measurements to even smaller and less luminous stars could reveal trends also in other regions. This would require observations more sensitive than those adopted for the initial ALMA surveys of nearby star-forming regions.

Finally, we would like to speculate on the possible time evolution of the $\log R_{\rm eff} - \log L_{\rm mm}$ relation utilizing the three regions that have been observed at a similar sensitivity with ALMA, i.e. Lupus, Cha I and USco. While Cha I and Lupus have overlapping ages with large uncertainties (1-3 and 2-3 Myrs respectively), if we take these ages at face value, we see a flattening of the $\log R_{\rm eff} - \log L_{\rm mm}$ relation moving from the youngest to the oldest region.

7. SUMMARY

Using ALMA archival data, we estimate the sizes of 152 protoplanetary disks in the three star-forming regions of Lupus, Cha I and USco. This results in the

first homogenous estimation of dust disk sizes between these regions. Because we use the same approach (visibility fitting using Nuker profiles) as in Tripathi et al. (2017) and Andrews et al. (2018a), we add to our analysis their disk-size estimates for Oph and Tau/Aur, for a total of 199 disk sizes from 5 different regions. While the 5 regions have had their disk-sizes estimated in a consistent way, Oph and Tau/Aur were observed with the SMA, hence are biased towards the brightest millimeter disks.

These 5 nearby regions cover the age range over which disks disperse (Ophiuchus: 1-2 Myr; Taurus & Auriga Complex: 1-3 Myr; Lupus: 1-3 Myr; Chamaeleon I: 2-3 Myr; Upper Scorpius OB: 5-11 Myr) and host stars that span the entire stellar mass, 0.08 to 4.68 $M_\star$; with typical (16-84% quantile range) stellar masses of 0.17 to 0.89 $M_\star$.

Of the 199 disk-size estimates in our entire sample, there are 130 resolved disks and 69 unresolved disks for which we provide upper limits in the dust radii. Estimated R_{68} disk sizes for the entire sample range from 8.5 to 177 au with a median of 39 au. For the 3 regions with R_{90} estimates (Lupus, Cha I and USco), we find that R_{90} range from 10-231 au with a median of 43 au.

Our main results can be summarized as follows:

- For disks around near solar mass stars ($M_\star \in [0.85 - 1.15 M\odot]$) R_{90} disk sizes range from 20-103 au. This suggests that the ~ 45 au outer-edge of the Solar System, if primordial in origin, is not an outlier when compared with typical 1-3 Myr disks, and that a truncating event (e.g. a stellar encounter or external photoevaporation) may not be required to explain its size. Additionally we find that the mass of solids in the Solar System falls within the range of estimated dust-disk masses estimated for our sample.

- We find that the disks in Cha I are not smaller than those in Lupus as previously suggested in Eisner et al. (2018), whose comparison was based on a sub-sample of Lupus as well as samples from Oph and Tau/Aur all of which were biased towards higher luminosity sources.

- USco disk sizes are not drawn from the same distribution of disk sizes as Lupus and Cha I. In agreement with previous findings, the older USco region appears to have a population of smaller disks, albeit not by a factor of 3 as reported in Barenfeld et al. (2017). We find that USco disks are also smaller than those in Cha I; our homogeneous analysis finds a difference in the median values of ~ 1.5.

- Dust disk radii correlate with millimeter luminosity in each of the 5 regions. However, we find that the $\log R_{\rm eff} - \log L_{\rm mm}$ relation is not the same in all regions but rather becomes flatter for older regions. Uncertainties in each region's age, lack of dynamic range in ages, and different stellar environments, impedes our ability to conclude that disk-size evolution with time is conclusively seen.

- We find no evidence for a correlation between the dust-disk outer radius and stellar mass in any of the 5 regions we tested.

- Only in the Lupus star-forming region is there a modest correlation between the dust outer radius and the stellar luminosity.

In relation to the last two points, one should keep in mind that we are examining only a subset of the entire disk population in each region. While we find a correlation between $L_{\rm mm}$ and $M_\star$ for our sub-samples, in each region the correlation is shallower than when the entire population is included (see Section 4.1 and Appendix D). Therefore, we can conclude that dust radii correlate less with $M_\star$ and $L_\star$ than the millimeter luminosity. Deeper ALMA observations, especially of disks around low-mass stars, will be necessary to test if a modest correlation is present between dust disk sizes and stellar properties.

APPENDIX

A. COMPARISON WITH LITERATURE RESULTS

A.1. *Lupus: comparing Andrews et al. (2018a) with this work*

Tripathi et al. (2017) and Andrews et al. (2018a) have used the same modeling approach to infer disk sizes and their papers combined provide the largest compilation available in the literature. To further expand upon their work, we have applied the same steps to model the disks in Cha I and USco. However, there are bound to be small differences in chosen modeling and fitting parameters and techniques, as well as differences in determining uncertainties and upper-limits, hence our re-analysis of the Lupus dataset and the comparison presented here.

Figure 10 shows our Lupus disk sizes vs those reported in Andrews et al. (2018a). For most models there is tight agreement in disk sizes between the two works and for almost all sources there is agreement within the uncertainties.

One caveat about Figure 10 is that it does not compare disks for which only an upper limit to the disk size could be estimated. In general, our method results in larger uncertainties than those given in Andrews et al. (2018a). For this reason our upper limits are typically larger, and consequently for 10 disks which Andrews et al. (2018a) report a size for, we only provide an upper limit. Figure 11 presents the results of Bayesian linear regression fitting (Kelly 2007) of both modeling results with these differences in uncertainties and upper limits included. Our fitting of both the Andrews et al. (2018a) sample and our sample gives results that are consistent with each other, see values in Figure 11 and in Table 1 of Andrews et al. (2018a).

A.2. *High- vs medium-resolution observations*

Due to the long exposure times required to make observations of disks at $\leq 0.1''$ like those in Long et al. (2018) and DSHARP (Andrews et al. 2018b), it is unlikely that large sample sizes required to compare disk demographics of star-forming regions will be available in the near-term at such high resolution. This means that medium-resolution observations, like those analyzed in this work, have an important role to play in establishing what are typical disk properties, e.g. disk sizes, and their spread. However, that can only be the case if these observations truly inform us about the disk size. Here, we test the agreement between disk sizes derived from high- and medium-resolution observations.

There are 26 Tau/Aur sources that are common between the high-resolution observations of Long et al. (2018), Huang et al. (2018) and Long et al. (2019) and the medium resolution observations of Tripathi et al. (2017). The medium-resolution disk sizes used here are from Andrews et al. (2018a) who updated the Tripathi et al. (2017) results by including GAIA DR2 distances. We use Eq. E2 (see Appendix E) to convert the Tripathi et al. (2017) disk sizes from R_{68} to the R_{90} radii. It should be noted that the high-resolution disk sizes include a mix of R_{95} and R_{90} emission radii but these values are so close to each other that we do not attempt to derive an additional scaling.

We directly compare the high- and medium-resolution disk size data in Figure 12 along with a 1:1 line (in blue) for reference. The relationship between the high-resolution (R_{high}) and low-resolution (R_{low}) disk sizes is fit using Bayesian linear regression fitting (Kelly 2007) and the best-fit is shown in black with the corresponding 1σ confidence interval in gray. The relationship is also given as Eq. A1.

Comparison of Lupus modeling
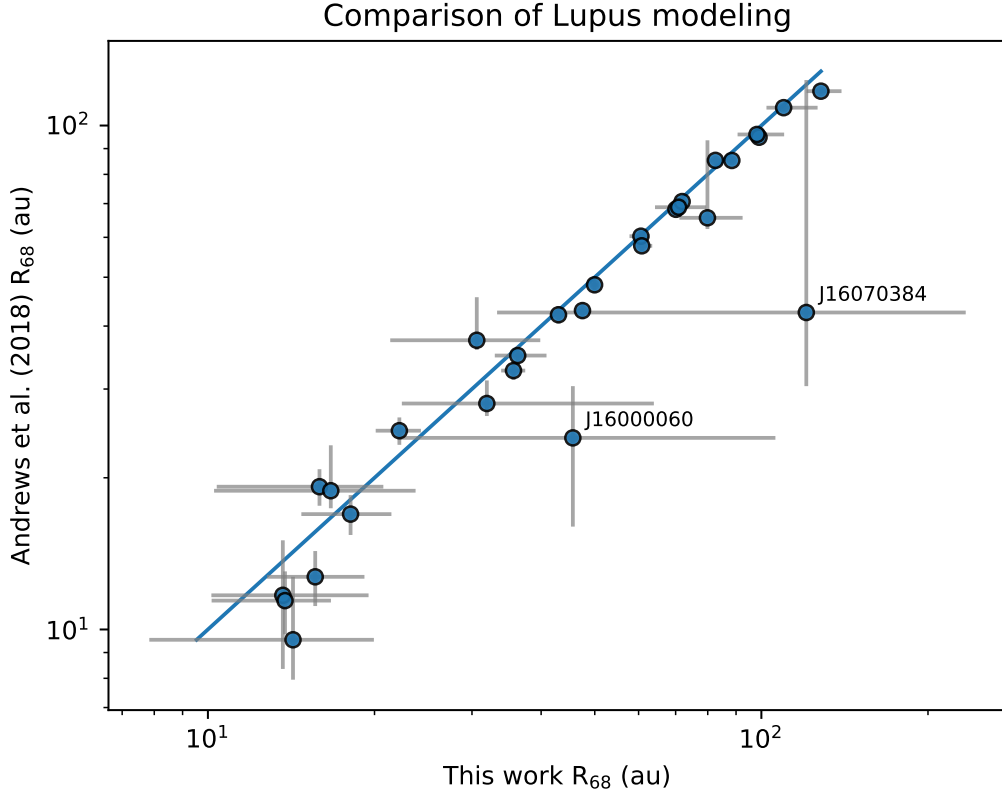
Figure 10. A comparison of disk sizes calculated in this work with sizes from Andrews et al. (2018a). The 1:1 line is shown in blue.
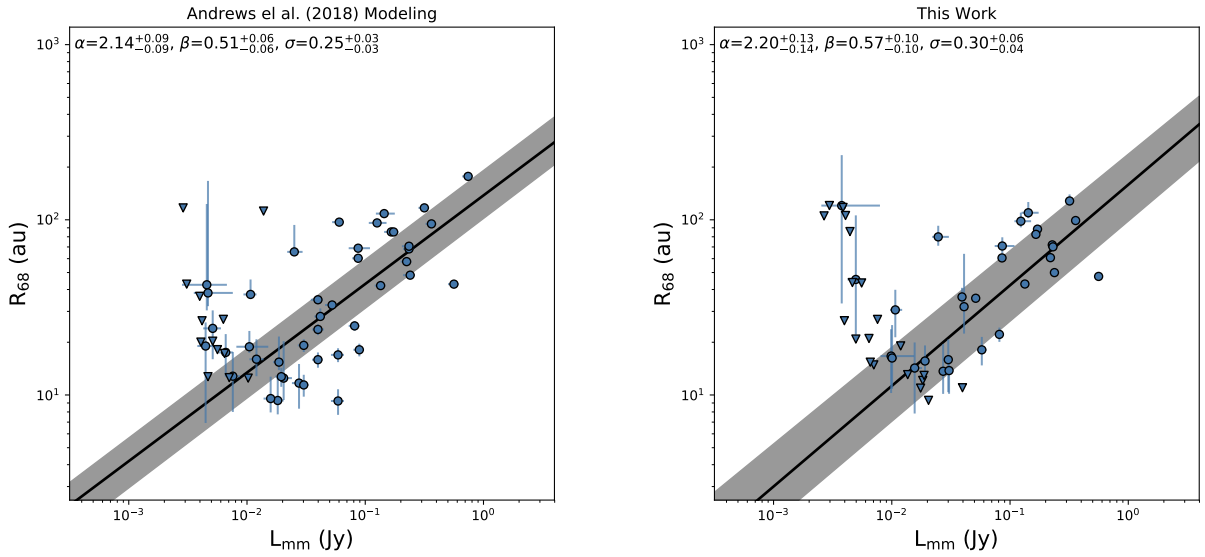
Figure 11. Two panels showing the results of Bayesian linear regression fitting using disk sizes from Andrews et al. (2018a) (left) and this work (right). The upper-left corner of each panel includes the best fit parameters (α and β) and scatter of the relation (σ), see eq. 2 in the main text.
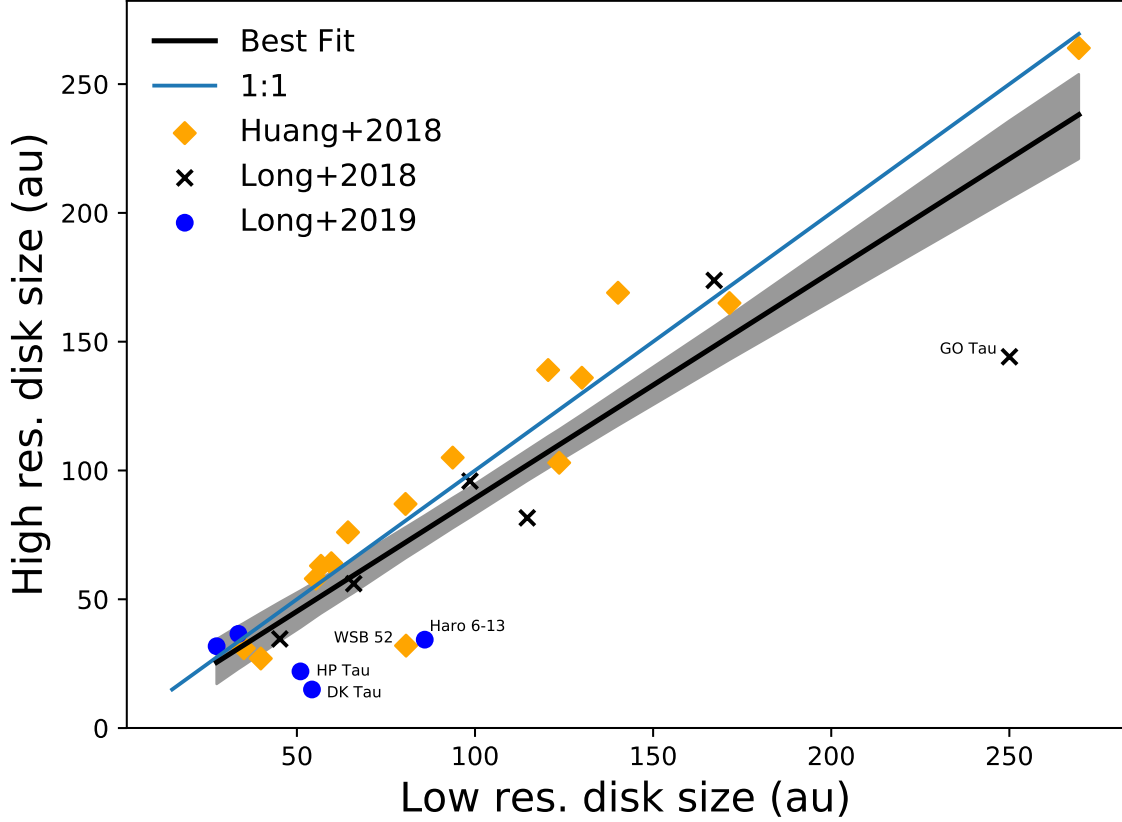
Figure 12. A comparison of disk size measurements for Tau/Aur disks that have been resolved at both high-resolution (ALMA) and medium-resolution (SMA). The medium resolution observations are taken from Tripathi et al. (2017). High-resolution observations are from Huang et al. (2018), Long et al. (2018) and Long et al. (2019) (indicated by a diamond, x and circle respectively). For each disk size measurement, the reported uncertainties are all 1 au or less. The best fit from Bayesian linear regression fitting is shown in black, while the corresponding 1σ confidence interval is shown in grey. A 1:1 relation line is shown in blue.

$$R_{\mathrm{high}}(R_{\mathrm{low}}) = 0.95(\mathrm{au}) + 0.88R_{\mathrm{low}}(\mathrm{au}) \tag{A1}$$

B. STELLAR AND DISK PROPERTIES

Table 7 lists stellar properties and derived stellar masses ($M_\star$) as described in Section 2.2.1. To derive stellar masses we follow the approach used in Pascucci et al. (2016) and assume an uncertainty of 0.02 dex in the stellar temperature for spectral types earlier than M3 and 0.01 dex for later spectral types, and a 0.1 dex uncertainty on all stellar luminosities.

Table 7. Stellar and Disk Properties

2MASS	Region	Distance	$\log(L_\star)$	T_{eff}	$\log(M_\star)$	L_{mm}[a]
		(pc)	$(L_\odot)$	(K)	$(M_\odot)$	(mJy)
J10533978-7712338	ChaI	$190.88^{+3.85}_{-3.70}$	$-1.70^{+0.01}_{-0.01}$	3560.00	$-0.48^{+0.10}_{-0.06}$	$6.95^{+0.59}_{-0.55}$

Table 7 continued

Table 7 (continued)

2MASS	Region	Distance	$\log(L_\star)$	T_{eff}	$\log(M_\star)$	L_{mm}[a]
		(pc)	$(L_\odot)$	(K)	$(M_\odot)$	(mJy)
J10555973-7724399	ChaI	$184.11^{+1.07}_{-1.06}$	$-0.74^{+0.11}_{-0.11}$	4060.00	$-0.11^{+0.14}_{-0.10}$	$58.97^{+3.00}_{-2.93}$
J10561638-7630530	ChaI	$195.52^{+4.15}_{-3.98}$	$-1.10^{+0.05}_{-0.05}$	2935.00	$-0.89^{+0.02}_{-0.02}$	$7.78^{+0.66}_{-0.61}$
J10563044-7711393	ChaI	$182.12^{+0.65}_{-0.64}$	$-0.37^{+0.25}_{-0.25}$	4060.00	$-0.14^{+0.19}_{-0.15}$	$198.98^{+3.30}_{-3.25}$
J10580597-7711501	ChaI	$185.69^{+3.70}_{-3.56}$	$-2.00^{+0.01}_{-0.01}$	3060.00	$-0.96^{+0.03}_{-0.02}$	$4.71^{+0.48}_{-0.45}$
J10581677-7717170	ChaI	$188.83^{+1.50}_{-1.48}$	$0.28^{+1.11}_{-1.11}$	5250.00	$0.21^{+0.16}_{-0.14}$	$564.26^{+10.87}_{-10.60}$
J10590108-7722407	ChaI	$184.23^{+0.65}_{-0.65}$	$-0.42^{+0.22}_{-0.22}$	4060.00	$-0.13^{+0.17}_{-0.15}$	$113.14^{+3.77}_{-3.72}$
J10590699-7701404	ChaI	$186.47^{+0.80}_{-0.80}$	$0.51^{+1.91}_{-1.91}$	5110.00	$0.27^{+0.33}_{-0.24}$	$784.48^{+8.14}_{-8.03}$
J11004022-7619280	ChaI	$190.50^{+1.58}_{-1.55}$	$-1.00^{+0.06}_{-0.06}$	3270.00	$-0.63^{+0.05}_{-0.03}$	$129.15^{+2.47}_{-2.41}$
J11022491-7733357	ChaI	$175.38^{+1.17}_{-1.16}$	$0.08^{+0.70}_{-0.70}$	4205.00	$-0.13^{+0.19}_{-0.15}$	$354.16^{+5.93}_{-5.80}$
J11025504-7721508	ChaI	$181.31^{+1.53}_{-1.50}$	$-0.82^{+0.09}_{-0.09}$	3200.00	$-0.72^{+0.02}_{-0.03}$	$1.95^{+0.31}_{-0.30}$
J11040425-7639328	ChaI	$191.36^{+3.53}_{-3.41}$	$-1.52^{+0.02}_{-0.02}$	3200.00	$-0.72^{+0.04}_{-0.04}$	$5.18^{+0.50}_{-0.47}$
J11040909-7627193	ChaI	$190.72^{+0.78}_{-0.77}$	$0.18^{+0.88}_{-0.88}$	4350.00	$-0.07^{+0.20}_{-0.18}$	$194.45^{+2.71}_{-2.67}$
J11044258-7741571	ChaI	$192.14^{+2.71}_{-2.64}$	$-1.05^{+0.05}_{-0.05}$	3270.00	$-0.62^{+0.05}_{-0.04}$	$7.82^{+0.53}_{-0.51}$
J11045701-7715569	ChaI	$193.46^{+3.24}_{-3.13}$	$-0.55^{+0.16}_{-0.16}$	3415.00	$-0.53^{+0.04}_{-0.03}$	$7.14^{+0.75}_{-0.71}$
J11062554-7633418	ChaI	$208.26^{+5.30}_{-5.04}$	$-1.52^{+0.02}_{-0.02}$	3060.00	$-0.88^{+0.03}_{-0.03}$	$101.91^{+5.60}_{-5.19}$
J11064510-7727023	ChaI	$184.49^{+1.28}_{-1.27}$	$-0.28^{+0.31}_{-0.31}$	4205.00	$-0.09^{+0.19}_{-0.17}$	$1.62^{+0.30}_{-0.30}$
J11065906-7718535	ChaI	$189.33^{+2.10}_{-2.06}$	$-0.49^{+0.19}_{-0.19}$	3200.00	$-0.63^{+0.02}_{-0.03}$	$44.41^{+1.65}_{-1.59}$
J11065939-7530559	ChaI	$195.30^{+4.40}_{-4.21}$	$-2.00^{+0.01}_{-0.01}$	3060.00	$-0.96^{+0.03}_{-0.02}$	$6.05^{+0.60}_{-0.56}$
J11070925-7718471	ChaI	$190.00^{+20.00}_{-20.00}$	$-0.60^{+0.15}_{-0.15}$	3415.00	$-0.54^{+0.04}_{-0.04}$	$1.20^{+0.65}_{-0.49}$
J11071206-7632232	ChaI	$194.65^{+0.84}_{-0.83}$	$-0.40^{+0.23}_{-0.23}$	3850.00	$-0.25^{+0.16}_{-0.13}$	$12.70^{+0.60}_{-0.59}$
J11071330-7743498	ChaI	$173.07^{+7.00}_{-6.48}$	$-0.66^{+0.13}_{-0.13}$	3342.00	$-0.59^{+0.04}_{-0.03}$	$3.41^{+0.55}_{-0.48}$
J11071860-7732516	ChaI	$198.81^{+13.57}_{-11.96}$	$-1.52^{+0.02}_{-0.02}$	3060.00	$-0.87^{+0.04}_{-0.03}$	$1.88^{+0.63}_{-0.50}$
J11072074-7738073	ChaI	$189.58^{+1.07}_{-1.06}$	$0.71^{+2.98}_{-2.98}$	5110.00	$0.33^{+0.37}_{-0.28}$	$48.34^{+3.26}_{-3.19}$
J11074366-7739411	ChaI	$193.76^{+2.21}_{-2.16}$	$-0.52^{+0.18}_{-0.18}$	3705.00	$-0.33^{+0.13}_{-0.10}$	$205.47^{+5.81}_{-5.60}$
J11074656-7615174	ChaI	$193.64^{+7.78}_{-7.21}$	$-2.00^{+0.01}_{-0.01}$	2935.00	$-1.13^{+0.03}_{-0.02}$	$4.17^{+0.67}_{-0.59}$
J11075730-7717262	ChaI	$187.37^{+12.74}_{-11.23}$	$-0.66^{+0.13}_{-0.13}$	3669.00	$-0.34^{+0.15}_{-0.11}$	$11.59^{+3.26}_{-2.61}$
J11075809-7742413	ChaI	$183.53^{+2.51}_{-2.44}$	$-0.80^{+0.09}_{-0.09}$	3415.00	$-0.52^{+0.05}_{-0.04}$	$12.22^{+0.62}_{-0.59}$
J11081509-7733531	ChaI	$190.00^{+20.00}_{-20.00}$	$0.10^{+0.74}_{-0.74}$	5110.00	$0.16^{+0.14}_{-0.13}$	$385.48^{+86.39}_{-77.52}$
J11083905-7716042	ChaI	$187.37^{+1.99}_{-1.95}$	$-0.28^{+0.31}_{-0.31}$	3955.00	$-0.22^{+0.17}_{-0.12}$	$25.27^{+1.98}_{-1.91}$
J11085367-7521359	ChaI	$187.26^{+0.82}_{-0.81}$	$-0.72^{+0.11}_{-0.11}$	3705.00	$-0.30^{+0.16}_{-0.12}$	$44.01^{+2.86}_{-2.81}$
J11085464-7702129	ChaI	$185.04^{+1.87}_{-1.83}$	$-0.89^{+0.08}_{-0.08}$	3780.00	$-0.17^{+0.55}_{-0.13}$	$7.04^{+0.43}_{-0.41}$
J11092379-7623207	ChaI	$191.25^{+0.83}_{-0.82}$	$-0.26^{+0.32}_{-0.32}$	3780.00	$-0.29^{+0.12}_{-0.11}$	$229.73^{+3.07}_{-3.02}$
J11094621-7634463	ChaI	$194.02^{+2.90}_{-2.82}$	$-1.22^{+0.04}_{-0.04}$	3415.00	$-0.48^{+0.07}_{-0.06}$	$9.08^{+1.84}_{-1.74}$
J11094742-7726290	ChaI	$192.14^{+5.47}_{-5.18}$	$-1.00^{+0.06}_{-0.06}$	3705.00	$-0.25^{+0.16}_{-0.13}$	$278.49^{+17.78}_{-16.34}$
J11095340-7634255	ChaI	$201.12^{+6.42}_{-6.04}$	$-0.32^{+0.28}_{-0.28}$	4060.00	$-0.17^{+0.18}_{-0.14}$	$157.05^{+14.20}_{-12.84}$
J11100369-7633291	ChaI	$199.94^{+3.21}_{-3.12}$	$-0.64^{+0.13}_{-0.13}$	3850.00	$-0.22^{+0.17}_{-0.13}$	$20.05^{+2.31}_{-2.18}$
J11100469-7635452	ChaI	$193.92^{+0.93}_{-0.92}$	$-0.47^{+0.20}_{-0.20}$	4060.00	$-0.13^{+0.17}_{-0.15}$	$14.83^{+1.65}_{-1.62}$
J11101141-7635292	ChaI	$194.31^{+2.09}_{-2.05}$	$-0.21^{+0.36}_{-0.36}$	4350.00	$0.01^{+0.97}_{-0.17}$	$142.21^{+5.83}_{-5.62}$
J11104959-7717517	ChaI	$184.20^{+1.49}_{-1.47}$	$-0.82^{+0.09}_{-0.09}$	3560.00	$-0.40^{+0.13}_{-0.10}$	$101.04^{+4.19}_{-4.07}$
J11105333-7634319	ChaI	$193.60^{+1.14}_{-1.13}$	$-0.80^{+0.09}_{-0.09}$	3415.00	$-0.52^{+0.05}_{-0.04}$	$59.32^{+3.20}_{-3.13}$

Table 7 continued

Table 7 *(continued)*

2MASS	Region	Distance	$\log(L_\star)$	$T_{\rm eff}$	$\log(M_\star)$	$L_{\rm mm}$[a]
		(pc)	$(L_\odot)$	(K)	$(M_\odot)$	(mJy)
J11105359-7725004	ChaI	$195.71^{+11.63}_{-10.41}$	$-1.40^{+0.02}_{-0.02}$	3125.00	$-0.78^{+0.04}_{-0.03}$	$15.40^{+2.63}_{-2.19}$
J11111083-7641574	ChaI	$190.00^{+20.00}_{-20.00}$	$-2.52^{+0.00}_{-0.00}$	3705.00	$-0.92^{+0.02}_{-0.02}$	$99.96^{+26.09}_{-22.52}$
J11113965-7620152	ChaI	$189.47^{+1.04}_{-1.03}$	$-0.54^{+0.17}_{-0.17}$	3340.00	$-0.57^{+0.03}_{-0.03}$	$39.34^{+1.91}_{-1.87}$
J11114632-7620092	ChaI	$191.45^{+0.89}_{-0.88}$	$0.01^{+0.60}_{-0.60}$	4900.00	$0.13^{+0.20}_{-0.12}$	$65.83^{+2.99}_{-2.94}$
J11120351-7726009	ChaI	$184.63^{+3.85}_{-3.69}$	$-1.15^{+0.04}_{-0.04}$	3060.00	$-0.86^{+0.02}_{-0.02}$	$5.13^{+0.51}_{-0.47}$
J11120984-7634366	ChaI	$192.18^{+1.89}_{-1.86}$	$-0.85^{+0.08}_{-0.08}$	3125.00	$-0.74^{+0.02}_{-0.02}$	$8.37^{+0.59}_{-0.57}$
J11122772-7644223	ChaI	$192.17^{+0.98}_{-0.97}$	$0.41^{+1.49}_{-1.49}$	5110.00	$0.24^{+0.21}_{-0.22}$	$111.26^{+3.60}_{-3.53}$
J11123092-7644241	ChaI	$194.92^{+1.79}_{-1.76}$	$-0.74^{+0.11}_{-0.11}$	3780.00	$-0.25^{+0.16}_{-0.13}$	$23.61^{+2.08}_{-2.01}$
J11132446-7629227	ChaI	$188.52^{+1.81}_{-1.78}$	$-0.96^{+0.06}_{-0.06}$	3270.00	$-0.63^{+0.05}_{-0.03}$	$14.63^{+1.74}_{-1.68}$
J11142454-7733062	ChaI	$188.00^{+2.94}_{-2.85}$	$-0.92^{+0.07}_{-0.07}$	3200.00	$-0.73^{+0.03}_{-0.03}$	$13.40^{+1.05}_{-1.00}$
J11160287-7624533	ChaI	$190.00^{+20.00}_{-20.00}$	$-2.47^{+0.00}_{-0.00}$	3955.00	$-0.87^{+0.02}_{-0.02}$	$23.63^{+9.02}_{-7.19}$
J11173700-7704381	ChaI	$187.36^{+0.86}_{-0.85}$	$-0.41^{+0.23}_{-0.23}$	3778.00	$-0.29^{+0.15}_{-0.11}$	$50.61^{+2.80}_{-2.75}$
J11183572-7935548	ChaI	$94.40^{+1.36}_{-1.32}$	$-0.59^{+0.15}_{-0.15}$	3125.00	$-0.81^{+0.03}_{-0.03}$	$6.60^{+0.36}_{-0.34}$
J11241186-7630425	ChaI	$183.82^{+2.48}_{-2.41}$	$-1.52^{+0.02}_{-0.02}$	3060.00	$-0.88^{+0.04}_{-0.03}$	$2.53^{+0.35}_{-0.33}$
J15354856-2958551	USco	$145.00^{+20.00}_{-20.00}$	$-0.60^{+0.15}_{-0.15}$	$3235.94^{+152.50}_{152.50}$	$-0.68^{+0.03}_{-0.03}$	$2.06^{+0.82}_{-0.65}$
J15392776-3446171	Lupus	$155.00^{+3.00}_{-3.00}$	$-0.06^{+0.51}_{-0.51}$	$4073.80^{+191.99}_{-183.35}$	$-0.17^{+0.18}_{-0.14}$	$81.27^{+4.32}_{-3.82}$
J15392828-3446180	Lupus	$156.00^{+4.00}_{-4.00}$	$-0.66^{+0.13}_{-0.13}$	$3388.44^{+78.93}_{-77.13}$	$-0.54^{+0.05}_{-0.04}$	$18.75^{+5.41}_{-1.18}$
J15450887-3417333	Lupus	$154.00^{+6.00}_{-6.00}$	$-1.20^{+0.04}_{-0.04}$	$3090.30^{+71.98}_{-70.34}$	$-0.83^{+0.04}_{-0.03}$	$57.72^{+5.50}_{-5.08}$
J15451741-3418283	Lupus	$154.00^{+3.00}_{-3.00}$	$-1.03^{+0.05}_{-0.05}$	$3235.94^{+75.37}_{-73.66}$	$-0.65^{+0.05}_{-0.03}$	$20.45^{+1.56}_{-1.25}$
J15464473-3430354	Lupus	$155.00^{+3.00}_{-3.00}$	$-0.48^{+0.19}_{-0.19}$	$3630.78^{+171.11}_{-163.41}$	$-0.38^{+0.12}_{-0.11}$	$230.69^{+10.93}_{-10.97}$
J15475062-3528353	Lupus	$155.00^{+3.00}_{-3.00}$	$-0.56^{+0.16}_{-0.16}$	$3548.13^{+167.22}_{-159.69}$	$-0.42^{+0.13}_{-0.09}$	$17.53^{+2.21}_{-1.14}$
J15475693-3514346	Lupus	$156.00^{+3.00}_{-3.00}$	$-0.34^{+0.27}_{-0.27}$	$4073.80^{+191.99}_{-183.35}$	$-0.07^{+0.73}_{-0.14}$	$40.85^{+3.01}_{-2.39}$
J15514032-2146103	USco	$141.66^{+2.15}_{-2.09}$	$-1.31^{+0.03}_{-0.03}$	$3235.94^{+152.50}_{152.50}$	$-0.68^{+0.04}_{-0.04}$	$0.78^{+0.19}_{-0.18}$
J15530132-2114135	USco	$145.81^{+2.58}_{-2.50}$	$-1.20^{+0.04}_{-0.04}$	$3235.94^{+152.50}_{152.50}$	$-0.66^{+0.04}_{-0.04}$	$6.27^{+0.38}_{-0.36}$
J15534211-2049282	USco	$135.25^{+3.48}_{-3.31}$	$-0.84^{+0.08}_{-0.08}$	$3311.31^{+156.06}_{156.06}$	$-0.59^{+0.04}_{-0.04}$	$2.73^{+0.43}_{-0.39}$
J15564230-3749154	Lupus	$159.00^{+3.00}_{-3.00}$	$0.16^{+0.85}_{-0.85}$	$4073.80^{+191.99}_{-183.35}$	$-0.20^{+0.16}_{-0.13}$	$561.21^{+23.12}_{-21.85}$
J15580252-3736026	Lupus	$152.00^{+3.00}_{-3.00}$	$-0.91^{+0.07}_{-0.07}$	$3162.28^{+73.66}_{-71.98}$	$-0.77^{+0.03}_{-0.03}$	$39.25^{+2.42}_{-2.21}$
J15582981-2310077	USco	$146.98^{+2.84}_{-2.74}$	$-1.31^{+0.03}_{-0.03}$	$3388.44^{+159.69}_{-159.69}$	$-0.51^{+0.06}_{-0.05}$	$6.46^{+0.46}_{-0.43}$
J15583692-2257153	USco	$165.48^{+4.13}_{-3.94}$	$0.47^{+1.73}_{-1.73}$	$5623.41^{+0.00}_{0.00}$	$0.24^{+0.17}_{-0.22}$	$244.39^{+12.75}_{-11.86}$
J15591647-4157102	Lupus	$161.00^{+3.00}_{-3.00}$	$-0.36^{+0.26}_{-0.26}$	$4073.80^{+191.99}_{-183.35}$	$-0.07^{+0.70}_{-0.14}$	$237.39^{+10.16}_{-10.04}$
J15592838-4021513	Lupus	$158.00^{+4.00}_{-4.00}$	$0.28^{+1.11}_{-1.11}$	$4897.79^{+230.83}_{-220.44}$	$0.15^{+0.21}_{-0.15}$	$358.67^{+20.53}_{-19.26}$
J16000060-4221567	Lupus	$160.00^{+4.00}_{-4.00}$	$-1.00^{+0.06}_{-0.06}$	$3235.94^{+75.37}_{-73.66}$	$-0.65^{+0.05}_{-0.03}$	$4.96^{+1.07}_{-0.74}$
J16000236-4222145	Lupus	$164.00^{+4.00}_{-4.00}$	$-0.78^{+0.10}_{-0.10}$	$3235.94^{+75.37}_{-73.66}$	$-0.71^{+0.03}_{-0.13}$	$165.49^{+10.62}_{-9.28}$
J16001844-2230114	USco	$138.05^{+8.95}_{-7.94}$	$-1.13^{+0.04}_{-0.04}$	$3162.28^{+149.03}_{149.03}$	$-0.73^{+0.04}_{-0.03}$	$3.78^{+0.67}_{-0.55}$
J16003103-4143369	Lupus	$160.00^{+3.00}_{-3.00}$	$-0.76^{+0.10}_{-0.10}$	$3548.13^{+167.22}_{-159.69}$	$-0.39^{+0.14}_{-0.10}$	$7.58^{+1.24}_{-0.78}$
J16004452-4155310	Lupus	$156.00^{+3.00}_{-3.00}$	$-0.06^{+0.51}_{-0.51}$	$5128.61^{+241.70}_{-230.83}$	$0.07^{+0.14}_{-0.10}$	$219.52^{+9.81}_{-9.32}$
J16004943-4130038	Lupus	$160.00^{+3.00}_{-3.00}$	$-0.82^{+0.09}_{-0.09}$	$3388.44^{+78.93}_{-77.13}$	$-0.53^{+0.05}_{-0.04}$	$11.89^{+1.26}_{-0.94}$
J16014086-2258103	USco	$145.00^{+20.00}_{-20.00}$	$-0.90^{+0.07}_{-0.07}$	$3235.94^{+152.50}_{152.50}$	$-0.66^{+0.04}_{-0.04}$	$3.70^{+1.29}_{-1.06}$
J16014157-2111380	USco	$144.20^{+2.54}_{-2.45}$	$-1.56^{+0.02}_{-0.02}$	$3235.94^{+152.50}_{152.50}$	$-0.70^{+0.04}_{-0.04}$	$0.70^{+0.18}_{-0.17}$
J16020757-2257467	USco	$139.73^{+1.26}_{-1.23}$	$-0.82^{+0.09}_{-0.09}$	$3467.37^{+163.41}_{163.41}$	$-0.45^{+0.12}_{-0.09}$	$5.24^{+0.37}_{-0.36}$

Table 7 continued

Table 7 (continued)

2MASS	Region	Distance	$\log(L_\star)$	$T_{\rm eff}$	$\log(M_\star)$	$L_{\rm mm}$[a]
		(pc)	$(L_\odot)$	(K)	$(M_\odot)$	(mJy)
J16024152-2138245	USco	$141.30^{+2.58}_{-2.49}$	$-1.44^{+0.02}_{-0.02}$	$3162.28^{+149.03}_{149.03}$	$-0.77^{+0.04}_{-0.03}$	$10.44^{+0.58}_{-0.55}$
J16030161-2207523	USco	$143.71^{+3.57}_{-3.40}$	$-1.59^{+0.02}_{-0.02}$	$3162.28^{+149.03}_{149.03}$	$-0.78^{+0.04}_{-0.03}$	$2.96^{+0.28}_{-0.26}$
J16032939-4140018	Lupus	$153.00^{+18.00}_{-10.00}$	$0.02^{+0.61}_{-0.61}$	$4365.16^{+205.72}_{-196.46}$	$-0.03^{+0.21}_{-0.17}$	$85.99^{+23.06}_{-11.81}$
J16035767-2031055	USco	$142.00^{+0.79}_{-0.78}$	$-0.17^{+0.40}_{-0.40}$	$4365.16^{+101.68}_{101.68}$	$0.01^{+0.80}_{-0.13}$	$4.42^{+0.45}_{-0.45}$
J16041740-1942287	USco	$160.55^{+2.49}_{-2.42}$	$-1.07^{+0.05}_{-0.05}$	$3311.31^{+156.06}_{156.06}$	$-0.59^{+0.04}_{-0.04}$	$1.17^{+0.23}_{-0.21}$
J16052556-2035397	USco	$142.11^{+3.34}_{-3.20}$	$-1.37^{+0.02}_{-0.02}$	$3090.30^{+145.64}_{145.64}$	$-0.84^{+0.04}_{-0.03}$	$1.58^{+0.29}_{-0.27}$
J16063539-2516510	USco	$145.00^{+20.00}_{-20.00}$	$-1.60^{+0.01}_{-0.01}$	$3162.28^{+149.03}_{149.03}$	$-0.78^{+0.04}_{-0.03}$	$1.81^{+0.74}_{-0.59}$
J16064102-2455489	USco	$151.65^{+3.00}_{-2.89}$	$-1.70^{+0.01}_{-0.01}$	$3162.28^{+149.03}_{149.03}$	$-0.79^{+0.04}_{-0.03}$	$3.58^{+0.31}_{-0.29}$
J16064385-1908056	USco	$144.23^{+7.04}_{-6.43}$	$-0.39^{+0.24}_{-0.24}$	$4168.69^{+97.10}_{97.10}$	$-0.05^{+0.66}_{-0.12}$	$0.89^{+0.26}_{-0.22}$
J16070384-3911113	Lupus	$152.00^{+21.00}_{-11.00}$	$-0.99^{+0.06}_{-0.06}$	$3235.94^{+75.37}_{-73.66}$	$-0.65^{+0.05}_{-0.03}$	$3.77^{+4.17}_{-1.24}$
J16070854-3914075	Lupus	$175.00^{+17.00}_{-10.00}$	$-0.86^{+0.08}_{-0.08}$	$3235.94^{+75.37}_{-73.66}$	$-0.66^{+0.04}_{-0.03}$	$142.66^{+31.88}_{-17.37}$
J16071007-3911033	Lupus	$160.00^{+3.00}_{-3.00}$	$-0.38^{+0.24}_{-0.24}$	$4073.80^{+191.99}_{-183.35}$	$-0.07^{+0.70}_{-0.14}$	$30.04^{+1.95}_{-1.74}$
J16072625-2432079	USco	$142.25^{+1.99}_{-1.94}$	$-0.92^{+0.07}_{-0.07}$	$3311.31^{+156.06}_{156.06}$	$-0.59^{+0.04}_{-0.04}$	$13.55^{+0.64}_{-0.61}$
J16072747-2059442	USco	$145.00^{+20.00}_{-20.00}$	$-0.99^{+0.06}_{-0.06}$	$3162.28^{+149.03}_{149.03}$	$-0.76^{+0.04}_{-0.03}$	$2.28^{+0.84}_{-0.68}$
J16073773-3921388	Lupus	$173.00^{+7.00}_{-7.00}$	$-1.05^{+0.05}_{-0.05}$	$3090.30^{+71.98}_{-70.34}$	$-0.84^{+0.03}_{-0.02}$	$4.43^{+1.36}_{-0.91}$
J16075230-3858059	Lupus	$157.00^{+3.00}_{-3.00}$	$-0.58^{+0.15}_{-0.15}$	$3388.44^{+78.93}_{-77.13}$	$-0.55^{+0.04}_{-0.04}$	$6.41^{+0.90}_{-0.61}$
J16075475-3915446	Lupus	$153.00^{+22.00}_{-11.00}$	$-0.98^{+0.06}_{-0.06}$	$3235.94^{+75.37}_{-73.66}$	$-0.65^{+0.05}_{-0.03}$	$4.06^{+4.85}_{-0.87}$
J16075796-2040087	USco	$197.84^{+8.33}_{-7.69}$	$-0.82^{+0.09}_{-0.09}$	$3715.35^{+175.10}_{175.10}$	$-0.30^{+0.16}_{-0.12}$	$46.91^{+4.29}_{-3.80}$
J16080017-3902595	Lupus	$159.00^{+4.00}_{-4.00}$	$-1.44^{+0.02}_{-0.02}$	$3090.30^{+71.98}_{-70.34}$	$-0.85^{+0.04}_{-0.03}$	$4.64^{+0.64}_{-0.60}$
J16081263-3908334	Lupus	$156.00^{+3.00}_{-3.00}$	$-0.38^{+0.24}_{-0.24}$	$3715.35^{+175.10}_{-167.22}$	$-0.33^{+0.13}_{-0.11}$	$4.97^{+0.84}_{-0.55}$
J16081497-3857145	Lupus	$145.00^{+30.00}_{-12.00}$	$-1.02^{+0.06}_{-0.06}$	$3090.30^{+71.98}_{-70.34}$	$-0.84^{+0.03}_{-0.02}$	$9.87^{+5.60}_{-1.84}$
J16081566-2222199	USco	$139.66^{+1.61}_{-1.58}$	$-0.85^{+0.08}_{-0.08}$	$3388.44^{+159.69}_{159.69}$	$-0.53^{+0.05}_{-0.05}$	$0.97^{+0.14}_{-0.14}$
J16082180-3904214	Lupus	$157.00^{+3.00}_{-3.00}$	$-0.99^{+0.06}_{-0.06}$	$3311.31^{+77.13}_{-75.37}$	$-0.59^{+0.04}_{-0.04}$	$7.04^{+0.66}_{-0.63}$
J16082249-3904464	Lupus	$156.00^{+3.00}_{-3.00}$	$0.18^{+0.89}_{-0.89}$	$4073.80^{+191.99}_{-183.35}$	$-0.20^{+0.16}_{-0.13}$	$318.85^{+15.35}_{-14.18}$
J16082324-1930009	USco	$137.48^{+1.12}_{-1.10}$	$-0.59^{+0.15}_{-0.15}$	$3890.45^{+90.62}_{90.62}$	$-0.13^{+0.61}_{-0.12}$	$41.65^{+1.47}_{-1.43}$
J16082576-3906011	Lupus	$136.00^{+4.00}_{-4.00}$	$-1.09^{+0.05}_{-0.05}$	$3090.30^{+71.98}_{-70.34}$	$-0.85^{+0.03}_{-0.03}$	$51.24^{+3.66}_{-3.50}$
J16082751-1949047	USco	$145.00^{+20.00}_{-20.00}$	$-1.16^{+0.04}_{-0.04}$	$3090.30^{+145.64}_{145.64}$	$-0.84^{+0.03}_{-0.03}$	$0.82^{+0.42}_{-0.31}$
J16083026-3906111	Lupus	$159.00^{+4.00}_{-4.00}$	$-0.93^{+0.07}_{-0.07}$	$3311.31^{+77.13}_{-75.37}$	$-0.59^{+0.04}_{-0.04}$	$15.61^{+2.42}_{-1.14}$
J16083070-3828268	Lupus	$155.00^{+3.00}_{-3.00}$	$0.26^{+1.06}_{-1.06}$	$4897.79^{+230.83}_{-220.44}$	$0.15^{+0.29}_{-0.15}$	$170.75^{+8.07}_{-7.61}$
J16083081-3905488	Lupus	$165.00^{+4.00}_{-4.00}$	$-1.15^{+0.04}_{-0.04}$	$3090.30^{+71.98}_{-70.34}$	$-0.85^{+0.03}_{-0.03}$	$5.56^{+0.86}_{-0.66}$
J16084940-3905393	Lupus	$159.00^{+6.00}_{-6.00}$	$-0.81^{+0.09}_{-0.09}$	$3311.31^{+77.13}_{-75.37}$	$-0.59^{+0.05}_{-0.04}$	$2.97^{+1.06}_{-0.46}$
J16085157-3903177	Lupus	$159.00^{+3.00}_{-3.00}$	$-0.76^{+0.10}_{-0.10}$	$3311.31^{+77.13}_{-75.37}$	$-0.60^{+0.04}_{-0.04}$	$19.09^{+1.66}_{-1.09}$
J16085324-3914401	Lupus	$167.00^{+4.00}_{-4.00}$	$-0.68^{+0.12}_{-0.12}$	$3388.44^{+78.93}_{-77.13}$	$-0.54^{+0.05}_{-0.04}$	$27.18^{+2.36}_{-1.69}$
J16085373-3914367	Lupus	$156.00^{+31.00}_{-14.00}$	$-1.02^{+0.06}_{-0.06}$	$3090.30^{+71.98}_{-70.34}$	$-0.84^{+0.03}_{-0.02}$	$3.97^{+2.63}_{-0.99}$
J16085468-3937431	Lupus	$157.00^{+3.00}_{-3.00}$	$-0.68^{+0.12}_{-0.12}$	$3715.35^{+175.10}_{-167.22}$	$-0.28^{+0.17}_{-0.13}$	$227.63^{+10.48}_{-10.19}$
J16085553-3902339	Lupus	$159.00^{+4.00}_{-4.00}$	$-0.92^{+0.07}_{-0.07}$	$3162.28^{+73.66}_{-71.98}$	$-0.77^{+0.03}_{-0.03}$	$6.58^{+1.01}_{-0.82}$
J16085780-3902227	Lupus	$163.00^{+4.00}_{-4.00}$	$-1.37^{+0.02}_{-0.02}$	$3235.94^{+75.37}_{-73.66}$	$-0.68^{+0.04}_{-0.04}$	$30.50^{+2.08}_{-1.99}$
J16090002-1908368	USco	$138.53^{+2.75}_{-2.65}$	$-1.33^{+0.03}_{-0.03}$	$3090.30^{+145.64}_{145.64}$	$-0.84^{+0.04}_{-0.03}$	$1.69^{+0.20}_{-0.19}$
J16090075-1908526	USco	$137.08^{+1.48}_{-1.45}$	$-0.45^{+0.21}_{-0.21}$	$3890.45^{+90.62}_{90.62}$	$-0.19^{+0.17}_{-0.14}$	$45.33^{+1.88}_{-1.81}$
J16090141-3925119	Lupus	$164.00^{+4.00}_{-4.00}$	$-1.04^{+0.05}_{-0.05}$	$3311.31^{+77.13}_{-75.37}$	$-0.58^{+0.05}_{-0.04}$	$24.70^{+5.68}_{-2.76}$

Table 7 continued

Table 7 (continued)

2MASS	Region	Distance	$\log(L_\star)$	$T_{\rm eff}$	$\log(M_\star)$	$L_{\rm mm}$[a]
		(pc)	$(L_\odot)$	(K)	$(M_\odot)$	(mJy)
J16090185-3905124	Lupus	$162.00^{+3.00}_{-3.00}$	$-0.69^{+0.12}_{-0.12}$	$3162.28^{+73.66}_{-71.98}$	$-0.73^{+0.02}_{-0.02}$	$133.50^{+6.38}_{-5.80}$
J16093558-1828232	USco	$164.63^{+2.81}_{-2.72}$	$-1.06^{+0.05}_{-0.05}$	$3388.44^{+159.69}_{159.69}$	$-0.52^{+0.05}_{-0.04}$	$0.95^{+0.25}_{-0.23}$
J16094434-3913301	Lupus	$158.00^{+3.00}_{-3.00}$	$-0.56^{+0.16}_{-0.16}$	$3311.31^{+77.13}_{-75.37}$	$-0.62^{+0.04}_{-0.03}$	$13.63^{+1.18}_{-0.88}$
J16094864-3911169	Lupus	$163.00^{+3.00}_{-3.00}$	$-0.14^{+0.42}_{-0.42}$	$4365.16^{+205.72}_{-196.46}$	$0.01^{+0.88}_{-0.15}$	$85.54^{+4.44}_{-4.03}$
J16095628-3859518	Lupus	$156.00^{+4.00}_{-4.00}$	$-1.81^{+0.01}_{-0.01}$	$3019.95^{+70.34}_{-68.74}$	$-1.00^{+0.03}_{-0.02}$	$10.06^{+1.04}_{-0.86}$
J16101984-3836065	Lupus	$158.00^{+4.00}_{-4.00}$	$-1.35^{+0.03}_{-0.03}$	$2951.21^{+68.74}_{-67.18}$	$-1.09^{+0.02}_{-0.02}$	$2.67^{+1.61}_{-0.50}$
J16102955-3922144	Lupus	$163.00^{+4.00}_{-4.00}$	$-0.99^{+0.06}_{-0.06}$	$3235.94^{+75.37}_{-73.66}$	$-0.65^{+0.05}_{-0.03}$	$10.71^{+1.53}_{-1.04}$
J16104636-1840598	USco	$142.59^{+2.84}_{-2.73}$	$-1.57^{+0.02}_{-0.02}$	$3162.28^{+149.03}_{149.03}$	$-0.78^{+0.04}_{-0.03}$	$1.85^{+0.25}_{-0.23}$
J16122737-2009596	USco	$146.64^{+4.10}_{-3.88}$	$-1.44^{+0.02}_{-0.02}$	$3162.28^{+149.03}_{149.03}$	$-0.76^{+0.04}_{-0.03}$	$0.58^{+0.22}_{-0.20}$
J16124373-3815031	Lupus	$159.00^{+3.00}_{-3.00}$	$-0.41^{+0.23}_{-0.23}$	$3715.35^{+175.10}_{-167.22}$	$-0.32^{+0.14}_{-0.11}$	$39.60^{+2.58}_{-2.23}$
J16133650-2503473	USco	$145.00^{+20.00}_{-20.00}$	$-1.00^{+0.06}_{-0.06}$	$3311.31^{+156.06}_{156.06}$	$-0.59^{+0.04}_{-0.04}$	$0.94^{+0.54}_{-0.39}$
J16134410-3736462	Lupus	$159.00^{+4.00}_{-4.00}$	$-1.37^{+0.02}_{-0.02}$	$3162.28^{+73.66}_{-71.98}$	$-0.76^{+0.04}_{-0.03}$	$3.87^{+1.15}_{-0.56}$
J16141107-2305362	USco	$145.00^{+20.00}_{-20.00}$	$0.43^{+1.57}_{-1.57}$	$4897.79^{+230.83}_{230.83}$	$0.67^{+0.11}_{-0.88}$	$5.12^{+1.70}_{-1.43}$
J16142029-1906481	USco	$142.46^{+2.57}_{-2.48}$	$-0.33^{+0.27}_{-0.27}$	$3890.45^{+90.62}_{90.62}$	$-0.21^{+0.18}_{-0.14}$	$42.13^{+1.77}_{-1.67}$
J16143367-1900133	USco	$141.47^{+2.27}_{-2.20}$	$-0.47^{+0.20}_{-0.20}$	$3388.44^{+159.69}_{159.69}$	$-0.56^{+0.04}_{-0.04}$	$1.27^{+0.21}_{-0.20}$
J16153456-2242421	USco	$145.00^{+20.00}_{-20.00}$	$-0.13^{+0.43}_{-0.43}$	$3890.45^{+90.62}_{90.62}$	$-0.23^{+0.15}_{-0.12}$	$12.60^{+3.88}_{-3.33}$
J16154416-1921171	USco	$131.34^{+2.19}_{-2.12}$	$-0.31^{+0.29}_{-0.29}$	$4365.16^{+101.68}_{101.68}$	$-0.03^{+0.19}_{-0.08}$	$20.74^{+0.84}_{-0.80}$
J16163345-2521505	USco	$161.92^{+1.49}_{-1.46}$	$-0.83^{+0.09}_{-0.09}$	$3801.89^{+88.56}_{88.56}$	$-0.16^{+0.54}_{-0.13}$	$3.85^{+0.48}_{-0.46}$
J16181904-2028479	USco	$137.45^{+2.47}_{-2.39}$	$-1.32^{+0.03}_{-0.03}$	$3162.28^{+149.03}_{149.03}$	$-0.75^{+0.04}_{-0.03}$	$4.45^{+0.28}_{-0.27}$
J16270942-2148457	USco	$139.66^{+2.81}_{-2.70}$	$-1.55^{+0.02}_{-0.02}$	$3162.28^{+149.03}_{149.03}$	$-0.78^{+0.04}_{-0.03}$	$2.86^{+0.24}_{-0.22}$

[a]For consistency, our definition of $L_{\rm mm}$ is the same as found in Andrews et al. (2018a). It is a flux density scaled to 140 pc.

C. DETERMINATION AND REMOVAL OF SPURIOUS MODELING

During our model fitting we realized that low signal-to-noise data can result in Nuker profiles that fit the noise with a disk model that is typically extended, faint, highly inclined and/or ring-like. An example is shown in Figure 13. In these cases the uncertainties on the disk sizes are large. In order to cull these models from our analysis, we examine by eye sources where the uncertainty in disk size is larger than 66% of the disk size. By observing the fitting in the UV plane, and comparing continuum images of the data and model, we can identify these cases. Of the 23 disks that meet this metric, we find 15 that are obviously problematic, and hence removed them from our analysis (see Section 4.1).

Sources removed from the Cha I sample are: J11100785-7727480, J11064180-7635489, J11092266-7634320, J11071206-7632232 and J11045701-7715569.

Sources removed from the USco sample are: J16095933-1800090, J16095361-1754474, J16115091-2012098, J16102857-
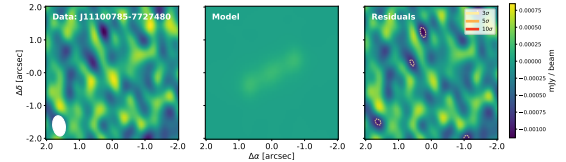
Figure 13. Example of a Nuker profile fitting the noise and not the faint disk emission from J11100785-7727480. The flux density is only 0.49 ± 0.16 mJy (Pascucci et al. 2016), a marginal 3σ detection.

1904469, J16073939-1917472, J15534211-2049282, J16035793-1942108, J16043916-1942459, J16135434-2320342 and J16303390-2428062

D. $\log L_{\rm mm} - \log M_\star$ RELATION

Our sample population is a subset of the entire disk population in each region, and is biased towards resolved sources. In order to understand this bias, we test our sample for a correlation between $L_{\rm mm}$ and $M_\star$ so that we can compare it to previously measured $L_{\rm mm}-M_\star$ correlations (e.g. Ansdell et al. 2016; Pascucci et al. 2016). We find a shallower slope for the $\log L_{\rm mm} - \log M_\star$ cor-

relation, and discuss this in detail at the end of Section 4.
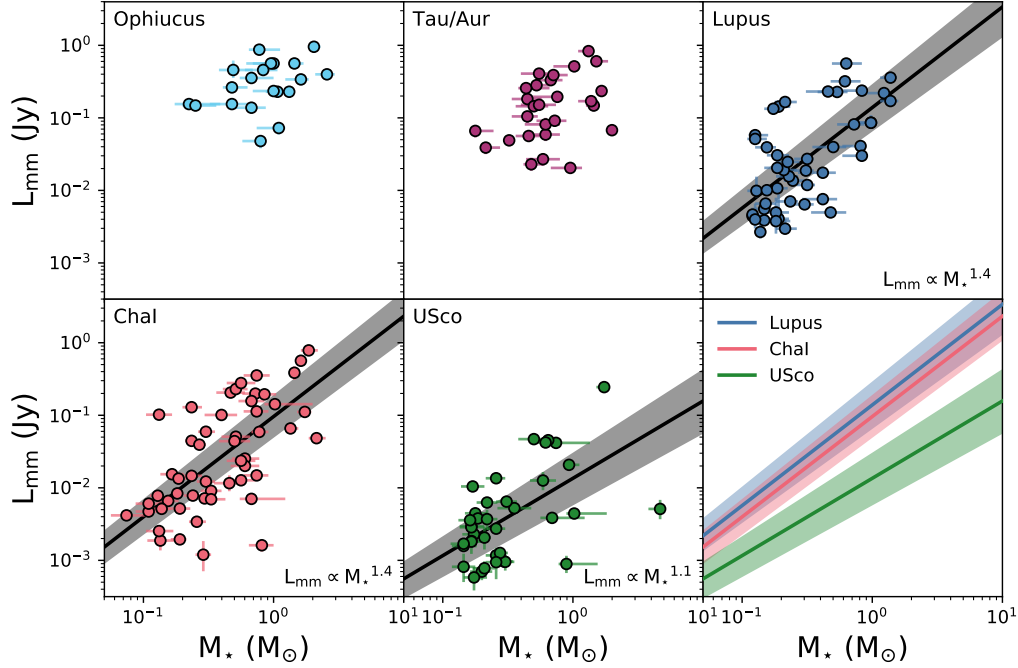
Figure 14. Fitting of $\log L_{\rm mm} - \log M_\star$. The first 5 panels (left to right; top to bottom; ordered by region age) show the model results of each region as circles (resolved) and triangles (upper-limits). The best fit from MCMC linear regression is plotted as a black line, and surrounded by our 68% confidence intervals in grey. The last panel replots the bests fits of each region (and the corresponding 68% confidence intervals) so that they can be directly compared. Fit parameters for each region are given in Table 8.

Table 8. $\log L_{\rm mm} - \log M_\star$ statistical tests

| Region | Shapiro $L_{\rm mm}$ | | Shapiro $M_\star$ | | Pearson r | | Spearman ρ | | Regression Parameters | | | |
	stat	p-value	stat	p-value	stat	p-value	stat	p-value	α	β	σ	$\hat{\rho}$
Oph	0.91	6.71e-02	0.91	5.66e-02	0.38	9.86e-02	0.30	2.01e-01	$-0.53^{+0.083}_{-0.08}$	$0.49^{+0.36}_{-0.36}$	$0.35^{+0.074}_{-0.056}$	$0.61^{+0.17}_{-0.28}$
Tau/Aur	0.87	3.25e-03	0.82	2.86e-04	0.37	6.06e-02	0.37	5.54e-02	$-0.77^{+0.1}_{-0.1}$	$0.75^{+0.36}_{-0.36}$	$0.43^{+0.074}_{-0.058}$	$0.66^{+0.12}_{-0.18}$
Lupus	0.77	2.89e-07	0.67	3.46e-09	0.56	3.82e-05	0.61	3.94e-06	$-0.86^{+0.2}_{-0.1}$	$1.4^{+0.2}_{-0.2}$	$0.51^{+0.06}_{-0.05}$	$0.81^{+0.05}_{-0.06}$
Cha I	0.8	1.19e-07	0.6	1.35e-11	0.61	2.78e-07	0.55	6.20e-06	$-1^{+0.1}_{-0.1}$	$1.4^{+0.2}_{-0.2}$	$0.56^{+0.06}_{-0.06}$	$0.82^{+0.05}_{-0.06}$
USco	0.45	8.04e-11	0.34	7.70e-12	0.29	7.48e-02	0.49	1.81e-03	$-1.9^{+0.2}_{-0.2}$	$1.1^{+0.3}_{-0.3}$	$0.52^{+0.07}_{-0.06}$	$0.75^{+0.08}_{-0.1}$

NOTE—Values we consider unreliable are greyed out (see Section 5.1).

E. CORRELATION OF R_{90} AND R_{68}

Different emission fractions have been used to define the location of R_{eff} in past works. For example, Tripathi et al. (2017) and Andrews et al. (2018a), who analyze low- and medium-resolution SMA and ALMA data, calculate the radius containing 68% of the total flux (R_{68}). However, high-resolution ALMA images have shown that R_{68} does not properly capture the radial extent of the disk, several sub-structures are left out, hence more recent works compute and analyze the 90% (R_{90}) or 95% (R_{95}) dust radius (see Long et al. 2018 and Huang et al. 2018). In order to compare the results of this work with disk sizes from the literature, we are interested in understanding if R_{68} is a reliable predictor of R_{90}.
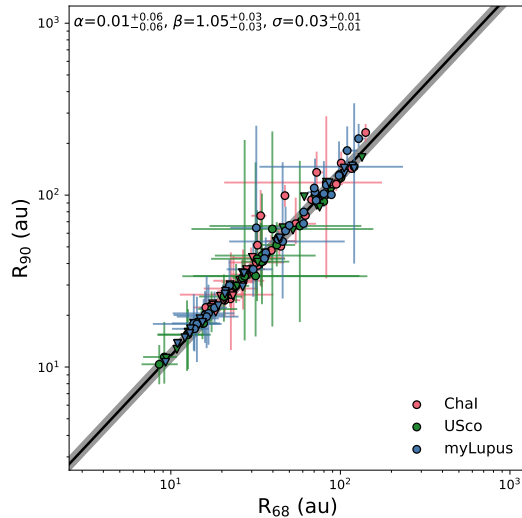
Figure 15. Here we compare our R_{68} dust-disk size estimates with the R_{90} size for each disk. Constrained disks sizes are plotted as circles while upper-limits are given as triangles. Symbols are color coded according to their associated region. The correlation between R_{68} and R_{90} is measured by fitting the values using linmix. The best fit is shown as a black line, with a 1-sigma confidence interval in gray. The parameters resulting from the mcmc chain are given in the upper left of the figure (see Equation E2).

The 68% and 90% emission radii we measure from modeled disks in Lupus, Cha I, and USco are shown in Figure 15. Visual inspection suggests that the two disk sizes are strongly correlated. We calculate the Spearman ρ rank-order correlation coefficient[6] to test the null hypothesis that the two variables are uncorrelated. As

shown in Table 9, the correlation coefficient is nearly unity (positive rank order) with an extremely low probability (p-value) that R_{68} and R_{90} are uncorrelated.

We then fit the data using the Bayesian linear regression method developed by Kelly (2007) and report the results in Table 9. Using these best fitting parameters, we can convert the R_{68} to a R_{90} disk size:.

$$\log R_{90} = -0.037(\mathrm{au}) + 1.1\log R_{68}(\mathrm{au}) \qquad (E2)$$

---

[6] We cannot apply the Pearson correlation test, which tests for a linear relationship between two quantities, because we find that R_{68} and R_{90} are not bivariate normally distributed.

Table 9. R_{90} vs R_{68} statistical analysis and fitting

	Shapiro R_{68}		Shapiro R_{90}		Spearman ρ		Regression Parameters			
	stat	p-value	stat	p-value	stat	p-value	α	β	σ	corr
R_{90} vs R_{68}	0.87	3.1e-07	0.84	4.1e-08	0.98	2.6e-63	$0.01^{+0.06}_{-0.06}$	$1.05^{+0.03}_{-0.03}$	$0.03^{+0.01}_{-0.01}$	$1.00^{+0.00}_{-0.00}$

F. INDIVIDUAL MODELING RESULTS

Table 10. Modeling Parameters

2MASS	R_{68} (")	R_{90} (")	R_t (")	f_0 (Jy/Sr)	α	β	γ	i (°)	PA (°)	dDec (")	dRA (")	hwcorr
J10533978-7712338	< 0.11	< 0.13	$0.11^{+0.05}_{-0.05}$	$9.98^{+0.52}_{-0.35}$	$60.00^{+32.12}_{-40.13}$	$9.37^{+3.55}_{-3.31}$	$-2.03^{+1.69}_{-2.69}$	$51.64^{+24.41}_{-28.56}$	$58.51^{+58.02}_{-37.85}$	$-0.01^{+0.03}_{-0.03}$	$-0.45^{+0.03}_{-0.03}$	$-0.96^{+0.00}_{-0.00}$
J10555973-7724399	$0.11^{+0.03}_{-0.01}$	$0.13^{+0.03}_{-0.03}$	$0.10^{+0.02}_{-0.02}$	$10.84^{+0.44}_{-0.16}$	$52.10^{+36.53}_{-26.66}$	$8.68^{+3.24}_{-3.09}$	$-2.75^{+2.09}_{-2.20}$	$43.74^{+11.77}_{-13.83}$	$88.60^{+29.78}_{-26.10}$	$-0.07^{+0.01}_{-0.01}$	$-0.07^{+0.01}_{-0.01}$	$-3.79^{+0.01}_{-0.01}$
J10561638-7630530	< 0.12	< 0.14	$0.10^{+0.04}_{-0.04}$	$10.23^{+0.49}_{-0.51}$	$56.36^{+35.09}_{-41.50}$	$9.79^{+3.28}_{-4.37}$	$-2.55^{+1.85}_{-1.57}$	$41.79^{+25.26}_{-17.18}$	$62.34^{+25.32}_{-23.98}$	$-0.07^{+0.02}_{-0.03}$	$-0.37^{+0.02}_{-0.01}$	$-0.49^{+0.01}_{-0.00}$
J10563044-7711393	$0.77^{+0.03}_{-0.03}$	$1.27^{+0.15}_{-0.15}$	$0.54^{+0.05}_{-0.04}$	$10.01^{+0.05}_{-0.10}$	$65.43^{+31.18}_{-46.05}$	$4.27^{+0.44}_{-0.36}$	$-3.57^{+1.37}_{-1.73}$	$51.64^{+1.27}_{-1.09}$	$167.35^{+1.37}_{-1.92}$	$0.06^{+0.01}_{-0.01}$	$-0.41^{+0.01}_{-0.01}$	$-3.88^{+0.01}_{-0.01}$
J10580597-7711501	< 0.11	< 0.13	$0.11^{+0.03}_{-0.05}$	$10.01^{+0.47}_{-0.70}$	$62.61^{+28.85}_{-29.76}$	$9.59^{+2.91}_{-3.74}$	$-2.06^{+1.74}_{-2.43}$	$55.33^{+18.43}_{-23.39}$	$147.06^{+17.04}_{-29.60}$	$-0.02^{+0.03}_{-0.03}$	$-0.37^{+0.03}_{-0.03}$	$-0.48^{+0.00}_{-0.00}$
J10581677-7717170	$0.62^{+0.01}_{-0.01}$	$0.76^{+0.03}_{-0.02}$	$0.57^{+0.02}_{-0.03}$	$10.43^{+0.06}_{-0.03}$	$65.83^{+27.95}_{-24.66}$	$7.60^{+1.27}_{-0.75}$	$-3.74^{+0.49}_{-0.86}$	$42.01^{+0.98}_{-0.77}$	$157.12^{+1.36}_{-1.56}$	$-0.06^{+0.00}_{-0.00}$	$-0.38^{+0.00}_{-0.00}$	$-4.10^{+0.01}_{-0.01}$
J10590108-7722407	$0.23^{+0.01}_{-0.01}$	$0.31^{+0.05}_{-0.03}$	$0.21^{+0.04}_{-0.04}$	$10.53^{+0.16}_{-0.29}$	$42.87^{+43.72}_{-29.18}$	$7.36^{+3.85}_{-2.48}$	$-2.89^{+2.14}_{-1.64}$	$31.40^{+4.96}_{-3.37}$	$-16.22^{+34.30}_{-5.49}$	$-0.16^{+0.01}_{-0.01}$	$-0.42^{+0.01}_{-0.00}$	$-3.82^{+0.01}_{-0.01}$
J10590699-7701404	$0.36^{+0.04}_{-0.03}$	$0.50^{+0.04}_{-0.03}$	$0.36^{+0.03}_{-0.04}$	$10.45^{+0.11}_{-0.05}$	$52.69^{+38.02}_{-28.69}$	$5.83^{+1.27}_{-1.10}$	$0.13^{+0.02}_{-0.04}$	$31.47^{+1.48}_{-1.86}$	$36.46^{+4.42}_{-3.16}$	$0.16^{+0.00}_{-0.00}$	$-0.42^{+0.00}_{-0.00}$	$-4.47^{+0.01}_{-0.01}$
J11004022-7619280	$0.25^{+0.01}_{-0.01}$	$0.52^{+0.08}_{-0.07}$	$0.16^{+0.07}_{-0.04}$	$10.29^{+0.26}_{-0.29}$	$35.15^{+50.60}_{-21.38}$	$3.68^{+0.85}_{-0.32}$	$-0.70^{+0.78}_{-2.17}$	$3.67^{+3.80}_{-2.35}$	$82.69^{+17.18}_{-24.61}$	$-0.01^{+0.00}_{-0.00}$	$-0.27^{+0.00}_{-0.00}$	$-0.58^{+0.00}_{-0.01}$
J11022491-7733357	$0.25^{+0.01}_{0.00}$	$0.29^{+0.01}_{-0.01}$	$0.25^{+0.02}_{-0.01}$	$10.97^{+0.07}_{-0.22}$	$49.20^{+35.35}_{-23.69}$	$12.16^{+1.94}_{-2.07}$	$-4.34^{+2.17}_{-1.31}$	$10.92^{+8.31}_{-5.57}$	$83.72^{+27.61}_{-20.18}$	$0.10^{+0.00}_{-0.00}$	$-0.49^{+0.00}_{-0.01}$	$-4.14^{+0.01}_{-0.01}$
J11023265-7729129	$0.42^{+0.48}_{-0.32}$	$0.61^{+0.87}_{-0.44}$	$0.39^{+0.31}_{-0.29}$	$8.02^{+0.75}_{-0.37}$	$58.20^{+24.08}_{-32.81}$	$9.00^{+3.82}_{-4.73}$	$-3.07^{+1.84}_{-2.06}$	$62.73^{+15.22}_{-44.60}$	$113.53^{+47.12}_{-76.85}$	$-1.56^{+0.23}_{-0.25}$	$-0.72^{+0.20}_{-0.23}$	$-0.96^{+0.00}_{-0.01}$
J11025504-7721508	< 0.23	< 0.30	$0.15^{+0.13}_{-0.09}$	$8.82^{+0.63}_{-0.64}$	$42.36^{+35.01}_{-23.83}$	$5.55^{+5.11}_{-2.67}$	$-2.69^{+1.91}_{-2.08}$	$53.30^{+19.94}_{-19.75}$	$162.52^{+21.91}_{-30.27}$	$0.01^{+0.13}_{-0.14}$	$-0.39^{+0.05}_{-0.09}$	$-0.47^{+0.00}_{-0.00}$
J11040425-7639328	< 0.09	< 0.12	$0.10^{+0.01}_{-0.04}$	$9.65^{+0.36}_{-1.37}$	$33.01^{+41.65}_{-21.70}$	$6.96^{+5.53}_{-3.20}$	$-0.33^{+0.56}_{-2.77}$	$33.79^{+15.48}_{-21.42}$	$54.00^{+24.09}_{-31.55}$	$-0.09^{+0.04}_{-0.04}$	$-0.40^{+0.02}_{-0.02}$	$-0.48^{+0.00}_{-0.00}$
J11040909-7627193	$0.18^{+0.02}_{-0.02}$	$0.22^{+0.02}_{-0.01}$	$0.18^{+0.02}_{-0.03}$	$10.77^{+0.27}_{-0.21}$	$65.72^{+30.64}_{-34.34}$	$9.05^{+3.19}_{-2.22}$	$-1.25^{+1.06}_{-2.99}$	$38.95^{+8.11}_{-16.83}$	$47.79^{+16.20}_{-8.93}$	$-0.08^{+0.00}_{-0.00}$	$-0.22^{+0.00}_{-0.00}$	$-3.96^{+0.01}_{-0.01}$
J11044258-7741571	$0.14^{+0.05}_{-0.05}$	$0.17^{+0.09}_{-0.05}$	$0.13^{+0.06}_{-0.05}$	$9.91^{+0.54}_{-0.62}$	$58.33^{+24.87}_{-32.95}$	$10.16^{+2.68}_{-4.19}$	$-3.01^{+3.09}_{-2.38}$	$58.40^{+12.25}_{-20.78}$	$79.18^{+19.56}_{-25.18}$	$-0.03^{+0.04}_{-0.03}$	$-0.30^{+0.02}_{-0.03}$	$-0.49^{+0.01}_{-0.01}$
J11045701-7715569	< 0.12	< 0.13	$0.09^{+0.06}_{-0.04}$	$10.06^{+0.99}_{-0.40}$	$47.21^{+28.55}_{-29.89}$	$10.09^{+3.52}_{-5.78}$	$-2.35^{+1.62}_{-2.26}$	$39.82^{+32.66}_{-31.70}$	$72.86^{+24.09}_{-46.51}$	$-0.06^{+0.03}_{-0.02}$	$-0.37^{+0.03}_{-0.03}$	$-0.95^{+0.00}_{-0.00}$
J11062554-7633418	$0.16^{+0.01}_{-0.02}$	$0.36^{+0.15}_{-0.13}$	$0.08^{+0.05}_{-0.02}$	$10.97^{+0.20}_{-0.32}$	$35.82^{+50.57}_{-16.53}$	$3.36^{+1.07}_{-0.41}$	$-2.35^{+1.41}_{-2.05}$	$53.42^{+4.13}_{-4.12}$	$31.46^{+4.63}_{-5.70}$	$-0.05^{+0.00}_{-0.00}$	$-0.42^{+0.00}_{-0.00}$	$-0.56^{+0.00}_{-0.00}$
J11064510-7727023	< 0.20	< 0.23	$0.19^{+0.08}_{-0.08}$	$9.14^{+0.67}_{-0.29}$	$44.01^{+28.92}_{-27.20}$	$8.23^{+3.17}_{-3.43}$	$-3.01^{+2.41}_{-1.68}$	$45.30^{+29.90}_{-31.16}$	$108.46^{+47.09}_{-69.55}$	$0.02^{+0.06}_{-0.04}$	$-0.06^{+0.06}_{-0.06}$	$-0.96^{+0.00}_{-0.01}$
J11065906-7718535	$0.12^{+0.01}_{-0.01}$	$0.13^{+0.02}_{-0.01}$	$0.10^{+0.01}_{-0.01}$	$10.76^{+0.12}_{-0.12}$	$72.57^{+26.67}_{-34.62}$	$10.71^{+2.73}_{-1.75}$	$-3.74^{+1.89}_{-1.75}$	$28.95^{+16.85}_{-7.13}$	$161.66^{+27.46}_{-34.25}$	$0.12^{+0.01}_{-0.00}$	$-0.48^{+0.00}_{-0.00}$	$-0.50^{+0.00}_{-0.00}$
J11065939-7530559	$0.12^{+0.09}_{-0.06}$	$0.13^{+0.10}_{-0.07}$	$0.10^{+0.07}_{-0.07}$	$9.71^{+0.67}_{-1.59}$	$78.46^{+13.10}_{-44.02}$	$10.45^{+2.36}_{-4.76}$	$-1.04^{+1.31}_{-2.80}$	$49.93^{+20.30}_{-30.04}$	$110.40^{+54.41}_{-70.98}$	$-0.05^{+0.06}_{-0.02}$	$-0.29^{+0.02}_{-0.03}$	$-0.48^{+0.01}_{-0.00}$
J11070925-7718471	< 0.25	< 0.33	$0.25^{+0.48}_{-0.17}$	$8.14^{+0.90}_{-0.46}$	$43.94^{+39.25}_{-37.28}$	$9.34^{+4.01}_{-3.74}$	$-3.90^{+2.80}_{-1.39}$	$41.62^{+33.89}_{-30.66}$	$99.42^{+44.00}_{-59.84}$	$0.14^{+0.30}_{-0.16}$	$-0.49^{+0.20}_{-0.28}$	$-0.96^{+0.00}_{-0.00}$
J11071206-7632232	$0.22^{+0.05}_{-0.04}$	$0.28^{+0.07}_{-0.05}$	$0.23^{+0.08}_{-0.05}$	$9.72^{+0.45}_{-0.45}$	$60.96^{+25.12}_{-35.79}$	$9.68^{+3.42}_{-2.72}$	$-2.49^{+2.15}_{-2.61}$	$63.02^{+11.34}_{-30.66}$	$114.64^{+10.45}_{-19.65}$	$-0.01^{+0.02}_{-0.02}$	$-0.42^{+0.01}_{-0.02}$	$-0.97^{+0.00}_{-0.00}$
J11071330-7743498	< 0.11	< 0.12	$0.09^{+0.09}_{-0.05}$	$10.17^{+0.86}_{-0.81}$	$66.05^{+18.58}_{-34.88}$	$11.24^{+2.73}_{-4.16}$	$-2.11^{+1.62}_{-2.64}$	$64.44^{+13.87}_{-31.30}$	$70.54^{+63.54}_{-56.50}$	$0.13^{+0.03}_{-0.03}$	$-0.65^{+0.03}_{-0.03}$	$-0.96^{+0.00}_{-0.00}$
J11071860-7732516	< 0.15	< 0.22	$0.13^{+0.21}_{-0.09}$	$8.53^{+1.28}_{-0.73}$	$48.93^{+45.19}_{-31.94}$	$9.72^{+2.96}_{-3.76}$	$-3.82^{+2.59}_{-1.29}$	$34.73^{+20.86}_{-21.95}$	$96.82^{+22.82}_{-34.87}$	$0.09^{+0.19}_{-0.22}$	$-0.45^{+0.14}_{-0.19}$	$-0.48^{+0.00}_{-0.00}$
J11072074-7738073	< 0.09	< 0.12	$0.06^{+0.03}_{-0.03}$	$10.05^{+1.22}_{-1.52}$	$66.39^{+20.46}_{-38.85}$	$6.78^{+1.87}_{-3.30}$	$0.13^{+0.19}_{-1.19}$	$45.33^{+17.53}_{-22.49}$	$37.64^{+103.18}_{-26.28}$	$-0.02^{+0.01}_{-0.01}$	$-0.42^{+0.01}_{-0.01}$	$-3.77^{+0.01}_{-0.01}$
J11074366-7739411	$0.17^{+0.01}_{-0.01}$	$0.20^{+0.03}_{-0.02}$	$0.16^{+0.06}_{-0.02}$	$11.06^{+0.12}_{-0.68}$	$75.09^{+23.28}_{-33.11}$	$8.62^{+3.88}_{-1.51}$	$-3.33^{+3.40}_{-1.50}$	$38.59^{+5.65}_{-14.07}$	$129.89^{+4.70}_{-7.51}$	$-0.05^{+0.00}_{-0.00}$	$-0.35^{+0.00}_{-0.00}$	$-3.93^{+0.01}_{-0.01}$
J11074656-7615174	< 0.09	< 0.12	$0.10^{+0.07}_{-0.04}$	$10.03^{+0.49}_{-0.68}$	$54.66^{+38.40}_{-36.42}$	$8.21^{+3.30}_{-3.48}$	$-1.92^{+1.90}_{-2.33}$	$63.22^{+14.18}_{-15.23}$	$93.97^{+25.73}_{-29.82}$	$0.10^{+0.04}_{-0.05}$	$-0.31^{+0.03}_{-0.03}$	$-0.48^{+0.01}_{-0.01}$
J11075730-7717262	< 0.15	< 0.17	$0.15^{+0.05}_{-0.07}$	$9.56^{+0.44}_{-1.68}$	$34.05^{+41.33}_{-21.32}$	$8.32^{+2.69}_{-3.65}$	$-1.29^{+1.58}_{-3.67}$	$30.10^{+17.99}_{-15.69}$	$-4.06^{+42.06}_{-22.15}$	$-0.05^{+0.05}_{-0.07}$	$-0.41^{+0.03}_{-0.05}$	$-3.75^{+0.01}_{-0.01}$

Table 10 continued

Table 10 *(continued)*

2MASS	R_{68} (″)	R_{90} (″)	R_t (″)	f_0 (Jy/Sr)	α	β	γ	i (°)	PA (°)	dDec (″)	dRA (″)	lnwcorr
J1075809-7742413	<0.08	<0.09	$0.07^{+0.05}_{-0.03}$	$10.58^{+0.98}_{-0.41}$	$56.38^{+29.16}_{-33.71}$	$9.59^{+4.01}_{-3.14}$	$-2.10^{+1.53}_{-2.12}$	$43.35^{+31.28}_{-30.26}$	$86.70^{+62.10}_{-46.34}$	$-0.02^{+0.01}_{-0.01}$	$-0.35^{+0.02}_{-0.01}$	$-0.96^{+0.00}_{-0.00}$
J1108002-7717304	<0.13	<0.16	$0.09^{+0.24}_{-0.08}$	$8.16^{+1.87}_{-0.45}$	$44.31^{+24.98}_{-35.08}$	$7.64^{+4.66}_{-3.73}$	$-2.68^{+2.04}_{-2.25}$	$47.22^{+32.04}_{-33.39}$	$93.32^{+68.02}_{-65.02}$	$0.46^{+0.19}_{-0.27}$	$0.53^{+0.18}_{-0.23}$	$-0.96^{+0.00}_{-0.00}$
J1081509-7733531	$0.33^{+0.02}_{-0.01}$	$0.40^{+0.02}_{-0.02}$	$0.31^{+0.06}_{-0.03}$	$10.65^{+0.11}_{-0.22}$	$65.90^{+27.72}_{-33.73}$	$8.55^{+4.66}_{-2.32}$	$-2.30^{+1.54}_{-1.62}$	$37.60^{+1.85}_{-2.40}$	$163.18^{+3.00}_{-3.62}$	$-0.25^{+0.00}_{-0.00}$	$0.99^{+0.00}_{-0.00}$	$-4.05^{+0.01}_{-0.01}$
J1083905-7716042	<0.09	<0.11	$0.08^{+0.10}_{-0.06}$	$10.05^{+0.77}_{-2.06}$	$28.11^{+42.67}_{-10.53}$	$12.44^{+1.59}_{-3.04}$	$-0.13^{+0.49}_{-3.26}$	$38.78^{+13.11}_{-21.39}$	$103.29^{+35.77}_{-17.28}$	$0.09^{+0.02}_{-0.02}$	$-0.38^{+0.01}_{-0.02}$	$-3.78^{+0.01}_{-0.01}$
J1085367-7521359	$0.15^{+0.03}_{-0.03}$	$0.18^{+0.04}_{-0.04}$	$0.15^{+0.04}_{-0.04}$	$10.39^{+0.28}_{-0.26}$	$49.40^{+28.33}_{-28.05}$	$10.10^{+3.06}_{-2.96}$	$-1.36^{+0.93}_{-2.58}$	$37.83^{+15.49}_{-22.38}$	$131.42^{+16.13}_{-18.44}$	$-0.02^{+0.01}_{-0.01}$	$-0.25^{+0.01}_{-0.01}$	$-3.81^{+0.01}_{-0.01}$
J1085464-7702129	<0.13	<0.16	$0.10^{+0.06}_{-0.03}$	$10.15^{+0.45}_{-0.41}$	$43.94^{+32.82}_{-27.15}$	$9.43^{+3.50}_{-3.63}$	$-3.16^{+2.03}_{-2.19}$	$49.12^{+27.85}_{-36.95}$	$66.05^{+73.92}_{-35.02}$	$-0.11^{+0.02}_{-0.02}$	$-0.15^{+0.02}_{-0.02}$	$-0.96^{+0.00}_{-0.01}$
J1092379-7623207	$0.17^{+0.01}_{-0.01}$	$0.27^{+0.07}_{-0.04}$	$0.14^{+0.02}_{-0.03}$	$10.87^{+0.15}_{-0.18}$	$60.40^{+38.00}_{-26.92}$	$5.19^{+2.21}_{-1.17}$	$-1.87^{+1.44}_{-2.12}$	$15.63^{+26.51}_{-10.29}$	$55.18^{+26.51}_{-33.20}$	$-0.05^{+0.00}_{-0.00}$	$-0.35^{+0.01}_{-0.02}$	$-3.94^{+0.01}_{-0.01}$
J1094621-7634463	<0.14	<0.19	$0.13^{+0.06}_{-0.05}$	$9.62^{+0.46}_{-0.28}$	$44.13^{+45.34}_{-25.03}$	$9.95^{+3.74}_{-5.10}$	$-2.03^{+1.65}_{-2.58}$	$23.95^{+14.42}_{-12.36}$	$148.16^{+34.58}_{-26.08}$	$-0.05^{+0.04}_{-0.07}$	$-0.43^{+0.03}_{-0.06}$	$-3.76^{+0.01}_{-0.01}$
J1094742-7726290	$0.53^{+0.02}_{-0.02}$	$0.80^{+0.13}_{-0.09}$	$0.49^{+0.06}_{-0.04}$	$9.87^{+0.06}_{-0.05}$	$69.02^{+26.36}_{-39.19}$	$4.83^{+1.58}_{-0.57}$	$0.12^{+0.02}_{-0.02}$	$54.12^{+1.27}_{-1.93}$	$29.37^{+1.85}_{-1.74}$	$-0.07^{+0.01}_{-0.01}$	$-0.41^{+0.00}_{-0.01}$	$-3.87^{+0.01}_{-0.01}$
J1095340-7634255	$0.36^{+0.03}_{-0.02}$	$0.67^{+0.22}_{-0.13}$	$0.24^{+0.05}_{-0.05}$	$10.24^{+0.30}_{-0.16}$	$55.32^{+28.30}_{-28.08}$	$3.76^{+0.66}_{-0.50}$	$-1.09^{+0.89}_{-3.16}$	$51.26^{+2.78}_{-3.23}$	$134.18^{+4.55}_{-3.08}$	$0.10^{+0.01}_{-0.01}$	$-0.33^{+0.01}_{-0.01}$	$-3.84^{+0.01}_{-0.01}$
J1100369-7633291	<0.15	<0.18	$0.14^{+0.34}_{-0.05}$	$10.16^{+0.99}_{-2.00}$	$33.46^{+34.57}_{-19.37}$	$6.84^{+3.87}_{-1.81}$	$-1.50^{+1.78}_{-2.86}$	$64.77^{+12.54}_{-13.92}$	$131.01^{+25.56}_{-20.69}$	$0.03^{+0.02}_{-0.02}$	$-0.31^{+0.01}_{-0.02}$	$-3.77^{+0.02}_{-0.01}$
J1100469-7635452	$0.18^{+0.07}_{-0.06}$	$0.22^{+0.13}_{-0.07}$	$0.18^{+0.22}_{-0.08}$	$9.88^{+0.47}_{-1.47}$	$54.18^{+38.14}_{-30.42}$	$8.77^{+3.62}_{-4.67}$	$-0.34^{+0.62}_{-2.60}$	$60.67^{+15.98}_{-25.29}$	$89.84^{+27.43}_{-14.71}$	$0.03^{+0.02}_{-0.03}$	$-0.34^{+0.02}_{-0.03}$	$-3.78^{+0.01}_{-0.01}$
J1101141-7635292	$0.14^{+0.02}_{-0.01}$	$0.18^{+0.02}_{-0.02}$	$0.15^{+0.01}_{-0.02}$	$11.01^{+0.17}_{-0.11}$	$55.55^{+25.36}_{-25.75}$	$12.14^{+1.53}_{-2.95}$	$-2.25^{+1.39}_{-2.33}$	$56.71^{+7.33}_{-13.78}$	$173.68^{+8.69}_{-11.46}$	$-0.02^{+0.01}_{-0.01}$	$-0.34^{+0.01}_{-0.00}$	$-3.91^{+0.01}_{-0.01}$
J1104959-7717517	$0.21^{+0.02}_{-0.02}$	$0.26^{+0.06}_{-0.03}$	$0.19^{+0.04}_{-0.03}$	$10.71^{+0.20}_{-0.09}$	$34.67^{+28.82}_{-21.56}$	$9.84^{+3.51}_{-5.33}$	$-1.64^{+1.16}_{-1.55}$	$61.71^{+10.22}_{-6.47}$	$59.76^{+6.48}_{-5.12}$	$0.04^{+0.01}_{-0.01}$	$-0.37^{+0.01}_{-0.00}$	$-3.82^{+0.01}_{-0.01}$
J1105333-7634319	$0.16^{+0.02}_{-0.03}$	$0.19^{+0.03}_{-0.03}$	$0.16^{+0.02}_{-0.02}$	$10.57^{+0.16}_{-0.30}$	$57.66^{+46.03}_{-23.44}$	$10.04^{+3.79}_{-2.97}$	$-2.81^{+2.39}_{-2.46}$	$46.76^{+13.83}_{-10.38}$	$24.56^{+20.27}_{-33.11}$	$-0.02^{+0.01}_{-0.01}$	$-0.27^{+0.01}_{-0.00}$	$-3.79^{+0.01}_{-0.01}$
J1105359-7725004	$0.12^{+0.05}_{-0.04}$	$0.15^{+0.05}_{-0.05}$	$0.11^{+0.08}_{-0.03}$	$10.35^{+0.26}_{-0.37}$	$45.16^{+34.71}_{-25.38}$	$10.26^{+3.62}_{-3.66}$	$-2.01^{+1.40}_{-2.70}$	$44.83^{+17.14}_{-13.10}$	$178.45^{+20.47}_{-25.86}$	$-0.07^{+0.01}_{-0.01}$	$-0.38^{+0.01}_{-0.01}$	$-0.49^{+0.01}_{-0.00}$
J1111083-7641574	$0.50^{+0.05}_{-0.05}$	$0.61^{+0.08}_{-0.05}$	$0.54^{+0.05}_{-0.11}$	$9.97^{+0.44}_{-0.20}$	$61.70^{+34.34}_{-22.59}$	$11.75^{+2.37}_{-5.96}$	$-0.01^{+0.12}_{-2.75}$	$76.72^{+5.65}_{-2.61}$	$144.14^{+1.42}_{-1.45}$	$0.30^{+0.01}_{-0.01}$	$-0.23^{+0.01}_{-0.01}$	$-3.80^{+0.01}_{-0.01}$
J1113965-7620152	<0.09	<0.12	$0.07^{+0.03}_{-0.01}$	$10.92^{+0.17}_{-0.19}$	$58.88^{+33.35}_{-35.35}$	$9.22^{+3.61}_{-2.72}$	$-3.21^{+2.34}_{-1.81}$	$24.03^{+18.42}_{-11.46}$	$113.13^{+26.59}_{-24.76}$	$0.33^{+0.02}_{-0.01}$	$-0.18^{+0.01}_{-0.01}$	$-3.79^{+0.01}_{-0.01}$
J1114632-7620092	$0.14^{+0.03}_{-0.03}$	$0.16^{+0.03}_{-0.03}$	$0.14^{+0.03}_{-0.03}$	$10.78^{+0.22}_{-0.20}$	$60.10^{+27.72}_{-38.03}$	$10.12^{+2.33}_{-3.63}$	$-2.14^{+1.83}_{-2.78}$	$56.51^{+8.03}_{-12.05}$	$136.42^{+15.63}_{-14.32}$	$0.40^{+0.01}_{-0.01}$	$-0.22^{+0.01}_{-0.01}$	$-3.80^{+0.01}_{-0.01}$
J1120351-7726009	<0.11	<0.14	$0.11^{+0.05}_{-0.04}$	$9.86^{+0.35}_{-0.28}$	$54.25^{+29.08}_{-30.04}$	$9.33^{+3.66}_{-4.09}$	$-3.19^{+2.07}_{-1.98}$	$47.71^{+16.94}_{-20.25}$	$125.17^{+24.64}_{-30.24}$	$0.06^{+0.03}_{-0.03}$	$-0.40^{+0.03}_{-0.02}$	$-0.49^{+0.01}_{-0.01}$
J1120984-7634366	<0.11	<0.14	$0.09^{+0.03}_{-0.04}$	$10.15^{+1.22}_{-0.28}$	$59.80^{+33.80}_{-37.59}$	$7.58^{+3.50}_{-2.14}$	$-1.81^{+1.19}_{-2.11}$	$43.50^{+11.75}_{-16.12}$	$156.92^{+24.31}_{-25.69}$	$0.09^{+0.03}_{-0.03}$	$-0.37^{+0.01}_{-0.01}$	$-0.48^{+0.01}_{-0.00}$
J1122772-7644223	$0.12^{+0.03}_{-0.03}$	$0.14^{+0.03}_{-0.03}$	$0.12^{+0.02}_{-0.04}$	$11.07^{+0.66}_{-0.16}$	$60.33^{+34.92}_{-19.22}$	$10.48^{+3.42}_{-3.11}$	$-1.93^{+1.22}_{-2.95}$	$51.81^{+10.91}_{-14.38}$	$144.73^{+23.25}_{-10.26}$	$0.17^{+0.01}_{-0.00}$	$-0.34^{+0.00}_{-0.00}$	$-3.87^{+0.01}_{-0.01}$
J1123092-7644241	<0.13	<0.16	$0.11^{+0.05}_{-0.05}$	$10.18^{+1.04}_{-0.34}$	$66.55^{+27.31}_{-43.58}$	$9.34^{+3.31}_{-4.64}$	$-2.27^{+1.75}_{-2.75}$	$24.56^{+19.26}_{-12.67}$	$102.37^{+30.73}_{-29.99}$	$0.29^{+0.03}_{-0.03}$	$-0.26^{+0.02}_{-0.02}$	$-3.80^{+0.01}_{-0.01}$
J1124268-7722230	<0.18	<0.23	$0.13^{+0.22}_{-0.10}$	$8.48^{+0.91}_{-0.67}$	$49.46^{+34.43}_{-34.07}$	$8.24^{+4.49}_{-4.88}$	$-2.72^{+1.83}_{-2.02}$	$59.40^{+34.07}_{-38.71}$	$73.10^{+57.56}_{-45.85}$	$-0.61^{+0.18}_{-0.26}$	$0.55^{+0.21}_{-0.18}$	$-0.96^{+0.01}_{-0.01}$
J1132446-7629227	$0.17^{+0.08}_{-0.05}$	$0.22^{+0.11}_{-0.07}$	$0.16^{+0.09}_{-0.05}$	$9.98^{+0.61}_{-0.36}$	$56.72^{+30.98}_{-39.50}$	$8.81^{+3.94}_{-3.82}$	$-1.82^{+1.39}_{-2.34}$	$59.91^{+14.46}_{-16.45}$	$19.33^{+25.92}_{-21.64}$	$-0.07^{+0.03}_{-0.04}$	$-0.40^{+0.02}_{-0.03}$	$-3.81^{+0.01}_{-0.01}$
J1142454-7733062	$0.12^{+0.01}_{-0.02}$	$0.15^{+0.02}_{-0.03}$	$0.11^{+0.02}_{-0.03}$	$10.20^{+0.12}_{-0.18}$	$58.92^{+33.74}_{-29.72}$	$9.73^{+2.64}_{-3.48}$	$-3.83^{+2.29}_{-1.48}$	$16.54^{+14.51}_{-10.42}$	$121.04^{+31.24}_{-34.91}$	$-0.19^{+0.02}_{-0.02}$	$-0.40^{+0.01}_{-0.01}$	$-0.48^{+0.01}_{-0.01}$
J1160287-7624533	$0.29^{+0.09}_{-0.06}$	$0.36^{+0.15}_{-0.09}$	$0.26^{+0.12}_{-0.10}$	$9.87^{+0.25}_{-0.28}$	$74.33^{+28.01}_{-43.73}$	$8.55^{+4.15}_{-4.08}$	$-2.32^{+1.92}_{-2.44}$	$70.85^{+7.85}_{-12.53}$	$132.49^{+10.80}_{-8.06}$	$-0.01^{+0.03}_{-0.03}$	$-0.40^{+0.01}_{-0.03}$	$-3.79^{+0.01}_{-0.01}$
J1173700-7704381	$0.16^{+0.03}_{-0.03}$	$0.20^{+0.07}_{-0.03}$	$0.13^{+0.04}_{-0.05}$	$10.57^{+0.13}_{-0.20}$	$38.63^{+30.55}_{-19.46}$	$6.06^{+4.39}_{-2.14}$	$-2.18^{+1.58}_{-1.53}$	$43.77^{+15.80}_{-19.46}$	$130.76^{+11.03}_{-16.15}$	$0.01^{+0.01}_{-0.01}$	$-0.42^{+0.01}_{-0.01}$	$-3.82^{+0.01}_{-0.01}$
J1183572-7935548	$0.17^{+0.03}_{-0.03}$	$0.24^{+0.05}_{-0.04}$	$0.14^{+0.04}_{-0.03}$	$10.36^{+0.51}_{-0.13}$	$69.16^{+33.69}_{-43.66}$	$6.19^{+3.07}_{-1.36}$	$-3.48^{+2.32}_{-1.96}$	$66.21^{+6.50}_{-10.60}$	$115.53^{+6.93}_{-11.50}$	$-0.33^{+0.01}_{-0.01}$	$0.19^{+0.01}_{-0.01}$	$-0.48^{+0.01}_{-0.01}$
J1241186-7630425	<0.12	<0.15	$0.13^{+0.06}_{-0.06}$	$9.35^{+0.34}_{-0.58}$	$46.26^{+36.29}_{-30.11}$	$10.78^{+2.75}_{-4.04}$	$-2.54^{+1.98}_{-2.01}$	$45.78^{+18.66}_{-23.68}$	$133.99^{+24.02}_{-36.09}$	$-0.17^{+0.11}_{-0.09}$	$-0.36^{+0.08}_{-0.05}$	$-0.48^{+0.00}_{-0.00}$

Table 10 continued

Table 10 (*continued*)

2MASS	R_{68} (")	R_{90} (")	R_t (")	f_0 (Jy/Sr)	α	β	γ	i (°)	PA (°)	dDec (")	dRA (")	lnwcorr
J15354856-2955551	< 0.18	< 0.24	$0.09^{+0.15}_{-0.04}$	$10.27^{+0.67}_{-0.80}$	$70.53^{+21.38}_{-38.19}$	$8.98^{+4.72}_{-3.81}$	$-1.64^{+1.55}_{-3.08}$	$70.45^{+15.50}_{-11.95}$	$88.67^{+33.06}_{-30.91}$	$-0.67^{+0.05}_{-0.03}$	$-0.95^{+0.03}_{-0.05}$	$-0.48^{+0.00}_{-0.00}$
J15392776-3446171	$0.14^{+0.01}_{-0.01}$	$0.19^{+0.08}_{-0.03}$	$0.13^{+0.05}_{-0.04}$	$10.93^{+0.28}_{-0.56}$	$45.10^{+37.82}_{-35.09}$	$6.66^{+4.01}_{-2.84}$	$-1.49^{+1.60}_{-3.09}$	$52.06^{+4.21}_{-2.30}$	$114.24^{+4.49}_{-2.16}$	$-0.17^{+0.00}_{-0.00}$	$-0.36^{+0.00}_{-0.00}$	$-0.53^{+0.01}_{-0.00}$
J15392828-3446180	< 0.08	< 0.10	$0.10^{+0.07}_{-0.04}$	$10.61^{+0.61}_{-1.40}$	$46.41^{+42.76}_{-35.89}$	$11.94^{+3.18}_{-4.90}$	$-0.95^{+1.18}_{-3.12}$	$40.45^{+21.22}_{-14.97}$	$59.51^{+22.40}_{-33.76}$	$-0.16^{+0.01}_{-0.01}$	$-0.26^{+0.01}_{-0.01}$	$-0.62^{+0.01}_{-0.01}$
J15450634-3417378	< 0.08	< 0.10	$0.07^{+0.03}_{-0.03}$	$11.13^{+0.34}_{-0.55}$	$63.22^{+23.66}_{-25.38}$	$11.48^{+2.89}_{-5.92}$	$-2.07^{+1.73}_{-2.61}$	$64.91^{+15.69}_{-18.01}$	$75.16^{+20.65}_{-32.65}$	$-0.11^{+0.01}_{-0.01}$	$-0.22^{+0.02}_{-0.02}$	$-0.49^{+0.01}_{-0.01}$
J15450887-3417333	$0.12^{+0.02}_{-0.02}$	$0.14^{+0.03}_{-0.03}$	$0.11^{+0.03}_{-0.03}$	$10.92^{+0.17}_{-0.24}$	$50.75^{+34.01}_{-34.13}$	$10.46^{+4.35}_{-5.14}$	$-1.82^{+1.39}_{-2.77}$	$44.12^{+19.76}_{-16.44}$	$95.87^{+19.09}_{-20.55}$	$-0.12^{+0.01}_{-0.00}$	$-0.34^{+0.01}_{-0.01}$	$-0.52^{+0.01}_{-0.01}$
J15451741-3418283	< 0.06	< 0.07	$0.06^{+0.03}_{-0.02}$	$11.03^{+0.36}_{-0.21}$	$40.13^{+32.86}_{-21.38}$	$11.96^{+3.80}_{-4.81}$	$-3.11^{+1.92}_{-2.12}$	$35.07^{+24.57}_{-14.42}$	$12.72^{+30.06}_{-18.83}$	$-0.17^{+0.01}_{-0.01}$	$-0.33^{+0.01}_{-0.01}$	$-0.50^{+0.01}_{-0.01}$
J15464473-3430354	$0.45^{+0.02}_{-0.01}$	$0.71^{+0.05}_{-0.04}$	$0.90^{+0.32}_{-0.48}$	$10.18^{+0.11}_{-0.12}$	$1.98^{+2.74}_{-0.40}$	$11.71^{+3.31}_{-7.10}$	$0.13^{+0.03}_{-0.03}$	$40.00^{+4.16}_{-1.99}$	$31.12^{+4.16}_{-3.18}$	$-0.57^{+0.01}_{-0.00}$	$-0.18^{+0.00}_{-0.00}$	$-0.53^{+0.00}_{-0.01}$
J15475062-3528353	< 0.07	< 0.09	$0.06^{+0.03}_{-0.02}$	$11.31^{+0.54}_{-0.47}$	$34.03^{+29.40}_{-18.95}$	$11.50^{+2.74}_{-4.60}$	$-3.06^{+2.33}_{-1.81}$	$57.75^{+19.03}_{-16.38}$	$6.92^{+27.88}_{-24.18}$	$-0.36^{+0.01}_{-0.01}$	$-0.21^{+0.01}_{-0.01}$	$-0.49^{+0.01}_{-0.01}$
J15475693-3514346	$0.20^{+0.21}_{-0.06}$	$0.41^{+1.21}_{-0.23}$	$0.12^{+0.06}_{-0.09}$	$10.69^{+0.55}_{-0.57}$	$43.40^{+33.13}_{-17.56}$	$5.15^{+9.58}_{-2.67}$	$-2.72^{+2.75}_{-2.14}$	$57.54^{+13.46}_{-12.25}$	$101.55^{+10.91}_{-18.96}$	$-0.38^{+0.01}_{-0.01}$	$-0.21^{+0.02}_{-0.01}$	$-0.51^{+0.01}_{-0.01}$
J15514032-2146103	< 0.62	< 0.74	$0.60^{+0.30}_{-0.49}$	$7.39^{+0.94}_{-2.34}$	$60.14^{+26.46}_{-32.17}$	$10.52^{+3.59}_{-4.55}$	$-3.36^{+3.17}_{-1.79}$	$43.60^{+21.65}_{-17.88}$	$82.04^{+21.65}_{-35.17}$	$-1.00^{+0.16}_{-0.22}$	$-0.50^{+0.15}_{-0.20}$	$-0.48^{+0.01}_{-0.01}$
J15530132-2114135	$0.09^{+0.03}_{-0.03}$	$0.11^{+0.04}_{-0.04}$	$0.08^{+0.04}_{-0.03}$	$10.40^{+0.52}_{-0.20}$	$54.80^{+32.54}_{-30.49}$	$11.13^{+4.30}_{-5.56}$	$-2.48^{+1.99}_{-2.15}$	$59.33^{+11.13}_{-17.32}$	$41.35^{+36.81}_{-24.02}$	$-0.30^{+0.01}_{-0.01}$	$-0.23^{+0.01}_{-0.01}$	$-0.48^{+0.01}_{-0.01}$
J15534211-2049282	$0.25^{+0.12}_{-0.06}$	$0.30^{+0.21}_{-0.08}$	$0.22^{+0.08}_{-0.08}$	$9.50^{+0.84}_{-0.49}$	$54.90^{+23.14}_{-31.97}$	$10.96^{+4.73}_{-7.06}$	$-2.34^{+2.12}_{-1.98}$	$74.77^{+7.75}_{-11.52}$	$78.06^{+14.60}_{-15.65}$	$-0.48^{+0.02}_{-0.04}$	$-0.62^{+0.07}_{-0.04}$	$-4.12^{+0.01}_{-0.01}$
J15564230-3749154	$0.30^{+0.01}_{-0.01}$	$0.39^{+0.15}_{-0.02}$	$0.30^{+0.02}_{-0.12}$	$10.54^{+0.40}_{-0.03}$	$33.60^{+28.78}_{-26.10}$	$6.44^{+1.66}_{-2.77}$	$0.16^{+0.01}_{-0.40}$	$15.59^{+5.05}_{-2.98}$	$89.58^{+9.33}_{-8.27}$	$-0.34^{+0.00}_{-0.00}$	$-0.18^{+0.00}_{-0.00}$	$-0.67^{+0.01}_{-0.01}$
J15580252-3736026	$0.24^{+0.03}_{-0.02}$	$0.30^{+0.07}_{-0.04}$	$0.23^{+0.05}_{-0.05}$	$10.54^{+0.22}_{-0.20}$	$56.50^{+26.56}_{-36.41}$	$7.85^{+6.67}_{-3.14}$	$-1.60^{+1.26}_{-2.94}$	$75.67^{+2.86}_{-6.93}$	$164.68^{+3.00}_{-2.63}$	$-0.40^{+0.01}_{-0.01}$	$-0.32^{+0.01}_{-0.00}$	$-0.50^{+0.01}_{-0.01}$
J15582981-2310077	$0.17^{+0.57}_{-0.09}$	$0.23^{+0.82}_{-0.13}$	$0.15^{+0.47}_{-0.08}$	$9.75^{+0.89}_{-3.02}$	$37.91^{+46.30}_{-23.55}$	$14.07^{+1.84}_{-6.70}$	$-0.04^{+0.41}_{-3.93}$	$46.74^{+24.83}_{-35.41}$	$100.51^{+43.05}_{-63.03}$	$-0.33^{+0.01}_{-0.01}$	$-0.09^{+0.02}_{-0.01}$	$-0.49^{+0.01}_{-0.01}$
J15583692-2257153	$0.48^{+0.00}_{-0.00}$	$0.55^{+0.00}_{-0.00}$	$0.53^{+0.01}_{-0.01}$	$9.96^{+0.01}_{-0.01}$	$68.28^{+20.64}_{-23.50}$	$14.38^{+1.47}_{-2.23}$	$-0.25^{+0.03}_{-0.04}$	$29.86^{+0.86}_{-1.02}$	$150.26^{+1.81}_{-1.54}$	$-0.29^{+0.00}_{-0.00}$	$-0.31^{+0.00}_{-0.00}$	$-0.61^{+0.00}_{-0.00}$
J15591647-4157102	$0.31^{+0.00}_{-0.01}$	$0.41^{+0.01}_{-0.02}$	$0.36^{+0.12}_{-0.06}$	$10.26^{+0.10}_{-0.04}$	$6.54^{+68.11}_{-3.12}$	$9.12^{+6.41}_{-3.36}$	$0.12^{+0.01}_{-0.03}$	$31.38^{+1.98}_{-1.81}$	$155.57^{+4.85}_{-4.37}$	$-0.37^{+0.00}_{-0.00}$	$-0.26^{+0.00}_{-0.00}$	$-0.52^{+0.00}_{-0.00}$
J15592838-4021513	$0.63^{+0.01}_{-0.01}$	$0.83^{+0.05}_{-0.04}$	$0.55^{+0.03}_{-0.03}$	$10.55^{+0.31}_{-0.09}$	$11.12^{+48.79}_{-5.74}$	$6.32^{+1.27}_{-0.71}$	$-2.02^{+0.46}_{-0.79}$	$67.71^{+0.52}_{-0.53}$	$108.87^{+0.52}_{-0.57}$	$-0.30^{+0.00}_{-0.00}$	$-0.23^{+0.00}_{-0.00}$	$-0.52^{+0.01}_{-0.01}$
J16000060-4221567	$0.29^{+0.38}_{-0.15}$	$0.34^{+0.64}_{-0.18}$	$0.23^{+0.23}_{-0.15}$	$9.39^{+0.80}_{-0.98}$	$41.71^{+42.75}_{-25.67}$	$7.53^{+7.14}_{-3.62}$	$-2.59^{+1.82}_{-2.52}$	$65.32^{+16.90}_{-16.68}$	$144.36^{+22.85}_{-27.36}$	$0.45^{+0.11}_{-0.10}$	$-0.41^{+0.10}_{-0.12}$	$-0.49^{+0.01}_{-0.01}$
J16000236-4222145	$0.50^{+0.01}_{-0.01}$	$0.70^{+0.05}_{-0.04}$	$0.59^{+0.27}_{-0.14}$	$9.97^{+0.09}_{-0.03}$	$5.43^{+45.97}_{-2.37}$	$8.28^{+6.51}_{-3.39}$	$0.12^{+0.01}_{-0.03}$	$64.53^{+1.05}_{-1.00}$	$161.71^{+1.24}_{-1.68}$	$0.53^{+0.00}_{-0.01}$	$-0.34^{+0.00}_{-0.00}$	$-0.50^{+0.01}_{-0.01}$
J16001844-2230114	< 0.09	< 0.12	$0.10^{+0.03}_{-0.03}$	$10.12^{+0.42}_{-0.23}$	$51.18^{+33.81}_{-32.93}$	$11.19^{+3.45}_{-4.83}$	$-2.60^{+1.89}_{-1.19}$	$50.37^{+14.94}_{-16.32}$	$47.61^{+22.85}_{-24.34}$	$-0.31^{+0.01}_{-0.01}$	$-0.30^{+0.02}_{-0.02}$	$-0.48^{+0.01}_{-0.00}$
J16003103-4143369	< 0.17	< 0.22	$0.17^{+0.71}_{-0.09}$	$9.35^{+1.01}_{-5.12}$	$55.34^{+34.25}_{-34.33}$	$10.46^{+4.01}_{-4.95}$	$-2.39^{+3.01}_{-4.96}$	$36.57^{+33.68}_{-27.55}$	$88.05^{+47.57}_{-55.56}$	$-0.11^{+0.04}_{-0.05}$	$-0.32^{+0.06}_{-0.08}$	$-0.50^{+0.01}_{-0.01}$
J16004452-4155310	$0.39^{+0.02}_{-0.01}$	$0.51^{+0.04}_{-0.03}$	$0.42^{+0.04}_{-0.05}$	$10.45^{+0.09}_{-0.06}$	$31.68^{+37.60}_{-25.04}$	$7.54^{+5.31}_{-1.99}$	$0.10^{+0.02}_{-0.03}$	$72.59^{+1.22}_{-1.56}$	$58.40^{+1.15}_{-0.91}$	$-0.07^{+0.00}_{-0.00}$	$-0.31^{+0.01}_{-0.00}$	$-0.52^{+0.01}_{-0.01}$
J16004943-4130038	< 0.12	< 0.14	$0.10^{+0.04}_{-0.03}$	$10.36^{+0.53}_{-0.32}$	$56.39^{+25.64}_{-30.87}$	$10.11^{+5.16}_{-4.29}$	$-2.52^{+1.89}_{-2.33}$	$52.46^{+20.39}_{-23.42}$	$133.70^{+36.12}_{-22.10}$	$-0.16^{+0.02}_{-0.02}$	$0.02^{+0.01}_{-0.02}$	$-0.49^{+0.01}_{-0.01}$
J16011549-4152351	$0.61^{+0.07}_{-0.05}$	$0.81^{+0.47}_{-0.11}$	$0.59^{+0.08}_{-0.12}$	$9.58^{+0.08}_{-0.06}$	$44.48^{+41.46}_{-22.33}$	$5.28^{+1.86}_{-0.99}$	$0.19^{+0.01}_{-0.02}$	$65.86^{+2.16}_{-3.71}$	$160.00^{+3.77}_{-3.51}$	$-0.24^{+0.02}_{-0.01}$	$-0.25^{+0.01}_{-0.01}$	$-0.51^{+0.01}_{-0.01}$
J16014086-2258103	< 0.10	< 0.13	$0.07^{+0.07}_{-0.06}$	$9.87^{+0.51}_{-0.78}$	$63.93^{+19.10}_{-36.07}$	$12.97^{+1.77}_{-7.25}$	$-2.18^{+2.38}_{-2.32}$	$32.85^{+14.07}_{-9.38}$	$176.94^{+18.10}_{-39.30}$	$-0.79^{+0.02}_{-0.02}$	$-0.27^{+0.01}_{-0.02}$	$-0.48^{+0.01}_{-0.01}$
J16014157-2111380	< 0.70	< 0.86	$0.49^{+0.53}_{-0.38}$	$7.92^{+0.77}_{-1.99}$	$35.64^{+32.39}_{-27.54}$	$10.71^{+4.44}_{-7.30}$	$-3.09^{+1.77}_{-2.32}$	$54.98^{+22.73}_{-16.15}$	$83.79^{+16.55}_{-29.24}$	$-0.32^{+0.20}_{-0.25}$	$1.82^{+0.20}_{-0.18}$	$-4.12^{+0.00}_{-0.00}$
J16020757-2257467	$0.17^{+0.03}_{-0.03}$	$0.21^{+0.07}_{-0.04}$	$0.16^{+0.04}_{-0.05}$	$9.66^{+0.23}_{-0.38}$	$57.05^{+29.61}_{-13.37}$	$10.90^{+4.47}_{-6.81}$	$-1.90^{+1.92}_{-2.08}$	$30.54^{+16.72}_{-13.37}$	$113.57^{+21.26}_{-30.65}$	$-0.50^{+0.02}_{-0.02}$	$-0.27^{+0.02}_{-0.03}$	$-0.47^{+0.00}_{-0.00}$
J16024152-2138245	$0.06^{+0.02}_{-0.01}$	$0.07^{+0.02}_{-0.02}$	$0.06^{+0.02}_{-0.01}$	$10.71^{+0.34}_{-0.16}$	$38.53^{+36.59}_{-22.45}$	$9.18^{+5.44}_{-4.10}$	$-1.79^{+1.33}_{-1.37}$	$28.22^{+16.15}_{-10.52}$	$54.55^{+17.28}_{-33.49}$	$-0.42^{+0.01}_{-0.01}$	$-0.15^{+0.01}_{-0.00}$	$-4.19^{+0.00}_{-0.01}$
J16030161-2207523	< 0.16	< 0.21	$0.12^{+0.56}_{-0.08}$	$6.36^{+3.63}_{-1.79}$	$65.09^{+?}_{-43.33}$	$11.15^{+3.73}_{-1.79}$	$0.47^{+0.17}_{-0.99}$	$43.88^{+23.88}_{-19.22}$	$88.41^{+30.56}_{-31.72}$	$-0.44^{+0.02}_{-0.01}$	$-0.23^{+0.01}_{-0.02}$	$-4.18^{+0.00}_{-0.00}$

Table 10 continued

Table 10 (continued)

2MASS	R_{68} ('')	R_{90} ('')	R_t ('')	f_0 (Jy/Sr)	α	β	γ	i (°)	PA (°)	dDec ('')	dRA ('')	lnwcorr
J16032939-4140018	$0.46^{+0.06}_{-0.04}$	$0.68^{+0.39}_{-0.12}$	$0.40^{+0.14}_{-0.16}$	$10.29^{+0.34}_{-0.27}$	$47.70^{+34.85}_{-37.27}$	$4.30^{+4.30}_{-1.18}$	$-0.01^{+0.13}_{-4.15}$	$77.72^{+2.89}_{-3.24}$	$126.45^{+1.78}_{-1.76}$	$0.59^{+0.01}_{-0.01}$	$-0.43^{+0.01}_{-0.01}$	$-0.51^{+0.01}_{-0.01}$
J16035767-2031055	$0.23^{+0.11}_{-0.11}$	$0.30^{+0.28}_{-0.13}$	$0.14^{+0.15}_{-0.08}$	$9.91^{+0.72}_{-0.63}$	$52.69^{+35.75}_{-35.09}$	$6.61^{+6.06}_{-3.22}$	$-1.88^{+1.47}_{-3.06}$	$49.71^{+24.31}_{-40.38}$	$128.62^{+37.57}_{-87.70}$	$-0.41^{+0.07}_{-0.06}$	$-0.16^{+0.03}_{-0.03}$	$-0.91^{+0.00}_{-0.00}$
J16041740-1942287	< 0.44	< 0.59	$0.33^{+0.72}_{-0.25}$	$6.89^{+2.51}_{-1.98}$	$49.61^{+39.53}_{-42.15}$	$10.27^{+4.59}_{-5.29}$	$-2.00^{+1.52}_{-3.09}$	$44.96^{+23.80}_{-10.79}$	$53.95^{+39.25}_{-16.13}$	$-0.46^{+0.15}_{-0.11}$	$-0.01^{+0.17}_{-0.18}$	$-4.13^{+0.00}_{-0.00}$
J16042165-2130284	$0.67^{+0.00}_{-0.00}$	$0.84^{+0.01}_{-0.01}$	$0.60^{+0.00}_{-0.00}$	$10.13^{+0.01}_{-0.01}$	$83.89^{+11.75}_{-21.31}$	$7.30^{+0.20}_{-0.16}$	$-5.88^{+0.16}_{-0.09}$	$10.15^{+1.33}_{-1.80}$	$137.28^{+7.30}_{-8.48}$	$-0.42^{+0.00}_{-0.00}$	$-0.19^{+0.00}_{-0.01}$	$-0.70^{+0.01}_{-0.01}$
J16052556-2035397	< 0.15	< 0.20	$0.14^{+0.16}_{-0.08}$	$9.33^{+0.76}_{-1.12}$	$46.03^{+29.90}_{-25.98}$	$8.34^{+4.89}_{-4.00}$	$-2.09^{+1.82}_{-3.00}$	$50.67^{+21.85}_{-35.96}$	$89.38^{+57.34}_{-57.41}$	$0.06^{+0.05}_{-0.08}$	$-0.23^{+0.10}_{-0.10}$	$-0.49^{+0.01}_{-0.01}$
J16062196-1928445	< 0.22	< 0.28	$0.24^{+0.52}_{-0.14}$	$9.37^{+0.56}_{-2.37}$	$55.02^{+31.31}_{-39.00}$	$9.14^{+5.56}_{-5.99}$	$-2.69^{+2.04}_{-1.57}$	$39.73^{+31.57}_{-25.91}$	$117.60^{+42.22}_{-72.48}$	$-0.14^{+0.10}_{-0.39}$	$-0.31^{+1.07}_{-0.13}$	$-1.04^{+0.01}_{-0.01}$
J16062277-2011243	0.55	0.79	$0.56^{+0.63}_{-0.40}$	$6.22^{+1.23}_{-0.96}$	$57.01^{+24.12}_{-35.17}$	$11.88^{+3.65}_{-5.25}$	$-2.71^{+2.30}_{-2.28}$	$41.50^{+28.70}_{-32.35}$	$71.68^{+57.65}_{-48.38}$	$-0.24^{+1.78}_{-1.00}$	$-0.09^{+1.16}_{-1.15}$	$-0.48^{+0.01}_{-0.01}$
J16063539-2516510	< 0.17	< 0.20	$0.14^{+0.08}_{-0.06}$	$9.52^{+0.31}_{-0.29}$	$48.11^{+36.77}_{-30.68}$	$10.02^{+5.43}_{-5.48}$	$-3.45^{+2.03}_{-1.54}$	$36.18^{+20.95}_{-23.03}$	$21.28^{+24.00}_{-26.96}$	$-0.54^{+0.05}_{-0.05}$	$-0.18^{+0.06}_{-0.03}$	$-0.48^{+0.01}_{-0.01}$
J16064102-2455489	$0.14^{+0.04}_{-0.04}$	$0.17^{+0.06}_{-0.05}$	$0.12^{+0.04}_{-0.04}$	$9.71^{+0.34}_{-0.21}$	$44.89^{+37.28}_{-25.99}$	$8.94^{+5.17}_{-4.37}$	$-3.39^{+2.72}_{-1.69}$	$38.69^{+9.99}_{-20.50}$	$118.27^{+25.38}_{-30.34}$	$-0.43^{+0.03}_{-0.02}$	$-0.25^{+0.02}_{-0.03}$	$-0.48^{+0.01}_{-0.01}$
J16064385-1908056	$0.40^{+0.52}_{-0.28}$	$0.46^{+0.64}_{-0.33}$	$0.37^{+0.45}_{-0.29}$	$7.95^{+1.11}_{-2.26}$	$41.61^{+23.74}_{-24.68}$	$11.10^{+4.37}_{-5.37}$	$-3.13^{+2.52}_{-2.13}$	$66.43^{+16.05}_{-9.29}$	$71.31^{+41.22}_{-26.62}$	$-0.48^{+0.15}_{-0.22}$	$-0.11^{+0.13}_{-0.15}$	$-4.12^{+0.00}_{-0.00}$
J16070384-3911113	$0.79^{+0.75}_{-0.57}$	$0.96^{+1.29}_{-0.70}$	$0.75^{+0.46}_{-0.45}$	$7.43^{+1.16}_{-1.16}$	$51.22^{+30.49}_{-32.87}$	$8.58^{+5.39}_{-4.83}$	$-2.65^{+2.28}_{-2.02}$	$60.84^{+20.15}_{-19.13}$	$134.06^{+33.79}_{-23.94}$	$0.28^{+0.15}_{-0.16}$	$-0.85^{+0.20}_{-0.16}$	$-0.49^{+0.01}_{-0.01}$
J16070854-3914075	$0.63^{+0.10}_{-0.04}$	$1.04^{+0.40}_{-0.25}$	$0.50^{+0.09}_{-0.07}$	$9.96^{+0.12}_{-0.09}$	$43.70^{+36.45}_{-33.33}$	$4.16^{+2.22}_{-0.72}$	$-0.35^{+0.30}_{-0.82}$	$72.41^{+1.92}_{-1.86}$	$154.02^{+1.74}_{-1.62}$	$-0.20^{+0.01}_{-0.02}$	$-0.37^{+0.01}_{-0.01}$	$-0.49^{+0.01}_{-0.01}$
J16071007-3911033	$0.10^{+0.03}_{-0.03}$	$0.13^{+0.05}_{-0.04}$	$0.08^{+0.04}_{-0.04}$	$11.05^{+0.55}_{-0.36}$	$54.50^{+34.57}_{-23.66}$	$11.47^{+3.63}_{-5.84}$	$-2.80^{+1.74}_{-1.87}$	$54.83^{+13.51}_{-17.46}$	$142.63^{+14.62}_{-34.49}$	$-0.15^{+0.01}_{-0.01}$	$-0.27^{+0.01}_{-0.01}$	$-0.49^{+0.01}_{-0.01}$
J16072625-2432079	$0.11^{+0.01}_{-0.01}$	$0.13^{+0.02}_{-0.01}$	$0.10^{+0.02}_{-0.01}$	$10.52^{+0.23}_{-0.20}$	$51.36^{+34.46}_{-30.42}$	$9.66^{+3.74}_{-3.28}$	$-3.32^{+2.50}_{-1.60}$	$28.83^{+24.92}_{-13.94}$	$180.44^{+27.74}_{-35.05}$	$-0.29^{+0.00}_{-0.01}$	$-0.15^{+0.01}_{-0.01}$	$-0.50^{+0.01}_{-0.01}$
J16072747-2059442	< 0.06	< 0.08	$0.06^{+0.04}_{-0.02}$	$9.90^{+0.45}_{-1.26}$	$39.15^{+27.41}_{-21.54}$	$13.41^{+2.58}_{-5.83}$	$-0.77^{+1.00}_{-3.36}$	$32.71^{+19.26}_{-19.84}$	$135.41^{+26.56}_{-16.57}$	$-0.27^{+0.01}_{-0.02}$	$-0.38^{+0.02}_{-0.02}$	$-4.17^{+0.00}_{-0.01}$
J16073773-3921388	< 0.50	< 0.68	$0.33^{+0.41}_{-0.25}$	$7.84^{+1.25}_{-1.76}$	$60.04^{+22.91}_{-32.76}$	$9.67^{+5.00}_{-5.26}$	$-2.10^{+1.34}_{-1.99}$	$22.78^{+19.36}_{-15.70}$	$159.82^{+32.94}_{-33.13}$	$-0.34^{+0.22}_{-0.18}$	$-0.08^{+0.23}_{-0.14}$	$-0.49^{+0.01}_{-0.01}$
J16075230-3858059	< 0.13	< 0.18	$0.11^{+0.10}_{-0.06}$	$10.17^{+0.53}_{-0.76}$	$49.98^{+34.64}_{-32.76}$	$9.72^{+5.10}_{-4.90}$	$-2.20^{+2.05}_{-2.14}$	$61.56^{+21.48}_{-14.71}$	$126.46^{+24.47}_{-25.22}$	$-0.19^{+0.04}_{-0.03}$	$-0.26^{+0.04}_{-0.04}$	$-0.49^{+0.01}_{-0.01}$
J16075475-3915446	< 0.69	< 0.88	$0.72^{+0.77}_{-0.53}$	$6.03^{+2.17}_{-2.15}$	$57.05^{+31.59}_{-40.88}$	$10.33^{+3.42}_{-6.63}$	$-6.16^{+4.88}_{-4.02}$	$42.12^{+33.31}_{-26.17}$	$91.82^{+49.25}_{-71.76}$	$0.02^{+1.90}_{-1.88}$	$0.10^{+2.00}_{-2.03}$	$-0.50^{+0.01}_{-0.01}$
J16075796-2040087	$0.08^{+0.02}_{-0.01}$	$0.09^{+0.02}_{-0.02}$	$0.09^{+0.05}_{-0.03}$	$10.84^{+0.68}_{-0.44}$	$75.57^{+18.48}_{-25.98}$	$10.94^{+3.00}_{-2.44}$	$-0.16^{+0.28}_{-2.26}$	$68.28^{+7.65}_{-17.95}$	$209.14^{+6.16}_{-8.62}$	$-0.37^{+0.00}_{-0.00}$	$-0.22^{+0.00}_{-0.00}$	$-4.19^{+0.00}_{-0.00}$
J16080017-3902595	< 0.28	< 0.35	$0.21^{+0.65}_{-0.14}$	$8.97^{+1.26}_{-1.65}$	$43.46^{+34.16}_{-28.27}$	$11.02^{+4.83}_{-5.88}$	$-2.17^{+2.50}_{-2.13}$	$47.97^{+25.03}_{-10.51}$	$164.31^{+30.23}_{-31.60}$	$-0.16^{+0.06}_{-0.08}$	$-0.55^{+0.05}_{-0.13}$	$-0.50^{+0.01}_{-0.01}$
J16081263-3908334	< 0.13	< 0.17	$0.12^{+0.07}_{-0.06}$	$10.09^{+0.60}_{-0.52}$	$50.37^{+29.82}_{-29.82}$	$9.62^{+4.49}_{-4.42}$	$-3.60^{+2.69}_{-1.47}$	$51.93^{+19.93}_{-21.14}$	$114.13^{+27.52}_{-31.65}$	$-0.33^{+0.06}_{-0.04}$	$-0.02^{+0.04}_{-0.04}$	$-0.50^{+0.01}_{-0.01}$
J16081497-3857145	$0.11^{+0.05}_{-0.04}$	$0.14^{+0.07}_{-0.05}$	$0.12^{+0.06}_{-0.05}$	$10.34^{+0.51}_{-0.41}$	$62.27^{+26.07}_{-13.70}$	$11.93^{+3.78}_{-4.25}$	$-1.92^{+1.89}_{-3.04}$	$55.60^{+18.60}_{-13.70}$	$96.02^{+26.98}_{-33.34}$	$-0.42^{+0.02}_{-0.01}$	$-0.00^{+0.03}_{-0.01}$	$-0.49^{+0.01}_{-0.01}$
J16081566-2222199	< 0.34	< 0.46	$0.29^{+0.29}_{-0.29}$	$5.54^{+2.26}_{-1.01}$	$39.99^{+48.68}_{-21.85}$	$1.25^{+4.02}_{-0.81}$	$0.50^{+0.12}_{-0.15}$	$12.18^{+6.11}_{-7.00}$	$107.65^{+41.52}_{-7.87}$	$-0.46^{+0.05}_{-0.04}$	$0.02^{+0.02}_{-0.02}$	$-4.16^{+0.00}_{-0.00}$
J16082180-3904214	< 0.09	< 0.12	$0.10^{+0.16}_{-0.05}$	$10.30^{+0.62}_{-1.60}$	$49.37^{+25.94}_{-30.68}$	$11.45^{+3.77}_{-5.23}$	$-1.24^{+1.49}_{-2.33}$	$73.54^{+10.24}_{-15.73}$	$75.93^{+21.21}_{-29.81}$	$-0.35^{+0.03}_{-0.02}$	$0.01^{+0.04}_{-0.03}$	$-0.49^{+0.01}_{-0.01}$
J16082249-3904464	$0.82^{+0.07}_{-0.05}$	$1.37^{+0.30}_{-0.15}$	$1.11^{+0.49}_{-0.66}$	$9.92^{+0.12}_{-0.03}$	$2.09^{+7.25}_{-2.49}$	$6.29^{+2.91}_{-3.78}$	$0.15^{+0.02}_{-0.03}$	$46.79^{+0.63}_{-2.21}$	$108.55^{+4.00}_{-0.98}$	$-0.85^{+0.01}_{-0.01}$	$-0.23^{+0.00}_{-0.01}$	$-0.51^{+0.00}_{-0.00}$
J16082324-1930009	$0.25^{+0.03}_{-0.03}$	$0.30^{+0.05}_{-0.03}$	$0.23^{+0.04}_{-0.05}$	$10.63^{+0.42}_{-0.20}$	$42.35^{+35.50}_{-22.51}$	$9.41^{+3.61}_{-3.63}$	$-3.14^{+1.48}_{-1.68}$	$70.25^{+1.74}_{-3.81}$	$126.62^{+4.08}_{-5.36}$	$-0.29^{+0.01}_{-0.01}$	$-0.28^{+0.01}_{-0.01}$	$-0.99^{+0.00}_{-0.00}$
J16082576-3906011	$0.26^{+0.01}_{-0.01}$	$0.31^{+0.03}_{-0.02}$	$0.24^{+0.04}_{-0.03}$	$10.43^{+0.14}_{-0.19}$	$40.97^{+43.85}_{-26.69}$	$8.52^{+5.18}_{-1.87}$	$-3.30^{+1.99}_{-1.85}$	$47.06^{+3.16}_{-4.05}$	$63.48_{-2.13}$	$-0.55^{+0.00}_{-0.00}$	$-0.16^{+0.00}_{-0.00}$	$-0.49^{+0.01}_{-0.01}$
J16082751-1949047	$0.27^{+0.80}_{-0.18}$	$0.44^{+1.18}_{-0.32}$	$0.34^{+0.72}_{-0.26}$	$6.99^{+1.77}_{-1.42}$	$46.67^{+30.26}_{-28.67}$	$10.47^{+4.27}_{-5.61}$	$-3.39^{+2.05}_{-2.00}$	$40.76^{+29.70}_{-28.67}$	$100.52^{+55.92}_{-78.33}$	$0.11^{+0.92}_{-0.93}$	$-0.09^{+1.33}_{-1.35}$	$-0.49^{+0.01}_{-0.01}$
J16083026-3906111	$0.09^{+0.04}_{-0.04}$	$0.11^{+0.05}_{-0.04}$	$0.08^{+0.04}_{-0.04}$	$10.79^{+1.03}_{-0.44}$	$64.68^{+23.14}_{-32.66}$	$9.60^{+4.08}_{-4.45}$	$-1.98^{+1.50}_{-2.39}$	$50.40^{+15.19}_{-17.47}$	$41.26^{+23.72}_{-30.95}$	$-0.43^{+0.01}_{-0.01}$	$-0.05^{+0.01}_{-0.01}$	$-0.50^{+0.01}_{-0.01}$
J16083070-3828268	$0.57^{+0.01}_{-0.01}$	$0.65^{+0.03}_{-0.02}$	$0.56^{+0.02}_{-0.04}$	$10.52^{+0.12}_{-0.07}$	$45.33^{+29.45}_{-30.86}$	$11.71^{+2.81}_{-3.18}$	$-3.69^{+0.80}_{-1.56}$	$72.43^{+0.67}_{-0.61}$	$106.19^{+0.97}_{-0.71}$	$-0.43^{+0.01}_{-0.01}$	$-0.19^{+0.01}_{-0.01}$	$-0.51^{+0.01}_{-0.01}$

Table 10 continued

Table 10 *(continued)*

2MASS	R_{68} ('')	R_{90} ('')	R_t ('')	f_0 (Jy/Sr)	α	β	γ	i (°)	PA (°)	dDec ('')	dRA ('')	lnwcorr
J16083081-3905488	< 0.26	< 0.34	$0.21^{+0.23}_{-0.14}$	$9.44^{+0.77}_{-2.13}$	$54.15^{+30.48}_{-32.23}$	$7.55^{+5.14}_{-5.18}$	$-1.51^{+1.85}_{-2.57}$	$57.95^{+22.14}_{-12.70}$	$127.29^{+31.51}_{-29.13}$	$-0.46^{+0.09}_{-0.11}$	$-0.13^{+0.09}_{-0.05}$	$-0.49^{+0.01}_{-0.01}$
J16084940-3905393	< 0.76	< 0.90	$0.53^{+0.73}_{-0.35}$	$6.85^{+0.94}_{-1.43}$	$50.43^{+35.35}_{-31.90}$	$9.77^{+5.79}_{-6.88}$	$-3.85^{+2.27}_{-1.53}$	$54.39^{+18.29}_{-21.24}$	$99.98^{+31.99}_{-22.74}$	$0.82^{+0.20}_{-0.16}$	$0.77^{+0.17}_{-0.21}$	$-0.49^{+0.01}_{-0.01}$
J16085157-3903177	$0.10^{+0.02}_{-0.02}$	$0.12^{+0.04}_{-0.02}$	$0.09^{+0.03}_{-0.04}$	$10.63^{+0.25}_{-0.24}$	$42.58^{+38.37}_{-26.72}$	$8.73^{+4.71}_{-4.21}$	$-1.95^{+1.58}_{-2.00}$	$32.42^{+15.68}_{-23.90}$	$174.60^{+26.49}_{-32.31}$	$-0.35^{+0.01}_{-0.01}$	$-0.14^{+0.01}_{-0.01}$	$-0.49^{+0.01}_{-0.01}$
J16085324-3914401	$0.08^{+0.04}_{-0.02}$	$0.11^{+0.05}_{-0.03}$	$0.09^{+0.08}_{-0.03}$	$11.03^{+0.51}_{-1.27}$	$49.31^{+37.43}_{-31.06}$	$10.62^{+4.01}_{-5.22}$	$-2.11^{+2.28}_{-2.95}$	$57.03^{+13.55}_{-7.57}$	$114.61^{+28.86}_{-17.42}$	$-0.24^{+0.00}_{-0.01}$	$-0.05^{+0.00}_{-0.00}$	$-0.50^{+0.01}_{-0.01}$
J16085373-3914367	< 0.17	< 0.19	$0.18^{+0.38}_{-0.13}$	$9.72^{+0.87}_{-1.37}$	$68.14^{+17.99}_{-46.11}$	$9.96^{+4.80}_{-5.19}$	$-2.14^{+2.34}_{-2.77}$	$66.88^{+15.97}_{-21.31}$	$33.52^{+25.02}_{-29.54}$	$-0.51^{+0.05}_{-0.04}$	$-0.10^{+0.07}_{-0.06}$	$-0.51^{+0.01}_{-0.01}$
J16085468-3937431	$0.46^{+0.00}_{-0.00}$	$0.59^{+0.03}_{-0.03}$	$0.40^{+0.02}_{-0.02}$	$10.46^{+0.06}_{-0.04}$	$49.98^{+33.64}_{-28.32}$	$6.43^{+0.90}_{-0.47}$	$-2.90^{+0.51}_{-0.75}$	$54.92^{+0.67}_{-0.65}$	$45.07^{+0.92}_{-1.00}$	$0.41^{+0.00}_{-0.00}$	$-0.10^{+0.00}_{-0.00}$	$-0.50^{+0.01}_{-0.01}$
J16085553-3902339	< 0.10	< 0.11	$0.09^{+0.15}_{-0.04}$	$10.01^{+0.48}_{-1.99}$	$63.01^{+26.75}_{-41.13}$	$12.53^{+3.10}_{-7.37}$	$-2.81^{+2.92}_{-2.33}$	$19.04^{+12.36}_{-10.86}$	$33.32^{+32.70}_{-21.07}$	$-0.40^{+0.04}_{-0.03}$	$-0.04^{+0.03}_{-0.03}$	$-0.49^{+0.01}_{-0.01}$
J16085780-3902227	$0.08^{+0.02}_{-0.02}$	$0.10^{+0.02}_{-0.03}$	$0.08^{+0.02}_{-0.02}$	$11.30^{+0.38}_{-0.41}$	$47.83^{+30.74}_{-16.04}$	$10.12^{+5.46}_{-4.34}$	$-3.03^{+2.20}_{-1.75}$	$61.03^{+15.60}_{-21.76}$	$21.46^{+11.03}_{-21.76}$	$-0.52^{+0.00}_{-0.01}$	$-0.12^{+0.01}_{-0.01}$	$-0.50^{+0.01}_{-0.01}$
J16090002-1908368	$0.20^{+0.84}_{-0.11}$	$0.24^{+1.27}_{-0.14}$	$0.26^{+0.91}_{-0.16}$	$7.44^{+2.03}_{-1.67}$	$49.66^{+27.64}_{-35.40}$	$9.28^{+4.64}_{-6.85}$	$0.24^{+0.19}_{-3.40}$	$39.24^{+28.55}_{-19.50}$	$74.74^{+61.76}_{-41.78}$	$-0.32^{+0.02}_{-0.03}$	$-0.05^{+0.03}_{-0.04}$	$-0.48^{+0.01}_{-0.01}$
J16090075-1908526	$0.19^{+0.02}_{-0.02}$	$0.24^{+0.06}_{-0.03}$	$0.17^{+0.03}_{-0.04}$	$10.73^{+0.17}_{-0.10}$	$53.55^{+8.60}_{-22.66}$	$7.74^{+6.80}_{-2.85}$	$-4.12^{+1.09}_{-1.22}$	$56.46^{+8.60}_{-12.23}$	$155.81^{+7.58}_{-6.82}$	$-0.42^{+0.01}_{-0.01}$	$-0.11^{+0.01}_{-0.00}$	$-1.03^{+0.01}_{-0.01}$
J16090141-3925119	$0.49^{+0.08}_{-0.05}$	$0.62^{+0.34}_{-0.10}$	$0.45^{+0.10}_{-0.09}$	$9.53^{+0.31}_{-0.22}$	$44.83^{+42.34}_{-28.01}$	$7.92^{+5.83}_{-4.01}$	$-0.64^{+0.54}_{-1.94}$	$72.99^{+5.41}_{-6.41}$	$0.31^{+4.62}_{-4.56}$	$-0.40^{+0.05}_{-0.04}$	$0.07^{+0.01}_{-0.02}$	$-0.50^{+0.01}_{-0.01}$
J16090185-3905124	$0.27^{+0.01}_{-0.01}$	$0.34^{+0.04}_{-0.02}$	$0.28^{+0.04}_{-0.02}$	$9.97^{+0.05}_{-0.04}$	$46.78^{+36.06}_{-34.80}$	$7.54^{+4.49}_{-1.89}$	$0.17^{+0.01}_{-0.01}$	$6.46^{+6.52}_{-4.95}$	$59.17^{+35.54}_{-34.78}$	$-0.30^{+0.00}_{-0.00}$	$-0.05^{+0.00}_{-0.00}$	$-0.51^{+0.01}_{-0.01}$
J16093558-1828232	< 0.81	< 1.01	$0.43^{+0.59}_{-0.30}$	$5.23^{+1.73}_{-1.10}$	$54.52^{+35.51}_{-35.54}$	$7.80^{+4.87}_{-5.19}$	$-1.61^{+1.37}_{-1.65}$	$36.12^{+17.25}_{-16.17}$	$60.56^{+35.44}_{-29.42}$	$1.34^{+0.15}_{-0.23}$	$-0.48^{+0.16}_{-0.17}$	$-4.11^{+0.00}_{-0.00}$
J16094098-2217594	< 0.50	< 0.60	$0.38^{+0.66}_{-0.29}$	$6.68^{+1.59}_{-1.54}$	$48.52^{+41.80}_{-34.87}$	$6.96^{+8.29}_{-3.24}$	$-1.53^{+1.69}_{-1.84}$	$32.66^{+19.08}_{-23.26}$	$38.64^{+19.30}_{-44.57}$	$1.82^{+0.18}_{-0.17}$	$-0.94^{+0.14}_{-0.24}$	$-4.15^{+0.00}_{-0.00}$
J16094434-3913301	< 0.08	< 0.11	$0.09^{+0.69}_{-0.04}$	$9.48^{+1.78}_{-3.01}$	$54.51^{+29.21}_{-41.53}$	$10.56^{+4.51}_{-4.43}$	$0.18^{+0.33}_{-3.49}$	$67.50^{+8.65}_{-20.27}$	$47.89^{+25.89}_{-37.43}$	$-0.21^{+0.01}_{-0.01}$	$0.12^{+0.02}_{-0.01}$	$-0.49^{+0.01}_{-0.01}$
J16094864-3911169	$0.37^{+0.01}_{-0.02}$	$0.42^{+0.03}_{-0.02}$	$0.37^{+0.05}_{-0.02}$	$10.40^{+0.15}_{-0.16}$	$48.20^{+35.71}_{-29.52}$	$11.89^{+3.63}_{-3.73}$	$-3.30^{+1.65}_{-1.82}$	$67.23^{+1.99}_{-3.21}$	$-5.42^{+3.07}_{-2.46}$	$-0.35^{+0.01}_{-0.01}$	$0.01^{+0.01}_{-0.01}$	$-0.49^{+0.01}_{-0.01}$
J16095441-1906551	< 0.62	< 0.74	$0.69^{+0.58}_{-0.40}$	$6.88^{+1.30}_{-1.60}$	$46.94^{+30.36}_{-31.55}$	$7.69^{+5.71}_{-4.48}$	$-2.74^{+1.65}_{-1.83}$	$63.71^{+15.14}_{-22.13}$	$25.31^{+47.22}_{-16.71}$	$-0.37^{+0.24}_{-0.18}$	$-0.88^{+0.23}_{-0.20}$	$-4.11^{+0.00}_{-0.00}$
J16095628-3859518	$0.10^{+0.06}_{-0.03}$	$0.13^{+0.09}_{-0.04}$	$0.10^{+0.03}_{-0.04}$	$10.58^{+0.54}_{-0.45}$	$43.44^{+39.70}_{-31.49}$	$10.17^{+5.03}_{-4.21}$	$-2.23^{+1.94}_{-2.78}$	$67.40^{+17.49}_{-22.68}$	$123.20^{+32.04}_{-17.48}$	$-0.22^{+0.01}_{-0.02}$	$-0.07^{+0.02}_{-0.02}$	$-0.50^{+0.01}_{-0.01}$
J16101984-3836065	< 0.67	< 0.91	$0.36^{+0.53}_{-0.29}$	$6.68^{+1.73}_{-1.10}$	$56.45^{+25.11}_{-38.65}$	$9.11^{+4.83}_{-6.01}$	$-2.43^{+1.96}_{-2.32}$	$25.28^{+16.32}_{-14.77}$	$21.98^{+27.49}_{-34.72}$	$-1.73^{+0.21}_{-0.19}$	$-1.16^{+0.16}_{-0.25}$	$-0.48^{+0.01}_{-0.01}$
J16102955-3922144	$0.19^{+0.06}_{-0.06}$	$0.23^{+0.10}_{-0.07}$	$0.16^{+0.06}_{-0.07}$	$10.16^{+0.70}_{-0.35}$	$58.96^{+25.92}_{-29.58}$	$11.85^{+3.41}_{-4.47}$	$-3.06^{+1.98}_{-2.02}$	$67.79^{+18.56}_{-13.62}$	$106.52^{+14.67}_{-19.58}$	$-0.14^{+0.02}_{-0.02}$	$-0.38^{+0.05}_{-0.03}$	$-0.49^{+0.01}_{-0.01}$
J16104636-1840598	< 0.10	< 0.13	$0.07^{+0.07}_{-0.03}$	$10.01^{+0.62}_{-0.64}$	$52.74^{+27.81}_{-32.04}$	$11.95^{+4.53}_{-4.52}$	$-2.03^{+1.43}_{-2.54}$	$52.98^{+18.77}_{-18.77}$	$159.03^{+16.50}_{-38.36}$	$-0.40^{+0.04}_{-0.04}$	$-0.06^{+0.04}_{-0.03}$	$-4.12^{+0.00}_{-0.00}$
J16122737-2009596	< 0.51	< 0.58	$0.66^{+0.39}_{-0.57}$	$6.59^{+2.58}_{-1.40}$	$62.71^{+30.08}_{-53.55}$	$8.24^{+6.99}_{-5.68}$	$-2.66^{+2.46}_{-1.07}$	$46.61^{+13.39}_{-23.06}$	$1.56^{+25.77}_{-27.75}$	$-0.34^{+0.13}_{-0.20}$	$-0.36^{+0.25}_{-0.11}$	$-4.12^{+0.00}_{-0.00}$
J16124373-3815031	< 0.07	< 0.09	$0.07^{+0.09}_{-0.02}$	$11.18^{+0.52}_{-0.87}$	$38.87^{+48.12}_{-26.63}$	$10.23^{+4.00}_{-3.67}$	$-1.38^{+1.52}_{-2.06}$	$62.94^{+12.24}_{-18.12}$	$40.32^{+23.78}_{-31.92}$	$-0.12^{+0.01}_{-0.01}$	$-0.13^{+0.01}_{-0.01}$	$-0.50^{+0.01}_{-0.01}$
J16133650-2503473	< 0.54	< 0.68	$0.39^{+0.32}_{-0.25}$	$6.95^{+1.76}_{-1.68}$	$49.93^{+31.99}_{-31.41}$	$7.97^{+6.61}_{-4.95}$	$-2.48^{+2.36}_{-1.87}$	$76.04^{+10.73}_{-10.22}$	$7.97^{+23.73}_{-23.57}$	$-0.53^{+0.17}_{-0.16}$	$-0.11^{+0.17}_{-0.21}$	$-0.47^{+0.01}_{-0.01}$
J16134410-3736462	< 0.74	< 0.93	$0.58^{+0.45}_{-0.37}$	$6.43^{+1.98}_{-0.96}$	$53.64^{+31.61}_{-35.07}$	$10.31^{+4.16}_{-6.53}$	$-2.15^{+1.50}_{-2.83}$	$54.84^{+22.10}_{-15.26}$	$39.97^{+37.93}_{-35.07}$	$-1.46^{+0.19}_{-0.20}$	$-1.58^{+0.22}_{-0.15}$	$-0.48^{+0.01}_{-0.01}$
J16141107-2305362	$0.12^{+0.03}_{-0.02}$	$0.15^{+0.04}_{-0.04}$	$0.13^{+0.20}_{-0.02}$	$9.93^{+0.28}_{-1.67}$	$40.14^{+28.70}_{-22.93}$	$13.54^{+2.46}_{-4.16}$	$-3.46^{+3.66}_{-1.59}$	$31.19^{+46.25}_{-18.34}$	$115.44^{+46.88}_{-73.21}$	$-0.35^{+0.01}_{-0.01}$	$-0.05^{+0.02}_{-0.02}$	$-0.48^{+0.01}_{-0.01}$
J16142029-1906481	$0.11^{+0.01}_{-0.01}$	$0.13^{+0.02}_{-0.01}$	$0.11^{+0.01}_{-0.01}$	$10.78^{+0.12}_{-0.19}$	$76.16^{+16.05}_{-33.28}$	$12.96^{+2.33}_{-3.65}$	$-0.85^{+0.58}_{-1.26}$	$22.53^{+13.81}_{-13.81}$	$36.50^{+100.49}_{-21.42}$	$-0.21^{+0.00}_{-0.00}$	$-0.32^{+0.00}_{-0.00}$	$-0.52^{+0.01}_{-0.01}$
J16143367-1900133	< 0.43	< 0.69	$0.50^{+0.74}_{-0.34}$	$6.06^{+1.75}_{-1.35}$	$58.66^{+30.44}_{-37.66}$	$8.70^{+5.63}_{-5.04}$	$-3.36^{+2.91}_{-1.41}$	$72.69^{+11.20}_{-14.28}$	$53.51^{+21.99}_{-41.12}$	$-0.52^{+0.12}_{-0.21}$	$-0.27^{+0.17}_{-0.20}$	$-4.12^{+0.00}_{-0.00}$
J16153456-2242421	$0.24^{+0.26}_{-0.11}$	$0.31^{+0.40}_{-0.15}$	$0.18^{+0.17}_{-0.06}$	$9.46^{+0.67}_{-0.95}$	$47.51^{+35.11}_{-25.59}$	$10.17^{+5.04}_{-5.57}$	$0.20^{+0.11}_{-0.08}$	$64.31^{+10.66}_{-12.92}$	$12.79^{+20.97}_{-10.54}$	$-0.99^{+0.00}_{-0.00}$	$0.02^{+0.01}_{-0.01}$	$-4.18^{+0.00}_{-0.00}$
J16154416-1921171	$0.07^{+0.01}_{-0.02}$	$0.09^{+0.05}_{-0.03}$	$0.05^{+0.02}_{-0.01}$	$11.47^{+0.26}_{-0.14}$	$49.00^{+23.45}_{-33.60}$	$6.89^{+4.34}_{-3.26}$	$-3.01^{+2.35}_{-1.99}$	$75.97^{+8.96}_{-8.28}$	$14.36^{+7.52}_{-7.92}$	$-0.54^{+0.00}_{-0.00}$	$-0.03^{+0.00}_{-0.00}$	$-4.19^{+0.00}_{-0.00}$

Table 10 continued

Table 10 *(continued)*

2MASS	R_{68}	R_{90}	R_t	f_0	α	β	γ	i	PA	dDec	dRA	lnwcorr
	$''$	$''$	$''$	(Jy/Sr)				(°)	(°)	($''$)	($''$)	
J16163345-2521505	$0.26^{+0.07}_{-0.06}$	$0.32^{+0.11}_{-0.08}$	$0.25^{+0.07}_{-0.07}$	$9.26^{+0.22}_{-0.23}$	$49.80^{+26.27}_{-29.24}$	$9.38^{+4.68}_{-4.77}$	$-2.61^{+1.85}_{-2.34}$	$66.19^{+14.42}_{-20.11}$	$61.35^{+14.04}_{-17.68}$	$-0.35^{+0.06}_{-0.03}$	$-0.20^{+0.05}_{-0.04}$	$-4.17^{+0.00}_{-0.00}$
J16181904-2028479	$0.09^{+0.03}_{-0.03}$	$0.11^{+0.07}_{-0.04}$	$0.07^{+0.03}_{-0.03}$	$10.85^{+0.24}_{-0.55}$	$59.77^{+21.80}_{-29.83}$	$10.30^{+4.71}_{-5.00}$	$-3.82^{+1.96}_{-1.51}$	$60.38^{+18.35}_{-13.79}$	$110.06^{+26.14}_{-32.21}$	$-0.28^{+0.01}_{-0.01}$	$-0.07^{+0.01}_{-0.01}$	$-4.17^{+0.01}_{-0.00}$
J16215466-2043091	< 0.48	< 0.58	$0.38^{+0.48}_{-0.30}$	$6.62^{+1.49}_{-2.07}$	$63.75^{+23.79}_{-35.42}$	$7.11^{+6.00}_{-4.51}$	$-3.08^{+2.23}_{-2.27}$	$34.72^{+13.58}_{-19.22}$	$59.71^{+23.64}_{-27.95}$	$-1.55^{+0.15}_{-0.12}$	$-0.03^{+0.17}_{-0.24}$	$-4.18^{+0.01}_{-0.00}$
J16270942-2148457	< 0.07	< 0.09	$0.06^{+0.04}_{-0.02}$	$10.37^{+0.26}_{-0.53}$	$43.26^{+35.76}_{-34.38}$	$12.60^{+3.39}_{-6.75}$	$-2.71^{+2.11}_{-1.41}$	$21.20^{+13.06}_{-12.60}$	$105.01^{+36.92}_{-27.81}$	$-0.34^{+0.02}_{-0.02}$	$-0.22^{+0.01}_{-0.01}$	$-4.17^{+0.00}_{-0.01}$

G. $\log L_{\mathrm{mm}} - \log L_\star$ RELATION

In our discussion on disk sizes scaling relations (see Section 6.3), we reproduce the temperature power law index (q) estimation following the method given in Andrews et al. (2018a). This approach requires us to know the $\log L_{\mathrm{mm}} - \log L_\star$ for our samples, which we provide here using the statistical methods described in Section 5.
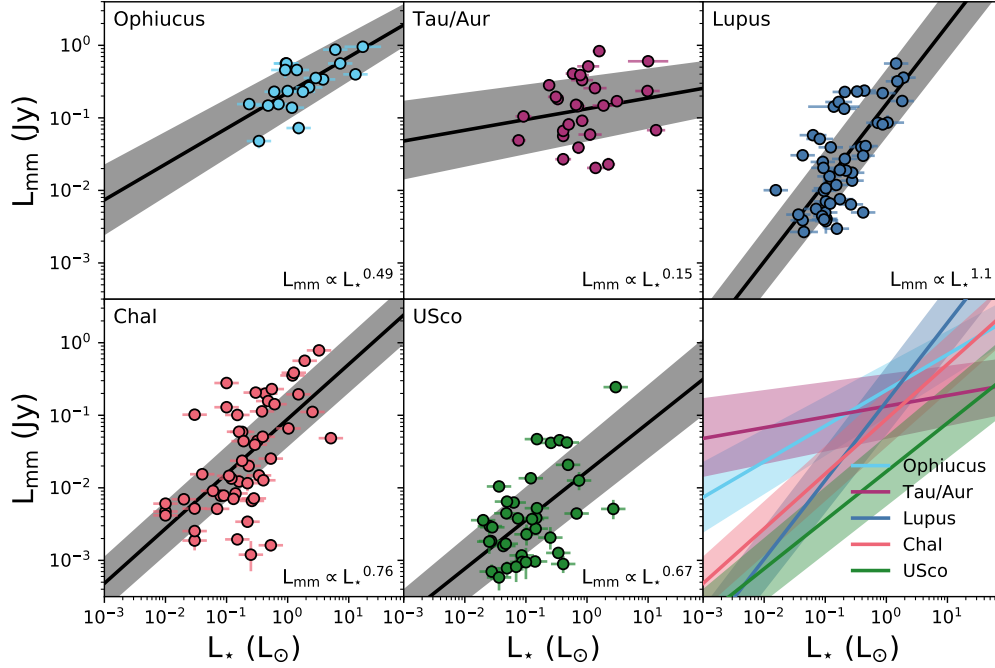
Figure 16. Fitting of $\log L_{\mathrm{mm}} - \log L_{\star}$. The first 5 panels (left to right; top to bottom; ordered by region age) show the model results of each region as circles (resolved) and triangles (upper-limits). The best fit from MCMC linear regression is plotted as a black line, and surrounded by our 68% confidence intervals in grey. The last panel replots the bests fits of each region (and the corresponding 68% confidence intervals) so that they can be directly compared. Fit parameters for each region are given in Table G.

Table 11. $\log L_{\mathrm{mm}} - \log L_{\star}$ statistical tests

| Region | Shapiro L_{mm} | | Shapiro $L_{\star}$ | | Pearson r | | Spearman ρ | | Regression Parameters | | | |
	stat	p-value	stat	p-value	stat	p-value	stat	p-value	α	β	σ	$\hat{\rho}$
Oph	0.66	1.3e-05	0.90	5.0e-02	0.66	1.6e-03	0.57	8.7e-03	$-0.65^{+0.07}_{-0.07}$	$0.49^{+0.2}_{-0.2}$	$0.27^{+0.07}_{-0.05}$	$0.84^{+0.08}_{-0.1}$
Tau/Aur	0.55	6.2e-08	0.82	3.5e-04	0.15	4.6e-01	0.16	4.2e-01	$-0.88^{+0.09}_{-0.09}$	$0.15^{+0.2}_{-0.2}$	$0.46^{+0.08}_{-0.06}$	$0.42^{+0.2}_{-0.2}$
Lupus	0.66	3.0e-09	0.67	3.5e-09	0.73	3.4e-09	0.63	1.7e-06	$-0.81^{+0.1}_{-0.1}$	$1.1^{+0.2}_{-0.2}$	$0.47^{+0.06}_{-0.06}$	$0.86^{+0.04}_{-0.06}$
Cha I	0.54	7.3e-12	0.62	1.1e-10	0.52	4.5e-05	0.54	1.8e-05	$-1.1^{+0.1}_{-0.1}$	$0.76^{+0.1}_{-0.1}$	$0.59^{+0.07}_{-0.06}$	$0.79^{+0.06}_{-0.07}$
USco	0.45	1.0e-10	0.34	7.7e-12	0.69	1.6e-06	0.46	3.9e-03	$-1.8^{+0.2}_{-0.2}$	$0.67^{+0.2}_{-0.2}$	$0.53^{+0.08}_{-0.06}$	$0.75^{+0.08}_{-0.1}$

NOTE—Values we consider unreliable are greyed out (see Section 5.1).

REFERENCES

Adams, F. C. 2010, ARA&A, 48, 47

Adams, F. C., Hollenbach, D., Laughlin, G., & Gorti, U. 2004, ApJ, 611, 360

Alcalá, J. M., Natta, A., Manara, C. F., et al. 2014, A&A, 561, A2

Allen, R. L., Bernstein, G. M., & Malhotra, R. 2001, ApJL, 549, L241

Anderson, T. W., & Darling, D. A. 1952, The annals of mathematical statistics, 23, 193

Andrews, S. M., Rosenfeld, K. A., Kraus, A. L., & Wilner, D. J. 2013, ApJ, 771, 129

Andrews, S. M., Terrell, M., Tripathi, A., et al. 2018a, ApJ, 865, 157

Andrews, S. M., Wilner, D. J., Hughes, A. M., Qi, C., & Dullemond, C. P. 2010, ApJ, 723, 1241

Andrews, S. M., Huang, J., Pérez, L. M., et al. 2018b, ApJL, 869, L41

Ansdell, M., Williams, J. P., van der Marel, N., et al. 2016, ApJ, 828, 46

Astropy Collaboration, Robitaille, T. P., Tollerud, E. J., et al. 2013, A&A, 558, A33

Astropy Collaboration, Price-Whelan, A. M., Sipőcz, B. M., et al. 2018, AJ, 156, 123

Bailer-Jones, C. A. L., Rybizki, J., Fouesneau, M., Mantelet, G., & Andrae, R. 2018, AJ, 156, 58

Barenfeld, S. A., Carpenter, J. M., Ricci, L., & Isella, A. 2016, ApJ, 827, 142

Barenfeld, S. A., Carpenter, J. M., Sargent, A. I., Isella, A., & Ricci, L. 2017, ApJ, 851, 85

Biazzo, K., Frasca, A., Alcalá, J. M., et al. 2017, A&A, 605, A66

Carpenter, J. M., Ricci, L., & Isella, A. 2014, ApJ, 787, 42

Chiang, E. I., & Goldreich, P. 1997, ApJ, 490, 368

Comerón, F. 2008, The Lupus Clouds, ed. B. Reipurth, Vol. 5, 295

D'Alessio, P., Cantö, J., Calvet, N., & Lizano, S. 1998, ApJ, 500, 411

Davidson-Pilon, C., Kalderstam, J., Zivich, P., et al. 2019, CamDavidsonPilon/lifelines: v0.21.3, , , doi:10.5281/zenodo.3240536. https://doi.org/10.5281/zenodo.3240536

de Zeeuw, P. T., Hoogerwerf, R., de Bruijne, J. H. J., Brown, A. G. A., & Blaauw, A. 1999, AJ, 117, 354

Duncan, M. J., Levison, H. F., & Budd, S. M. 1995, AJ, 110, 3073

Eisner, J. A., Arce, H. G., Ballering, N. P., et al. 2018, ApJ, 860, 77

Evans, A. 1994, The dusty universe

Facchini, S., Clarke, C. J., & Bisbas, T. G. 2016, MNRAS, 457, 3593

Foreman-Mackey, D., Hogg, D. W., Lang, D., & Goodman, J. 2013, PASP, 125, 306

Frasca, A., Biazzo, K., Alcalá, J. M., et al. 2017, A&A, 602, A33

Gerbig, K., Lenz, C. T., & Klahr, H. 2019, A&A, 629, A116

Guilloteau, S., Dutrey, A., Piétu, V., & Boehler, Y. 2011, A&A, 529, A105

Huang, J., Andrews, S. M., Dullemond, C. P., et al. 2018, ApJL, 869, L42

Ida, S., Larwood, J., & Burkert, A. 2000, ApJ, 528, 351

Isella, A., Carpenter, J. M., & Sargent, A. I. 2009, ApJ, 701, 260

Kelly, B. C. 2007, ApJ, 665, 1489

Kenyon, S. J., & Bromley, B. C. 2004, Nature, 432, 598

Krijt, S., Ormel, C. W., Dominik, C., & Tielens, A. G. G. M. 2015, A&A, 574, A83

Lauer, T. R., Ajhar, E. A., Byun, Y. I., et al. 1995, AJ, 110, 2622

Lenz, C. T., Klahr, H., & Birnstiel, T. 2019, ApJ, 874, 36

Long, F., Herczeg, G. J., Pascucci, I., et al. 2018, ApJ, 863, 61

Long, F., Herczeg, G. J., Harsono, D., et al. 2019, ApJ, 882, 49

Luhman, K. L. 2004, ApJ, 617, 1216

Luhman, K. L., & Rieke, G. H. 1999, ApJ, 525, 440

Luhman, K. L., Allen, L. E., Allen, P. R., et al. 2008, ApJ, 675, 1375

Manara, C. F., Fedele, D., Herczeg, G. J., & Teixeira, P. S. 2016, A&A, 585, A136

Manara, C. F., Testi, L., Herczeg, G. J., et al. 2017, A&A, 604, A127

Manara, C. F., Tazzari, M., Long, F., et al. 2019, A&A, 628, A95

McMullin, J. P., Waters, B., Schiebel, D., Young, W., & Golap, K. 2007, in Astronomical Society of the Pacific Conference Series, Vol. 376, Astronomical Data Analysis Software and Systems XVI, ed. R. A. Shaw, F. Hill, & D. J. Bell, 127

Merín, B., Jørgensen, J., Spezzi, L., et al. 2008, ApJS, 177, 551

Morbidelli, A., Levison, H. F., & Gomes, R. 2008, The Dynamical Structure of the Kuiper Belt and Its Primordial Origin, ed. M. A. Barucci, H. Boehnhardt, D. P. Cruikshank, A. Morbidelli, & R. Dotson, 275–292

Mulders, G. D., Pascucci, I., & Apai, D. 2015, ApJ, 798, 112

Nakajima, Y., Tamura, M., Oasa, Y., & Nakajima, T. 2000, AJ, 119, 873

Ormel, C. W., Liu, B., & Schoonenberg, D. 2017, A&A, 604, A1

Pascucci, I., Mulders, G. D., Gould, A., & Fernand es, R. 2018, ApJL, 856, L28

Pascucci, I., Wolf, S., Steinacker, J., et al. 2004, A&A, 417, 793

Pascucci, I., Testi, L., Herczeg, G. J., et al. 2016, ApJ, 831, 125

Pecaut, M. J., Mamajek, E. E., & Bubar, E. J. 2012, ApJ, 746, 154

Petit, J.-M., Kavelaars, J. J., Gladman, B. J., et al. 2011, AJ, 142, 131

Pinilla, P., Birnstiel, T., Benisty, M., et al. 2013, A&A, 554, A95

Preibisch, T., Brown, A. G. A., Bridges, T., Guenther, E., & Zinnecker, H. 2002, AJ, 124, 404

Ricci, L., Testi, L., Natta, A., et al. 2010, A&A, 512, A15

Roccatagliata, V., Sacco, G. G., Franciosini, E., & Rand ich, S. 2018, A&A, 617, L4

Rosotti, G. P., Booth, R. A., Tazzari, M., et al. 2019, MNRAS, 486, L63

Sacco, G. G., Spina, L., Randich, S., et al. 2017, A&A, 601, A97

Shapiro, S. S., & Wilk, M. B. 1965, Biometrika, 52, 591. https://doi.org/10.1093/biomet/52.3-4.591

Slesnick, C. L., Hillenbrand, L. A., & Carpenter, J. M. 2008, ApJ, 688, 377

Tazzari, M. 2017, doi:10.5281/zenodo.1003113

Tazzari, M., Beaujean, F., & Testi, L. 2018, MNRAS, 476, 4527

Tazzari, M., Testi, L., Natta, A., et al. 2017, A&A, 606, A88

Tripathi, A., Andrews, S. M., Birnstiel, T., & Wilner, D. J. 2017, ApJ, 845, 44

Wasserburg, G. J., Karakas, A. I., & Lugaro, M. 2017, ApJ, 836, 126

Wilking, B. A., Meyer, M. R., Robinson, J. G., & Greene, T. P. 2005, AJ, 130, 1733

Winter, A. J., Clarke, C. J., Rosotti, G., et al. 2018, MNRAS, 478, 2700

Zinner, E. 2014, Presolar Grains, ed. A. M. Davis, Vol. 1, 181–213